ABSTRACT

LIU, LU. Fabrication and Characterization of Poly(vinyl alcohol) Magnetic Fibers with High Loadings of Fe_3O_4 Nanoparticles via Dry-jet Wet Spinning. (Under the direction of Dr. Stephen Michielsen).

Magnetic fibers are a new class of magnetic materials that combine the unique properties of fibers and magnetic materials together. Magnetic fibers have shown promising potential in applications such as micro-sensors, flexible microwave absorption textiles, data storage media, metal ion filtration membranes, and biomedical scaffolds. However, the magnetic performance of current magnetic fibers is very low compared to traditional inorganic magnetic materials, due to the low magnetic nanoparticle (MNPs) loadings in the fibers, which can be attributed to the fiber fabrication method of electro-spinning.

The main objective of this study was to obtain highly magnetically responsive magnetic fibers via the industrialized fiber production technique of dry-jet wet spinning. The main hypothesis was that dry-jet wet spinning technique would enable higher MNPs concentration in the system compared to electro-spinning.

In the study, magnetic PVOH fibers with superparamagnetic Fe_3O_4 MNPs were spun at various MNPs loadings (0%wt, 10%wt, 20%wt, 40%wt, and 60%wt upon polymer weight) to study the effect of MNPs concentration on fiber properties. Ferromagnetic Fe_3O_4 MNPs were also dry-jet wet spun into fibers at a high loading ratio of 60%wt to understand the effect of MNPs species on fiber performance. Fibers were evaluated for different properties such as fiber morphology, crystal structure, thermal performance, mechanical properties, and magnetic performance.

The results of this study showed that the fiber production technique of dry-jet wet spinning was able to generate magnetic fibers at high MNPs loadings that had not been achieved by electro-spinning before, and superparamagnetic fiber exhibited magnetism saturation value (Ms) as high

as 67% as compared to bare superparamagnetic Fe_3O_4 MNPs. Meanwhile, ferromagnetic fibers were also successfully fabricated with Ms value of 46% as compared to bare ferromagnetic Fe_3O_4 MNPs. To the author's best knowledge, these fibers were the most magnetically responsive fibers that have been reported in literature. These high-MNPs-loading fibers demonstrated uniform fiber structure and sufficient fiber mechanical performance, with competitive magnetic performance as compared to traditional inorganic magnetic materials, along with unique properties of a fiber. The magnetic fibers from this study could potentially be utilized in traditional magnetics applications as well as in other innovative ways.

Fabrication and Characterization of Poly(vinyl alcohol) Magnetic Fibers with High Loadings of Fe_3O_4 Nanoparticles via Dry-jet Wet Spinning

by
Lu Liu

A dissertation submitted to the Graduate Faculty of
North Carolina State University
in partial fulfillment of the
requirements for the degree of
Doctor of Philosophy

Fiber and Polymer Science

Raleigh, North Carolina
2019

APPROVED BY:

Dr. Stephen Michielsen Committee Chair	Dr. Richard Kotek
Dr. Ericka Ford	Dr. Joseph Tracy

DEDICATION

To my family, especially my mother Liping Jiang, my father Pingyi Liu,

my husband Brian Bernard Eller, and my daughter Zoe Liu Eller.

BIOGRAPHY

Lu Liu originally came from the city of Jilin in Northeast China. She graduated with a bachelor's degree in chemical and Biomolecular Engineering from Zhejiang University, China, in 2010. Following undergraduate studies, Lu enrolled in the master's degree program in the Department of Chemical & Biomolecular Engineering at North Carolina State University, Raleigh, NC, where she had worked on polymer surface modification in Dr. Jan Genzer's group and combustion molecular simulation in Dr. Phillip Westmoreland's group.

Lu later joined the PhD program of Fiber and Polymer Science, Textile at North Carolina State University and worked on experiments and computation simulation of polymer surface modification for pathogen removal with Dr. Julie Willoughby and Dr. Melissa Pasquinelli. In 2013, Lu joined the research group of Dr. Stephen Michielsen, where she started the doctoral research project of dry-jet wet spinning magnetic fibers.

In addition to her research, Lu has served as the President of Chinese Students and Scholars Association (CSSFA) at NCSU in 2011-2012; and has worked as a product engineer at Fredenburg Filtration Technologies in Kentucky in 2015-2017. Outside the lab, Lu enjoys exploring nature, watching science fiction shows, and playing the traditional Chinese instrument the Guzheng.

ACKNOWLEDGMENTS

First and most importantly, I would like to offer my sincerest gratitude to Dr. Stephen Michielsen, my advisor and committee chair, for the extreme patience and courage he had given me in both research and life in the past few years, as well as for the financial support. His professionalism as a researcher and kindness as an advisor are more than a student and friend could ask for, and I am so grateful to have this learning experience from Dr. Michielsen, which I wish I would inherit and influence others the same way one day.

I would like to truly thank my committee members for their valuable inputs and support to this study: Dr. Richard Kotek for the encouragement throughout the project and instruction on the experiments, Dr. Ericka Ford for sharing the instrument and giving much guidance on fiber spinning, and Dr. Joseph Tracy for the education on the topic of magnetic materials and help with magnetism analysis.

I would also like to express my gratitude to everyone that helped me along this research project: Dr. William Oxenham for giving me the opportunity to join Dr. Michielsen's group, Dr. Sam M. Hudson for wet spinning equipment and experiments instruction, Dr. Ford's research group for bouncing great ideas with, Dr. Ching-Chang Chung for WAXD analysis, Dr. Lewis Reynolds for SQUID test, Ms. Birgit Andersen for TGA analysis, Ms. Judy Elson for optical analysis, Ms. Teresa White for tensile test, Mr. Hai Bui and Dzung Nguyen for helping me build parts in the machine shop. It was also a great joy to work with other members in Dr. Michielsen's group, especially Dr. Jingyao Li, who all had helped me with ImageJ analysis and encouraged me throughout the study.

Last but not least, I am sincerely thankful for all the love and support from my family and friends, especially my parents, Liping Jiang and Pingyi Liu, my parents in law, Dr. Wendy Rey

and Dr. Mark Eller, and my dearest husband, Brian Bernard Eller. Brian's encouragement and patience have made this work grow, so made me grow. We just introduced a new little member to the family on Oct 1st, 2018, Zoe Liu Eller, who has been accompanying me for the last part of this journey and giving me force since the first day she existed in this world! I hope one day she will read her mom's dissertation and be proud of being part of it.

TABLE OF CONTENTS

LIST OF TABLES

LIST OF FIGURES

CHAPTER 1 INTRODUCTION

Magnetic fibers are a new class of materials that are actively under development. Magnetic fibers combine magnetic properties of traditional inorganic magnetic materials and unique properties of fibers such as lightness in weight, transparency, unique physical geometry, and flexibility of scale. These advantages give magnetic fibers the potential to be utilized in diverse applications, such as micro-sensors, artificial muscles, flexible microwave absorption textiles, data storage media, metal ion filtration membrane, and biomedical scaffolds et al.[1-7]

Electro-spinning has served as the main method to fabricate magnetic fibers to date, as electro-spinning is easy to configure in laboratory and can produce fibers at nanoscale. However, electro-spinning also faces many challenges when it comes to magnetic fiber production. For example, the magnetic response of electro-spun magnetic fibers is usually much lower than bare magnetic nanoparticles (MNPs), with magnetism saturation values less than 5 emu/g compared to 50 emu/g of bare MNPs.[8] This is because the MNPs loading in an electro-spun setup is usually small, as high MNPs concentration could cause significant MNPs agglomeration at spinneret tip, which is due to the imbalanced force of surface tension and electro-field at the spinneret tip. Furthermore, it is also difficult to produce single magnetic fibers with sufficient mechanical properties via electro-spinning.[9] Finally, electro-spinning still faces many challenges such as low production rate and high cost compared to other fiber spinning techniques.

There is no apparent way to produce highly magnetically responsive single fibers cost-effectively to date. The goal of this study is to fill this gap with the fabrication of highly magnetic responsive single fibers embedded with ferromagnetic/superparamagnetic

Fe_3O_4 MNPs via a cost-effective fiber production method: dry-jet wet spinning. Dry-jet wet spinning is capable of producing single fibers with outstanding mechanical performance at low-cost and at industrial scale. The central hypothesis of this study is that: 1) high loadings of MNPs can be achieved with dry-jet wet spinning, as no electro-field is involved in the process; 2) the fiber products could maintain sufficient fiber structure and properties.

The study will be conducted in three stages:

- To identify the optimum spinning dope for dry-jet wet spinning magnetic PVOH fibers
- To fabricate superparamagnetic PVOH fibers with 20nm Fe_3O_4 MNPs at different MNPs loadings, and to study the effects of MNPs concentration on fiber performance
- To fabricate ferromagnetic fibers with 80nm Fe_3O_4 MNPs at high MNPs loading and to compare the impact of MNPs species on fiber properties

CHAPTER 2 LITERATURE REVIEW

2.1 Magnetism

Every material has a magnetic property, which is usually defined as inner magnetic response when the object is placed in a magnetic field (*H),* and this response is called the induction (*B),* which is a function of external the magnetic field (*H)* and the material magnetization *(M) (*Equation 2-1). The ratio of *M* over *H* is defined as magnetic susceptibility (χ), and χ is an index that reflects the pairing condition of molecule electrons.

$$B = H + 4\pi \mathrm{M} \qquad 2\text{-}1$$

$$\chi = M/H \qquad 2\text{-}2$$

If the electrons in a molecule are in pairs, the electrons will form closed orbital rings when put in an external magnetic field, and a negligible internal magnetic field of the molecule would consequently be generated. This magnetism performance is called *diamagnetism*. Diamagnetic materials have a very small magnetic susceptibility (χ), and are generally considered "non-magnetic".

For materials with electrons not paired, the magnetic induction (*B)* cannot be neglected in an external magnetic field, and such magnetic behavior is called *paramagnetism,* the so-called "magnetic responsive".[10] In the category of paramagnetic materials, the magnetic susceptibility χ ((Equation 2-3) is used to describe magnetic properties, which is determined by the number of unpaired electrons (represented by Curie constant *C)* and influenced by temperature *T (Kelvin).* The calculation of Curie constant *C* against the number of unpaired electrons (*g*) is shown in Equation 2-4, where *β* refers to effective magnetic moments, *S* is the spin angular momentum, and *k* is Boltzmann's constant, and *N* is the number of magnetic atoms/molecule per volume.[10]

$$\chi = C/T \qquad 2\text{-}3$$

$$\mathrm{C} = \frac{N^2 g\beta^2 S(S+1)}{3k} \qquad 2\text{-}4$$

Magnetic performance of a paramagnetic material can be divided into four categories based on the types of magnetic interaction among the electron spins: paramagnetic, ferromagnetic, ferrimagnetic, and anti-ferromagnetic. A brief comparison of these four categories is included in Table 2.1,with typical magnetization curves shown in Figure 2.1. When ferromagnetic and ferrimagnetic materials are placed in a magnetic field, the coupling forces cause magnetic moments of neighboring atoms to align and to accumulate into a very large internal magnetic field that is 10- 100 times the external magnetic field strength (Table 2.1). This fact distinguishes ferro/ferri-magnetism from paramagnetism, as the magnetic moments in paramagnetic materials respond to external magnetic fields independently without lining up with each other which lead to weak internal magnetic fields. Furthermore, ferromagnetic and ferrimagnetic materials can retain permanent magnetism after an external magnetic field is removed. As shown in Figure 2.1 (x-axis: external magnetic field, y-axis: internal magnetic field), ferromagnetic and ferrimagnetic materials still contained an induced internal magnetic field when the external magnetic field is removed at $x = 0$. This is because magnetic moments are forced to line up forming internal magnetic field when an external magnetic field is added; once the external magnetic field is removed, not all magnetic moments have enough energy to rotate back to their original chaotic states. Therefore, the material retains its magnetism even when the external magnetic field is removed. As the environmental temperature increases (Curie temperature for ferromagnetic materials, and Neel temperature for antiferromagnetic materials), magnetic moments have more thermal energy to overcome the coupling forces

induced by the external magnetic field. In such circumstances, the magnetic moments are able to fluctuate randomly again as soon as the external magnetic field is removed. In this case, there would be no permanent internal magnetic field left in the material, which is known as superparamagnetism.

Table 2.1 Categories of magnetism[10].

Category	Magnetism	Spin
Paramagnetism	Each spin oriented randomly and independently to external magnetic field, with no interaction with each other	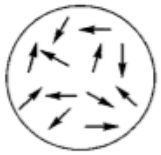
Ferromagnetism	Magnetic moments of neighboring atoms align which results in very large internal magnetic fields	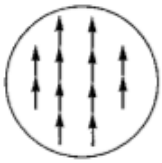
Ferrimagnetism	Two kinds of spins exist among magnetic moments, which are antiparallel to each other. One orientation dominates, which leads to large internal magnetic fields	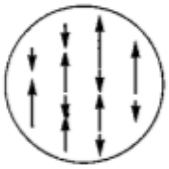
Anti-ferromagnetism	Two kinds of spins exist among magnetic moments, with neighboring spins always pointing antiparallel	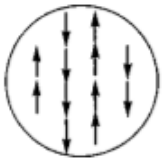

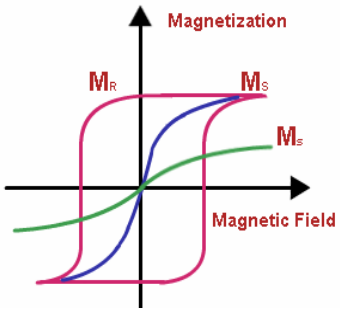

Figure 2.1 Magnetic hysteresis curves for ferromagnetism (red), paramagnetism (green), superparamagnetism (blue) [10].

Nanoparticles (NPs) such as Fe_3O_4 NPs with a diameter smaller than 25nm exhibit superparamagnetic properties at room temperature. The thermal energy (crystalline anisotropy energy) provided for these small magnetic nanoparticles at room temperature is sufficient to flip magnetic spins once the external magnetic field disappears. This is the result of the existence of single magnet domains in the small size of the Fe_3O_4 NPs, which requires very low thermal energy to flip magnetic moments. Therefore, superparamagnetism commonly exists in nanoparticles (NPs) of ferro- and ferrimagnetic materials at room temperature.

2.2 Magnetic Fibers

2.2.1 Introduction

As a relatively new group of materials, magnetic fibers have shown great potential in many diverse applications.[1-7] Patents have been filled related to magnetic fibers or magnetic organic gels for commercialization, such as "Process for Obtaining Magnetic Cellulose Paper and the Respective Product" (US20140231035A1) [11], "Magnetothermal Fibers" (WO2014084853A1)[12], and "Process for Treating Concentrated Salt Solutions Containing DOC" (US7540965B2)[13].

One promising potential application for highly magnetic fibers is for use as artificial muscles or linear actuators. Artificial muscles are materials or devices that can reversibly contract, expand or rotate in response to environmental conditions such as voltage, temperature, light, pH and magnetic field.[14] A living skeletal muscle can contract 30% in length in $10^{-3} \sim 10^{-2}$ s, but pH triggered artificial muscle materials take 20s to reach 80% deformation because it takes a relatively long time for polymers to relax and to reform when induced by pH change.[15] Magnetic field induced artificial muscle can achieve a much

shorter response time with an accurate elongation/contraction behavior as all the magnet spins in the material respond spontaneously and uniformly to magnetic field change.[14, 16] Compared to induction of light or voltage driven artificial muscles, the magnetic response is only related to magnetic nanoparticles (MNPs) embedded in fibers, which frees up the choice of polymers for other performance requirements. Magnetism triggered artificial muscles can be programmed for specific movement patterns by controlling magnetic field strength and location. Magnetostrictive polymer composite gels such as polydimethylsilicone containing Fe_3O_4 magnetic particles have been studied as artificial muscles by some researchers, but there have been few studies to explore the potential of magnetic fibers. It is worthwhile to mention the interesting work from Dr. Baughman's group[17], who fabricated carbon nanotube yarns as artificial muscle (**Figure 2.2**). In this product, the fibers responded to voltage for expansion and contraction movements. The author believes magnetic fibers would be able to achieve these movements by alternation of external magnetic fields.

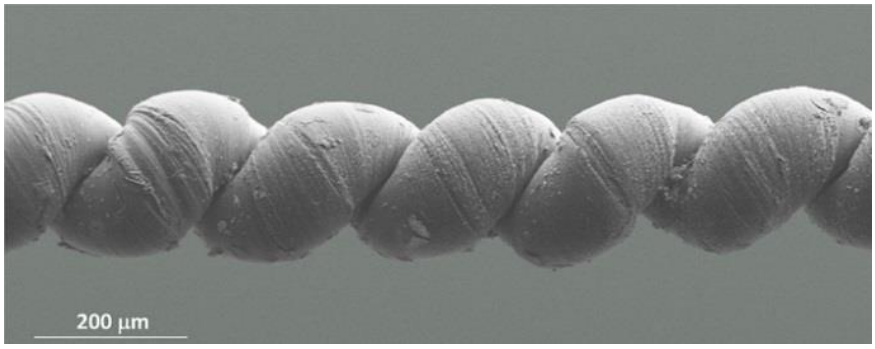

Figure 2.2 Artificial muscle made from carbon nanotube yarns with paraffin wax and twists[17].

Another promising application for highly ferromagnetic responsive fibers is magnetic filtration, such as for water/oil filtration to remove corrosive materials from

industrial process fluids, automotive filtration to maintain the effectiveness of lubricants (Figure 2.3), and bio-separation membranes to purify cells and proteins from bioreactor streams. [18-20] With high MNPs loadings, ferromagnetic fibers produced in this study have the potential to improve the filtration capacity of magnetically-sensitive materials at a small extra cost.

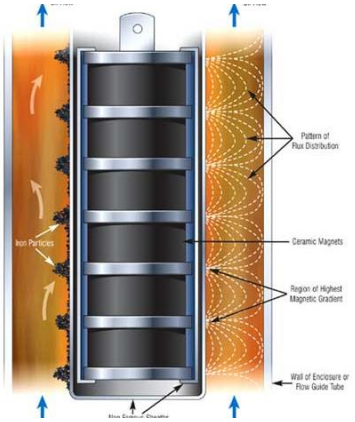

Figure 2.3 Magnetic filter with flux distribution and iron particles collection [18].

Magnetic fibers can be divided into three categories based on magnetism mechanism: 1) pure organic polymers with magnetic properties coming from organic radicals of the polymer backbones and /or side branches; 2) polymers with paramagnetic ions chemically bonded to polymer chains; 3) polymer systems with magnetic nanoparticles (MNPs) physically mixed in.[10] Among these three systems, the polymer-MNPs system is the most studied so far, as the magnetic fibers produced from this system have a much higher magnetic response compared to the ones from the other two systems, which gives it competitiveness to inorganic magnetic materials in practical applications. The polymer-MNPs system is the system selected in this study for magnetic fiber studies, and all following sections from here is based on this system unless otherwise claimed.

2.2.2 Challenges and Recent Studies

To produce magnetic fibers with desired mechanical and magnetic performance, researchers face many challenges, such as the uniformity of magnetic nanoparticles (MNPs) dispersion in fibers, the magnetic performance of final fiber products, mechanical and thermal properties of magnetic fibers. In this section, recent work on these challenges are discussed in depth.

2.2.2.1 Uniformity of MNPs Dispersion

To produce consistent and continuous magnetic fibers, it is essential to obtain uniform and stable polymer-MNPs spinning dope. An uncontrolled polymer solution could lead to defects in fibers, or even inhibit fibers from being formed properly. However, by nature, MNPs tend to agglomerate in polymer solution, as MNPs exhibit dipole-dipole interaction with each other. Furthermore, the large surface energy difference of polymers and MNPs tend to separate the two phases.

Many approaches have been explored to achieve a homogenous MNPs suspension, such as adding co-solvents into the solution, treating MNPs surfaces, and implementing special spinning techniques.

Co-solvents of sodium citrate, polyacid, or oleic acid have been added to stabilize the MNPs polymer dispersion.[21] Surface treatment on MNPs is also an effective way to reduce the surface energy difference between polymers and MNPs, including silanization[22], coating with polymer brushes[23, 24], grafting[25], and chemisorption. For example, Shan et al[21] have synthesized magnetic Fe_3O_4 MNPs in PLLA shells (Fe_3O_4@PLLA) to achieve homogenous spinning (Figure 2.4) where PLLA magnetic nanofibers were successfully produced. In another study, Mincheva et al[26] synthesized

Fe_3O_4 MNPs directly in the spinning solution of polyelectrolyte n-carboxyethyl chitosan (CECh), which formed a uniform MNPs dispersion with very fine MNPs diameters (Figure 2.5). This produced MNP-CECh homogenous solution that remained stable for 40 days without precipitation.

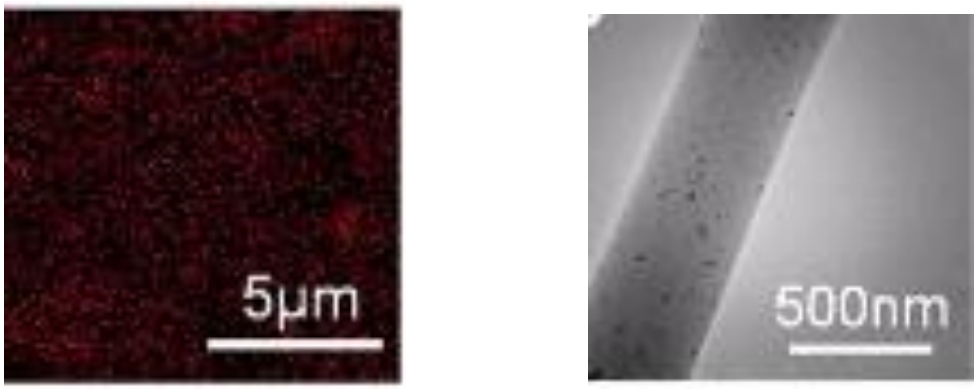

Figure 2.4 PLLA/Fe_3O_4 nanofibers with Fe_3O_4@PLLA MNPs loaded: (left) iron element mapping, and (right) TEM image [21].

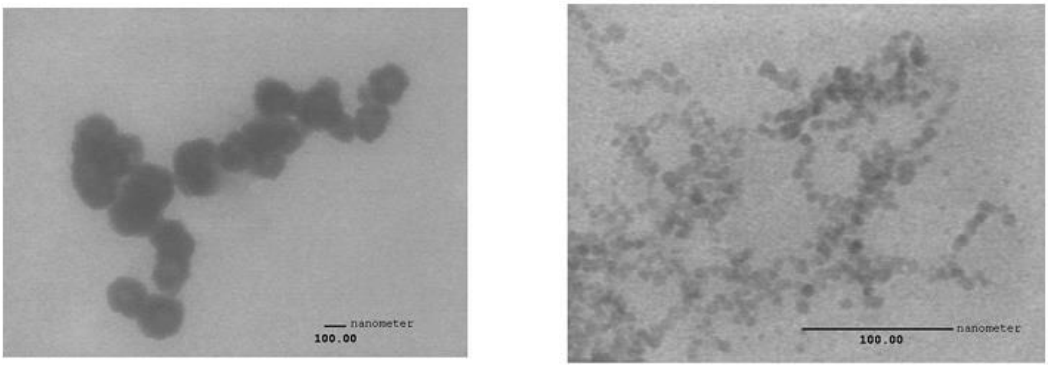

Figure 2.5 TEM image of (left) bare Fe_3O_4 nanoparticles and (right) Fe_3O_4 + CECh nanoparticles [26].

Another way to control MNPs dispersion without worrying about MNPs and polymer dispersion is to apply coaxial spinning (Figure 2.6). In this setup, the outside spinneret dope is pure polymer solution, and the inner spinneret solution only contain

MNPs and solvent. Song et al[27] have successfully embedded FePt MNPs (MNPs diameter of 17.6nm) in one-dimensional array in PCL nanofibers with coaxial spinning for 3000nm (Figure 2.6).

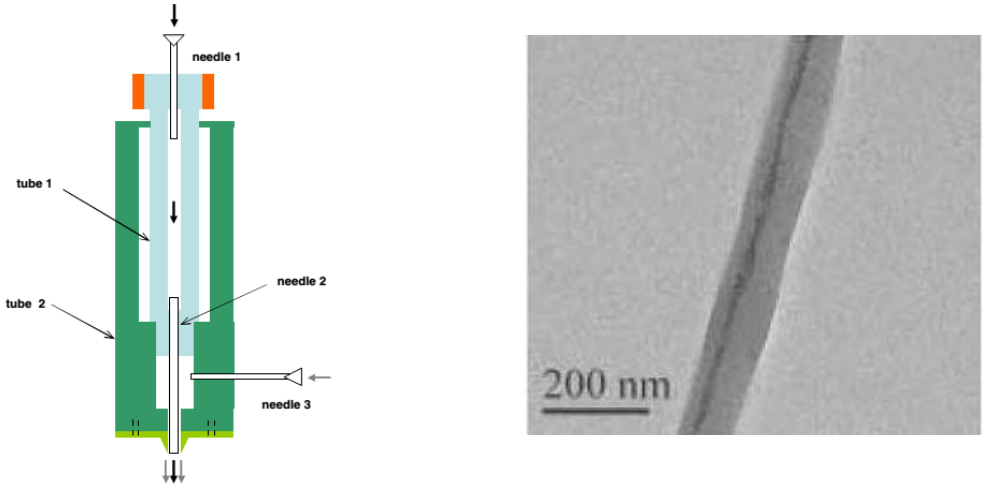

Figure 2.6 Coaxial electro-spinning setup (left), and TEM image of the produced magnetic PCL nanofibers with FePt self-assembled array along fiber axis (right) [27].

It is more difficult to obtain homogeneous spinning dope with the increase of the MNPs loading ratio, as MNPs are more likely to agglomerate. Miyauch et al observed strong agglomeration in the polyvinylpyrrolidone/Fe_3O_4 MNPs (50%wt/50%wt) fibers (Figure 2.9), which spinning dope contained 2-propanol as surfactant. However, it was doubtful whether the actual MNPs ratio had reached as high as 50%wt, as the saturated magnetic value of final fibers was much lower than 50% of that value as of pure MNPs.[9]

2.2.2.2 MNPs Topology

Another topic that has been briefly explored is the MNPs topology in magnetic fibers. In one study, all MNPs lined up in the fiber when a magnetic field was added perpendicular to the fiber axis during the spinning process, causing MNPs topology to change from random distribution (Figure 2.7 left) to alignment along the fiber axis (Figure

2.7 right). The magnetic saturation value (M_s) of the MNPs-aligned fiber was similar to that of magnetic fiber with random MNPs distribution, which indicated the alignment of MNPs in fibers did not alter the behavior of MNPs matrix and did not form a connected nanowire.[28]

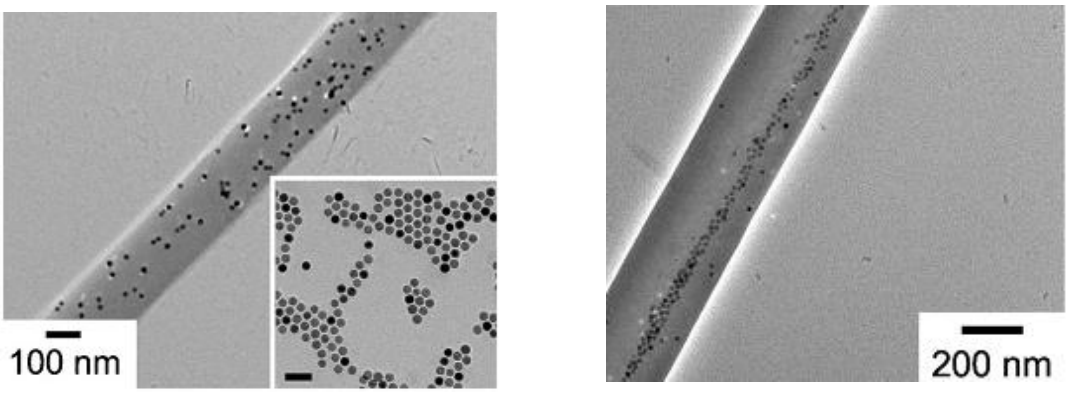

Figure 2.7 TEM images of (left) randomly dispersed superparamagnetic iron oxide nanoparticles (0.5 vol%) in electro-spun polycaprolactone (PCL) microfibers; (right) magnetic field-aligned SPIONs in PCL microfibers with long, contiguous arrays [28].

2.2.2.3 High MNPs Loadings

In order to be competitive in some magnetic applications, magnetic fibers need to reach a high magnetic response. The M_s value of most magnetic fibers currently reported in the literature is lower than 5 emu/g, compared to around 50 emu/g as for pure inorganic MNPs. Since M_s value is proportional to the loading ratio of MNPs in polymer matrix,[21] the challenge has become how to embed high MNPs loadings in magnetic fibers, which can be divided into two tasks: 1) to obtain stable homogenous solution with high MNPs loadings, 2) to spin fibers from high MNPs loaded solution.

The first task has been discussed in Section 2.2.2.1, which involves co-solvents, MNPs surface treatment, and a tailored spinning technique. Regarding the second task of

spinning fibers from high MNPs loaded solution, the current common spinning method of magnetic fibers, electro-spinning, is typically incapable of producing such fibers. This is because the interaction of MNPs and electric field at high MNPs loading is so high that MNPs tend to agglomerate at the spinning tip interrupting the continuous formation of uniform fibers. Therefore, the MNPs loading in electro-spinning process is usually less than 10%wt, which results in magnetic performance of final products that are much lower than inorganic magnetic materials.

One of the highest MNPs loading ratio via electro-spinning was claimed by Wang's group[29], in which the weight ratio of Fe_3O_4 MNPs and poly(vinyl pyrrolidone) (PVP) in spinning dope was 3:1. However, the actual MNPs loading in the final fiber product was not examined, and the saturation magnetization of prepared Fe_3O_4/PVP fiber was only 0.33 emu/g compared to the value of 93 emu/g for bare Fe_3O_4 MNPs. Therefore, the actual loading ratio of MNPs in their magnetic fibers is suspected by the author to be much lower than the initial loading in the polymer solution. Another high MNPs loading ratio of electro-spun magnetic fibers was from Miyauch's group,[9] where 50%wt of ferromagnetic Fe_3O_4 MNPs was embedded in PVP fiber spinning solution. However, according to the hysteresis loop (Figure 2.9), the M_s value was much smaller than 50% of M_s value of bare MNPs, which indicated the actual MNPs loading in the magnetic fibers was not as high as 50%wt.

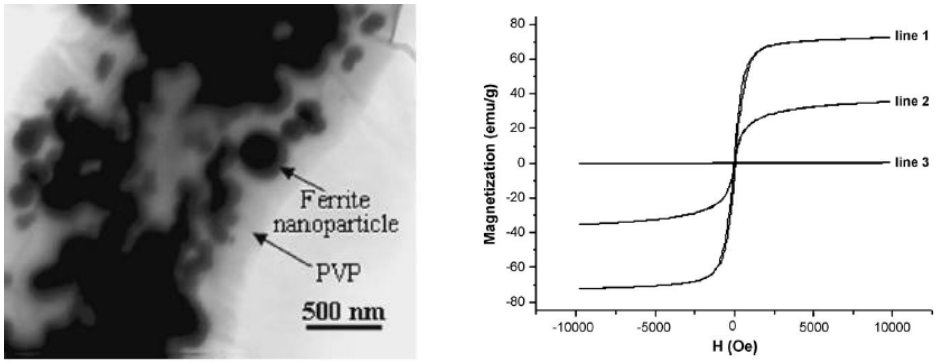

Figure 2.8 TEM image of PVP/ Fe_3O_4 composite nanofibers (left), and Fe_3O_4 MNPs hysteresis loops (right): Fe_3O_4 MNPs with diameter of 250nm (line 1), Fe_3O_4 MNPs with diameter of 20nm (line 2), Fe_3O_4 MNPs-250nm/PVP nanofibers (line 3) [29].

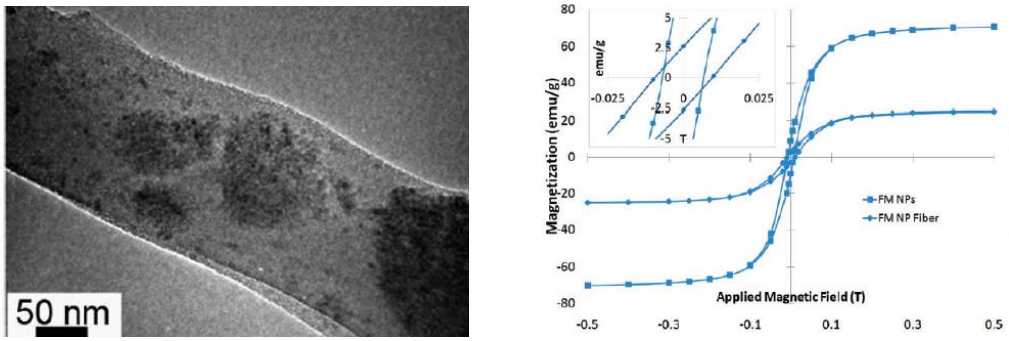

Figure 2.9 TEM image of magnetic nanofiber of PVP/SPM=50/50 %wt (left), and hysteresis loops (right) of electro-spun PVP/ferro-Fe_3O_4-MNPs magnetic fiber with 50%wt MNPs loading [9].

One interesting phenomenon has been reported about MNPs, MNPs become magnetically harder in a polymer matrix with higher M_s value per weight, once embedded in magnetic fibers. This effect is possibly caused by the reduction of dipolar-dipolar interaction between MNPs when immobilized in polymer phases.[30]

2.2.2.4 MNPs with Different Sizes

Despite the challenge to achieve high MNPs loadings, it is also difficult to incorporate MNPs with large diameters into magnetic fibers. This is true for fibers at both nanoscale as well as micro-scale, especially when the diameter of MNPs is larger than 200nm.

In one study, magnetic polyvinylpyrrolidone (PVP) fibers were successfully fabricated with a mixture of Fe_3O_4 ferromagnetic MNPs and Fe_3O_4 superparamagnetic MNPs.[9] No magnetic particle coupling was observed among two MNPs species in the magnetic fibers, which was different from some earlier research. Further investigation is needed for a thorough understanding on this topic.

2.2.2.5 MNPs Effects on Fiber Performance

The incorporation of MNPs affect various fiber properties, such as crystal structure, thermostability, and mechanical performance.

For example, MNPs can reinforce magnetic fiber crystallinity at low loading ratios. In an earlier work of PAN/Fe_3O_4 magnetic nanofibers, the wide-angle X-ray diffraction (WAXD) graphs showed the polymer crystal (PAN-2,0,0) peak at $2\theta \sim 17°$ (Figure 2.10 b-e) becoming sharper and more noticeable as the MNPs concentration increased from 0%wt to 9%wt. This is because the addition of MNPs as well as other nano-fillers restrict the mobility of polymer chains in certain directions, which makes the polymers more likely to align and form crystalline regions through drawing. This improved crystallinity at low MNPs loadings is expected to benefit the mechanical performance of magnetic fibers.

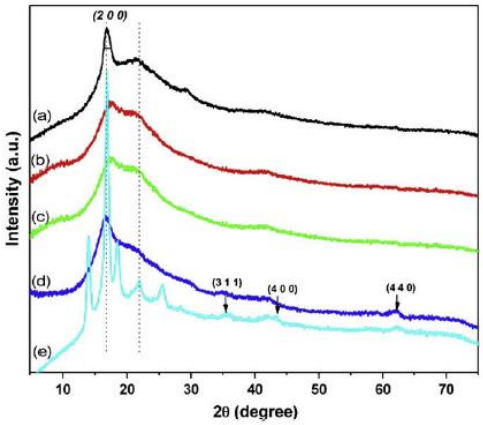

Figure 2.10 WAXD patterns of PAN/Fe_3O_4 magnetic nanofibers with different MNPs loadings: a) 0%wt (as-received PAN powder), b) 0%wt (pure PAN fibers), c) 1 %wt Fe_3O_4, d) 5 %wt Fe_3O_4, e) 9% Fe_3O_4 [30].

The addition of MNPs at a low concentration has been illustrated to benefit fiber mechanical properties. [31]As shown in Figure 2.11, the tensile strength of nylon-strontium magnetic fiber increased as MNPs volume was 5%vol.[4]. Beside the future development of crystal regions because of MNPs incorporation, a good filler-polymer interface is also likely to form at low MNPs loadings, which will help the stress transfer within materials under tension.

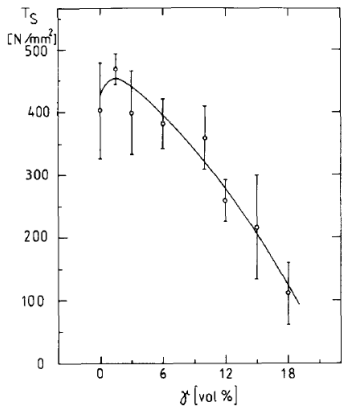

Figure 2.11 Tensile strength of nylon fibers with various loadings of strontium ferrite [4]

However, as the MNPs loading increases, the quantity and size of MNPs clusters in the fibers are likely to grow and form defects in the fibers, which would lead to weakened fiber mechanical performance. This effect is also seen in Figure 2.11, in which the tensile strength of magnetic fiber decreased as MNPs concentrations exceeded 5%vol. [4] This can be explained as the mobility of polymers is restricted so extensively at high MNPs concentrations that the growth of polymer crystal regions is inhibited. Under this circumstance, magnetic fibers of high MNPs loadings could experience high porosity with low crystallinity, which is reflected by poor mechanical strength and reduced thermal stability. For instance, Chien[32] et al. have reported a decrease of 18% on fiber modulus caused by 10%wt superparamagnetic Fe_3O_4 MNPs in PAN fibers. Other research has found a reduction of 50% on initial modulus value for magnetic PVOH fibers with the magnetic iron ion ratio of 17.63 %wt.[33]

The incorporation of MNPs on magnetic fiber thermostability has been explored with thermogravimetric analysis (TGA). As shown in Figure 2.12, magnetic fibers had a delayed starting point (~280°C) for major stage decomposition compared to pure PAA/PVOH fibers, but the former experienced a much faster weight loss right after. [34] In another study, it was considered the addition of MNPs enhanced fiber thermostability, as there was less weight lost till 300°C for magnetic fibers before the major degradation started (Figure 2.13). The author found this analysis doubtful, as the reduced weight loss could be caused by the lower weight ratio of polymer content in magnetic fibers and MNPs did not lose as much weight in this temperature range. Thus, further work is necessary to test the analysis.

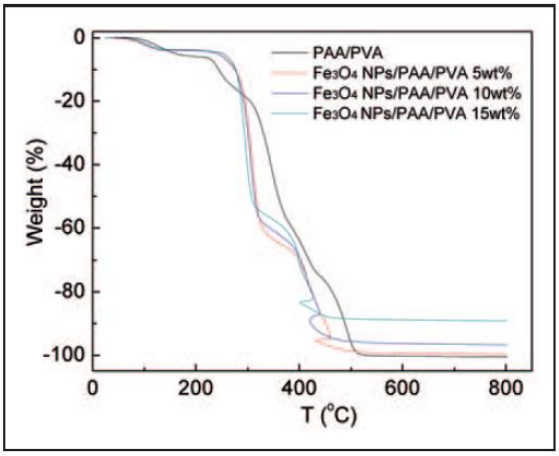

Figure 2.12 TGA curves of PAA/PVOH fibers and Fe_3O_4-MNPs/PAA/PVOH magnetic fibers [34].

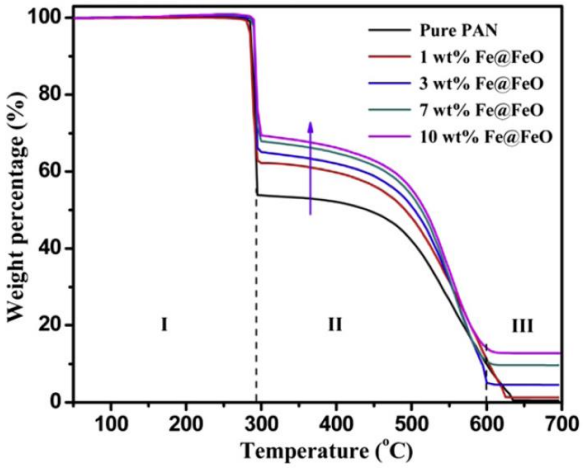

Figure 2.13 TGA curves of electro-spun PAN fibers and PAN/Fe@FeO magnetic fibers [35].

2.2.2.6 MNPs Effects on Spinning Dope Viscosity

The spinning solution of magnetic fibers is a typical non-Newton fluid, and the presence of MNPs enhances the non-Newton behavior even more. For instance, Zhang et al [30] prepared PAN spin dope with Fe_3O_4 MNPs at loading ratios of 5 %wt and 9 %wt. The solution viscosity analysis (Figure 2.14) showed that the shear thinning effect was more severe for 9 %wt MNPs spinning dope as the shear rate increased. This is because the strong

interaction between MNPs and polymers accelerates the alignment of polymer molecules under shear stress. The higher the concentration of MNPs is, the more shear thinning effect would be observed. This negative impact of MNPs on solution viscosity makes it possible to spin polymer solutions at a higher polymer concentration.

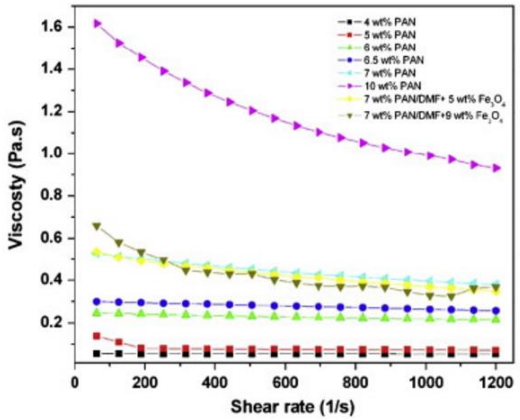

Figure 2.14 Rheological behavior of PAN and PAN/ Fe_3O_4 spinning dopes [30].

2.3 Magnetic Nanoparticles (MNPs)

2.3.1 Introduction

Magnetic nanoparticles (MNPs) are a group of materials that exhibit observable internal magnetic response once placed in external magnetic field and the induced internal magnetic fields could be ferromagnetic (Ferro), superparamagnetic (SPM), ferrimagnetic (Ferri), or antiferromagnetic (Anti-Ferro). MNPs have become popular materials for research, as they can provide benefits as magnetic material as well as being blended with other chemicals to create multi-functional materials. MNPs have been utilized in various applications, such as probes of biological separation, magnetic resonance imaging (MRI), and targeted drug delivery in blood.[24, 36, 37]

Several researchers have embedded MNPs in magnetic fibers. Within this body of work, some researchers have used MNPs with diameters less than 30 nm and

superparamagnetic performance and have embedded these MNPs in magnetic fibers; this choice of MNPs with these characteristics resulted in magnetic fibers, which were also superparamagnetic. Such small MNPs are chosen because it easier to achieve a homogeneous state with small MNPs, both in spinning solution preparation as well as during extrusion.[9] There are also a few approaches to embed larger ferromagnetic MNPs into magnetic fiber systems as discussed in Section 2.2.2.4. Various MNPs have been studied for magnetic fiber fabrication, such as Fe_3O_4[30,38], FePt[27], Fe@FeO (Core@shell structure for a metal NPs with an oxide shell) [8].

2.3.2 MNPs Synthesis

To achieve well-controlled magnetic fibers, MNPs must have a uniform shape with a narrow size distribution. Three methods are qualified to synthesize magnetic particles for such requirements, which are high temperature method, co-precipitation method, and microemulsion method. A summary of these synthesis methods is included in Table 2.2.

Table 2.2 Synthesis methods of MNPs [39, 40]

Method	Particle size produced (nm)	Advantages	Disadvantages
High temperature	5-22	Relatively easy particle size control and narrow size distribution	High temperature required, challenging for scale-up
Co-precipitation	5-200	Simple and rapid route, large scale, ambient conditions	Hard to control particle size
Microemulsion	1-50	Can be utilized at room temperature, good size control	Difficult to scale up

2.3.2.1 High Temperature Method

The high temperature synthesis method can produce uniform MNPs with a narrow size distribution. For this method, MNPs are first formed via nucleation from precursors in high concentration solution that exceeds its critical supersaturation loading, then MNPs grow following the La Mer colloidal growth law.[41] The size, shape and uniformity are controlled by nucleation time, reaction environment, and other kinetic factors. For example, FeO MNPs with a diameter of 14 nm were produced via high temperature synthesis in a solution of oleic acid and oleylamine at 300°C for 30 minutes, and the MNPs diameter could grow up to 100nm if the reaction time was extended (Figure 2.15). [42] Surfactant molecules are sometimes added to help prevent particle aggregation during the synthesis process, as surfactants interact with the unsaturated atoms on particle surfaces and stabilize the solution.[43] The surfactants can also be tailored for further functionalization of final MNPs products.

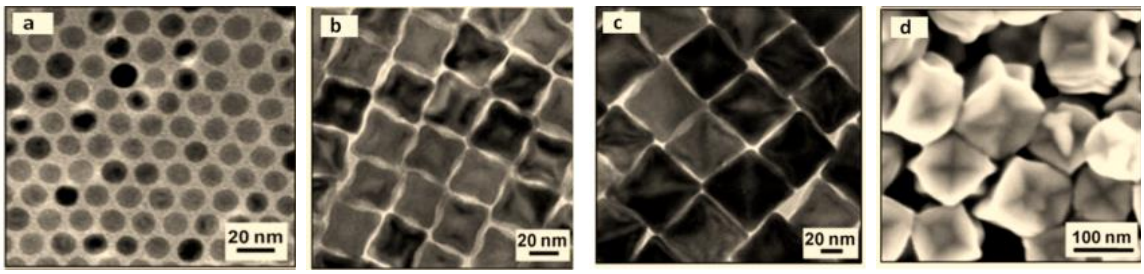

Figure 2.15 TEM images of truncated octahedral FeO NPs with diameter of a) 14nm spherical, b) 32nm cubic, c) 53 nm cubic; d) SEM image of 100 nm truncated octahedral NPs [42].

Two routes are illustrated here as high temperature synthesis methods. Route 1 can produce MNPs up to 100nm[42], and Route 2 is very reliable to generate monodisperse MNPs (up to 40g) in the diameter range of 5-22 nm at large scale [41].

Route 1 [42]:

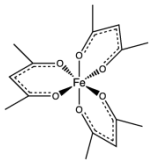

$Fe(acac)_3$ $+ Diphenyl\ ether\ \frac{1,2-hexadecanediol,}{265℃, oleic\ acid, oleylamine}\ Fe_3O_4\ \ MNPs\ (4nm)$ 2-5

$Fe_3O_4\ \ MNPs\ (4nm)\ \frac{further\ decompostion\ of\ Fe(acac)_3}{Fe_3O_4\ \ MNPs\ (4nm)\ growth}\ Fe_3O_4\ \ MNPs\ (20-160\ nm)$ 2-6

Or

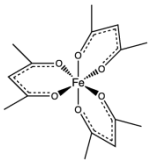

$Fe(acac)_3$ $\frac{265℃, oleic\ acid, oleylamine}{265℃, oleic\ acid, oleylamine}\ small\ FeO\ \ MNPs$ 2-7

$small\ FeO\ \ MNPs\ \frac{further\ decompostion\ of\ Fe(acac)_3}{FeO\ NPs\ growth}\ large\ FeO\ \ MNPs$ 2-8

Route 2 [41]:

$FeCl_3 \cdot 6H_2O + \ sodium\ oleate\ \frac{ethanol, water, hexane}{70℃}$ Fe − oleate complex 2-9

Fe − oleate complex $\frac{high-boiling-point\ solvent}{300℃\ thermal\ decompostion}\ iron\ oxide\ \ NPs$ 2-10

Most of the magnetic nanoparticles synthesized via high temperature method exhibit diameters smaller than 25nm, which are of interest in most MNPs studies. Fe_3O_4 nanoparticles with diameter range of 200~800nm can also been prepared via high temperature method via a modified reduction reaction of $FeCl_3$ and ethylene glycol in a hydrothermal system.[44] In this process, $FeCl_3$ was first dissolved in ethylene glycol, then

sodium acetate and poly(ethylene glycol) were added, stirred and heated to 190°C for 24 h. This process could produce ferrite spherical products with diameter of 200~800 nm with a narrow size distribution (Figure 2.16).

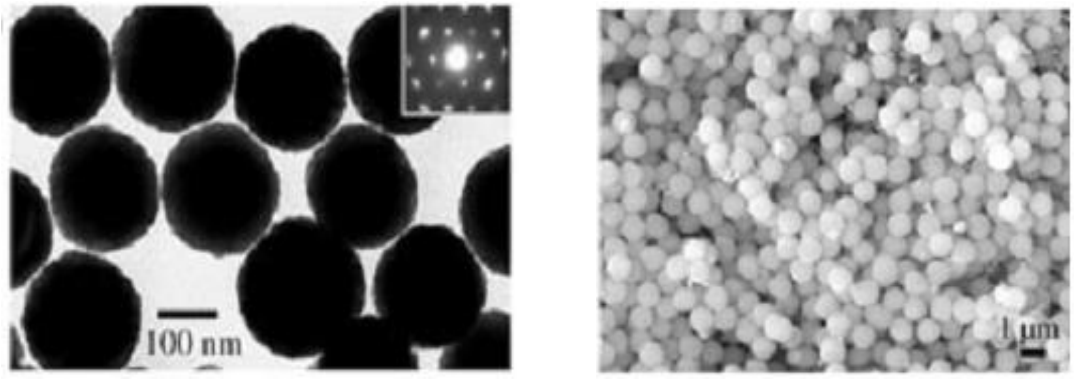

Figure 2.16 TEM image (left) and SEM image (right) of Fe_3O_4 MNPs synthesized via high temperature method [44].

2.3.2.2 Co-precipitation Method

Co-precipitation is the most commonly employed method to synthesize MNPs for magnetic fiber applications. Stone et al [38] have wet spun sodium alginate magnetic fibers with Fe_3O_4 MNPs produced via co-precipitation, in which the diameter of MNPs was 10nm with a size of 196 nm for agglomerated MNPs clusters in the fiber. Shan et al [21] have synthesized Fe_3O_4 MNPs encapsulated in PLLA shell via one-step modified co-precipitation method, aiming to obtain a uniform MNPs suspension solution in an easy way. In Shan's synthesis, PLLA-TFE solution was added into Fe^{3+}/Fe^{2+} mixture, and the final Fe_3O_4–PLLA MNPs had an overall diameter of 100~200 nm. These MNPs were electro-spun into magnetic poly(L-lactide) (PLLA) nanofibers products.

In co-precipitation process, the size and shape of MNPs are controlled by reaction parameters such as pH, ionic concentration, temperature, ratio of ferrous and ferric

hydroxide, and salt species. There are two commonly applied synthesis routes: 1) partially oxidizing ferrous hydroxide, 2) aging ferrous and ferric hydroxides in solution with stoichiometric mixing ratio (Equation 2-11). The optimized reaction condition[45] for the latter route is with pH value of 8~14 and Fe^{3+}/Fe^{2+} ratio of 2:1 (Figure 2.17).

$$2Fe^{3+} + Fe^{2+} + 8OH^{-} \rightarrow Fe_3O_4 + 4H_2O \qquad 2\text{-}11$$

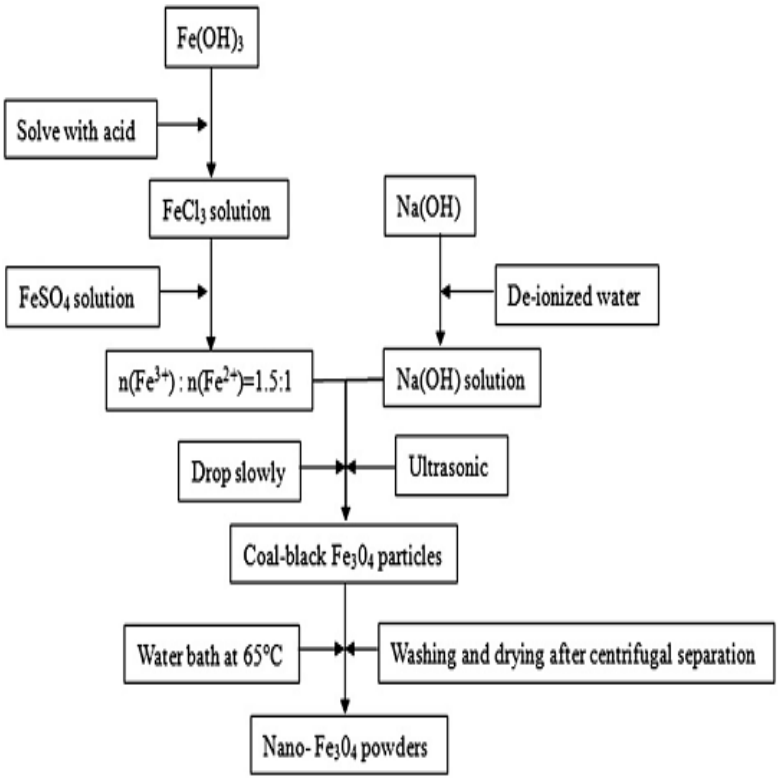

Figure 2.17 A typical route for Fe_3O_4 MNPs synthesis via co-precipitation method [46].

2.3.2.3 Micro-emulsion Method

With micro-emulsion synthesis, MNPs are generated at the interface of water and oil phases of the solution. The micro-emulsion has two reaction systems: oil-in-water system and water-in-oil system. In water-in-oil systems, water is the disperse phase containing metal ions, and oil is the continuous phase enclosing precipitating agents. When

the reaction is initiated, each water nanodroplet behaves as a nanoreactor where MNPs grows on the oil-water interface. To achieve a stable dispersion for reaction, amphiphilic surfactants are usually added to form an interfacial film between water and oil phases to lower the surface energy difference. The size of produced MNPs is controlled by the concentration of reactant, volume ratio of water droplet and surfactants, as well as reaction conditions including temperature, reaction time, and gas environment.[43] Once the MNPs are formed, further coating and function-group can be added with surfactants. One example of Fe_3O_4 MNPs synthesized via micro-emulsion is shown in Figure 2.18. [43]

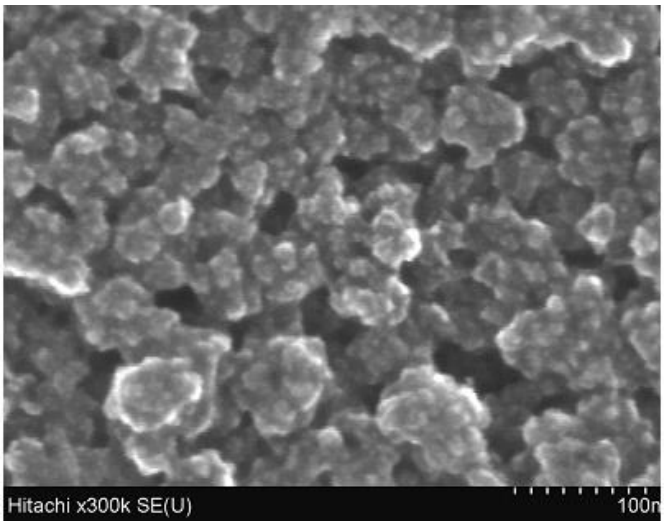

Figure 2.18 SEM image of Fe_3O_4 magnetite nanoparticles synthesized via micro-emulsion method [43].

2.3.3 Fe_3O_4 MNPs

2.3.3.1 Introduction

Compared to other MNPs, Fe_3O_4 MNPs offer a variety of choices in sizes, shapes,[47] and surface properties[21,26,48], and Fe_3O_4 MNPs have also been manufactured at industrial scale with a reasonable cost. Fe_3O_4 MNPs are also recognized as being more stable than

other MNPs at room temperature. With such benefits, Fe_3O_4 MNPs have been utilized in diverse applications, including magnetic resonance imaging (MRI) [49], drug delivery[50], separation of metals[51], microwave absorption[47], as a shape memory material [52], and for data storage media[53].

Fe_3O_4 MNPs are the most commonly used MNPs in magnetic fiber applications, in which most are superparamagnetic (SPM) Fe_3O_4 MNPs with diameters less than 30 nm. Fe_3O_4 SPM MNPs have been electro-spun into polymer matrix such as polyacrylonitrile (PAN)[30,32], poly(L-lacitide) (PLLA)[8], polyvinylpyrrolidone (PVP)[9], poly(vinyl alcohol) (PVOH)[54], poly(ethylene oxide) (PEO)[55], and poly(ethylene terephthalate) (PET)[56]. Fe_3O_4 MNPs have also been (dry-jet) wet spun into magnetic fibers of cellulose[57], alginate[38], and PAN[32].

With all the prior art, Fe_3O_4 MNPs have been chosen as the MNPs for this study. To explore the effects of MNPs on fiber structure and properties, two species of Fe_3O_4 MPs have been employed: 1) 20 nm Fe_3O_4 MNPs with superparamagnetic performance; 2) 80nm Fe_3O_4 MNPs with ferrimagnetic performance.

2.3.3.2 Characterization

Fe_3O_4 MNPs exhibit SPM performance when particle diameter is less than 30 nm[32], and show ferrimagnetism (FM) when the particle diameter is larger than 30 nm. Magnetic hysteresis loops of the MNPs in this study are included in the results sections.

The crystal structure of Fe_3O_4 MNPs can be studied through WAXD analysis, and a typical Fe_3O_4 MNPs pattern is shown in Figure 2.19 (ICDD PDF reference number of 00-019-0629).

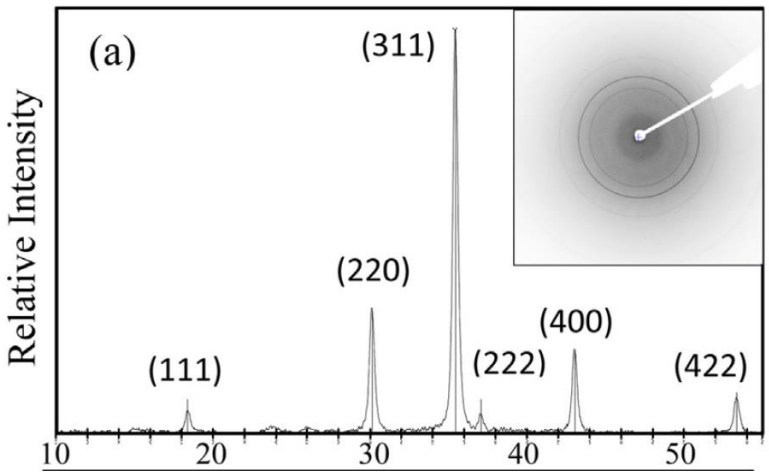

Figure 2.19 WAXD results of superparamagnetic Fe_3O_4 MNPs with diameter of 10-15nm [32].

The thermostability of Fe_3O_4 MNPs can be studied by TGA in air or nitrogen environment (Figure 2.20). In TGA degradation, Fe_3O_4 MNPs decompose from Fe_3O_4 to Fe_3C when annealed in nitrogen environment, while oxidized to Fe_2O_3 in an air environment.[32]

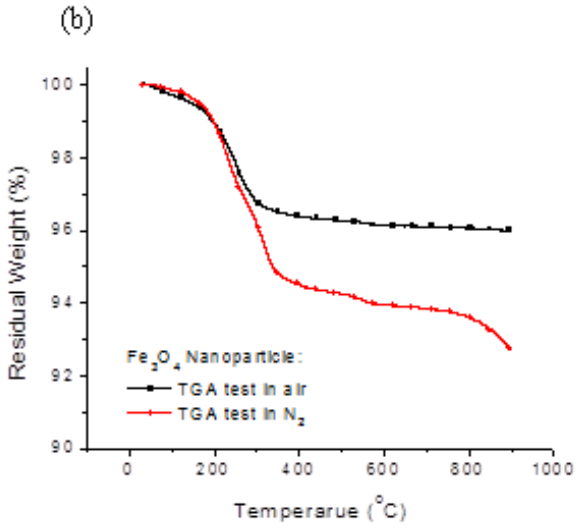

Figure 2.20 TGA graph of Fe_3O_4 MNPs in air and nitrogen environment from room temperature to 900°C with heating rate of 5°C/min [32].

2.4 Fiber System

2.4.1 Introduction

Magnetic fiber system of polymer-MNPs that the author has discussed so far belong to the category of synthetic fibers. Generally, there are two types of fibers in the world: synthetic fibers and natural-based fibers. Synthetic fibers refer to the ones made from synthetic polymers or small molecules. Synthetic fibers occupy more than half of the overall global fiber market, with the advantages of long durability, good tensile strength, design flexibility, and high production rate.

2.4.2 Fiber Synthesis Methods

Synthetic fibers can be produced via four spinning techniques: melt spinning, dry spinning, wet spinning, and electro spinning. A general comparison of these four techniques are included in **Table 2.3**.

In a generic flow chart of fiber spinning (Figure 2.21), polymer solution or polymer melt at a proper viscosity is first prepared, then this polymer suspension is pushed through a metering gear pump and filters, being extruded from spinneret holes into air or liquid phase to form fiber shape, and this fiber shape is maintained as the polymer melt cools down in air or the solvents in polymer solution evaporate/diffuse out. Sometimes post treatments such as drawing are performed to improve fiber crystallinity and mechanical performance.

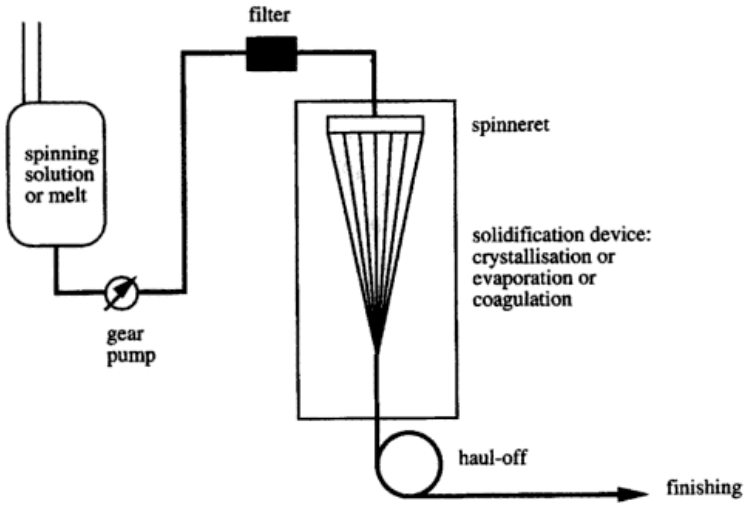

Figure 2.21 Generic graph of fiber spinning process [58].

Table 2.3 Synthesis methods of fibers.

Processing	Requirements for polymers	Solidification mechanism	Production rate (m/min)
Melt-spinning	Melt before degradation	• Solidification and crystallization during cooling, • initial molecular entanglements	4000-10 000
Dry-spinning	Can be dissolved in specific solution with proper elastic-viscosity	• Solvent evaporation • initial molecular entanglements	200-800
Wet-spinning	Can be dissolved in specific solution with proper elastic-viscosity	• Diffusion or reaction • initial molecular entanglements	45-150
Dry-jet Wet Spinning (Gel-spinning)	Can be dissolved in specific solution forming gel state	• Solvent evaporation in gas • Coagulation or reaction in liquid • initial molecular entanglements	Similar to wet spinning
Electro-spinning	Can be dissolved in specific solution with proper elastic-viscosity	• Solvent evaporation • initial molecular entanglements	Mostly nanoscale

2.4.2.1 Melt Spinning

Melt spinning[58] is a preferred method for fiber production when polymer raw materials can be melted without degradation. In a melt spinning process (Figure 2.22), polymer granules are dried and melted in an extruder, led through metering pumps and filters, extruded through spinneret, and finally forming fiber shape with crystallization by passing through a cooling air gap. Fiber strength are initially obtained as the winding-up speed was higher than extrusion speed, during which fiber chains are stretched between entanglement points to form aligned crystal-like regions (Figure 2.23). Further mechanical strength can be achieved via post-drawing. The air flow of solidification step in melt spinning plays an important role in fiber properties, as it determines solvent evaporation rate and polymer crystallization condition. A lot of work has been done exploring the melt-spinning process[59,60], such as nucleation, primary crystallization, spindle mode, but is beyond the interest of this study.

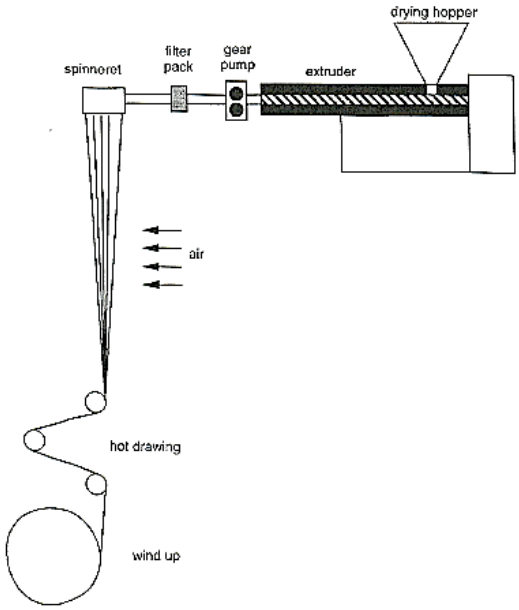

Figure 2.22 Schematic demonstration of melt spinning process [58].

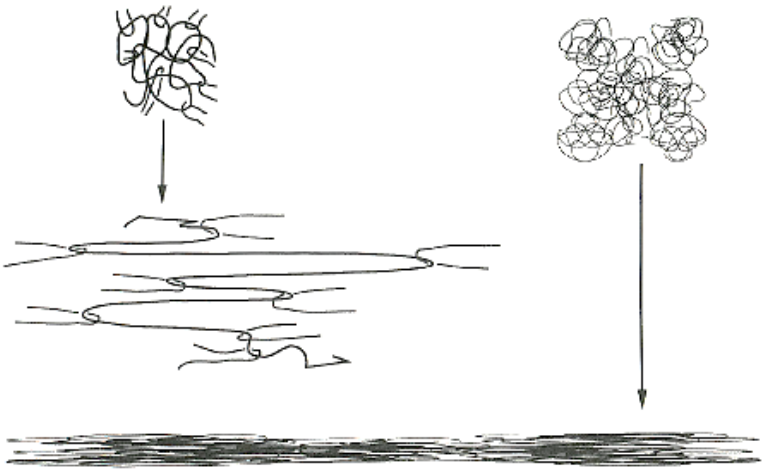

Figure 2.23 Schematic graph of the deformation effect on local structure of polymer chains in melt spinning process [58].

2.4.2.2 Dry/Wet Spinning

When a polymer exhibits a lower decomposition temperature than its melting temperature, fibers cannot be produced via melt-spinning. Under this circumstance, dry spinning and wet spinning are utilized to produce fibers. Polymers are dissolved in liquid solvent, then spun to form a fiber shape at temperatures lower than polymer decomposition temperature, solidified via solvent removal, and finally drawn to achieve proper fiber strength. According to the solvent removal process, the spinning technique is divided into dry spinning and wet spinning.

In dry spinning (Figure 2.24), the polymer solution is extruded from spinneret holes into a chamber with hot gas circulation, and solvent is removed through solvent evaporation in the gas flow. The dry spinning production rate can be as high as 500-1000 m/min and is much higher than wet spinning process.[61]

In wet spinning [62], polymer solution is extruded into a liquid coagulation bath with a spinneret immersed inside the liquid phase. As fibers travel through the coagulation bath, the solvents in polymer gel diffuses out leaving the polymers alone to form intermolecular and

intramolecular bonding. The polymer gel gradually becomes a nascent fiber with sufficient mechanical strength for handling, and by the time fibers are wound onto the collection rollers, polymers have formed a cross-linked structure with little solvent left in-between. There are many parameters to be adjusted to achieve the optimized condition in wet spinning, including coagulation chemicals, coagulation bath temperature, coagulation residence time, and winding speed.[32]. The coagulation process of wet spinning follows Fick's diffusion law, and this process is a critical step in the wet spinning process, as it determines the initial fiber structure such as porosity and potential for drawing.[58] Compared to dry spinning, it is easier to control fiber structure and performance with wet spinning, as it is a gentler and slower process.

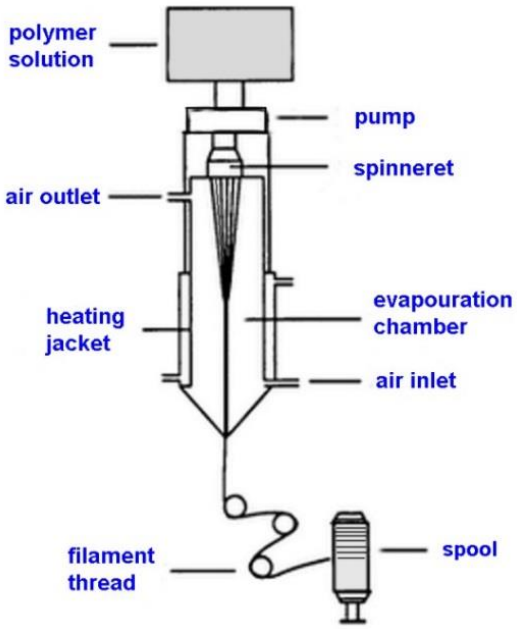

Figure 2.24 Schematic graph of dry spinning process [63].

2.4.2.3 Dry-jet Wet Spinning

Dry-jet wet spinning, also known as gel spinning, can produce fibers with high mechanical performance. Dry-jet wet spinning is similar to wet spinning, except that the spinneret tip (Figure 2.25) is placed slightly above the coagulation bath rather than being immersed in the bath. In dry-

jet wet spinning, the spinning dope passes through an air gap before entering the liquid coagulation bath once extruded. This air gap allows the polymer solution to release the stress of passing through the tiny spinneret hole as a non-Newtonian fluid before entering the coagulation bath, and thus, reduces the formation of voids and defects in fiber structure.

Dry-jet wet spun fibers tend to have a more uniform and dense structure, which benefits the fiber mechanical performance with higher draw ratio and higher crystallinity.[58] Spinning dope with a lower polymer concentration is allowed in dry-jet wet spinning, as compared to other fiber production methods, and this low polymer concentration results in fewer polymer entanglements, which allows fibers to be elongated further, or drawn to a higher ratio, with high crystallinity and improved mechanical strength. Furthermore, the dry-jet wet spinning technique maintains the high production rate from dry spinning and combines this with the benefits of controllable fiber properties from wet spinning.[61] Therefore, dry-jet wet spinning appears to be an attractive technique to produce high-strength fibers for commercial applications. More discussion about dry-jet wet spinning parameters is included in Section 2.4.3.4 for the production of PVOH fibers via dry-jet wet spinning technique.

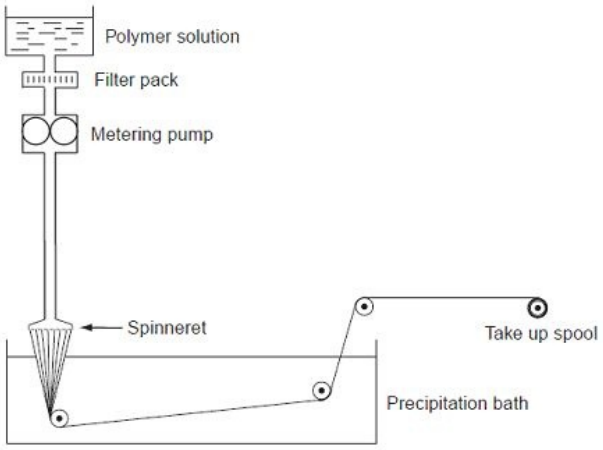

Figure 2.25 Schematic graph of dry-jet wet spinning process [64].

2.4.2.4 Electro Spinning

Electro spinning has a similar fiber production process to dry spinning except that an electrical field is used as the driving force to form fibers (Figure 2.26). Continuous fine strings of polymer gel are pulled out of a spinneret tip under the combined force of columbic repulsion and surface tension of the spinning solution, then fibers are solidified through solvent evaporation while travelling to the collector, and finally collected on the substrate. Compared to other fiber fabrication methods, electro-spinning usually does not require high temperature or a coagulation bath.

The advantage of electro spinning over other processes is that it allows for the creation of fibers with very fine diameters even at nanoscale fiber diameters. Nanofibers have become a popular topic among material scientists and researchers, because nanofibers offer unique benefits such as high porosity and large surface-to-volume ratio. Nanofibers have shown potential in various applications including uses as filters, semiconductors, composites, and ceramics.[35] However, when fabricating nanofibers electro-spinning is not as well-developed as other fiber fabrication methods, an electro-spinning still has a long way to go before it can be competitive at the production volume, rate, and cost as compared to other fiber fabrication methods.

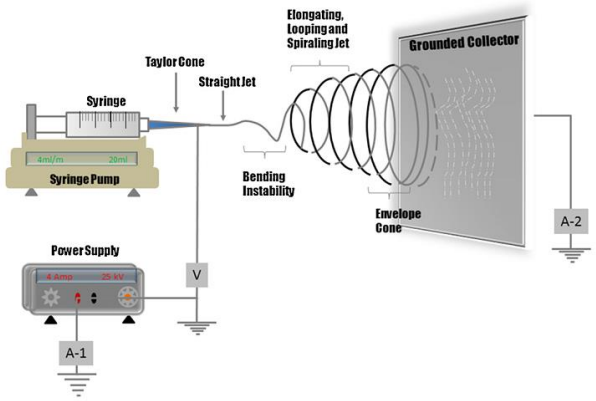

Figure 2.26 Schematic diagram of electro-spinning process [65].

2.4.3 PVOH Fibers

2.4.3.1 Introduction

Polyvinyl alcohol (PVOH) (Figure 2.27) is a polymer with simple structure: carbon backbone, $–CH_2$ and –OH function groups, which are commonly seen in polymer structures. This makes it possible to extend the research findings of PVOH polymers to many other polymer systems.

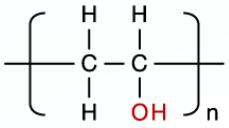

Figure 2.27 Chemical structure of poly(vinyl alcohol) polymer.

PVOH fiber is one of the most commercialized synthetic fibers in the world with many attractive properties such as high chemical resistance, high tensile strength, and human biocompatibility. PVOH fibers have been utilized in various applications including ropes, fishing nets, reinforcement materials in cement products, as well as a rubber material.

As the decomposition temperature of PVOH polymer is lower than its melting point, PVOH fibers cannot be fabricated via melt spinning techniques. Therefore, PVOH fibers are manufactured with a wet spinning process by industry. In recent years, dry-jet wet spinning has been developed successfully to generate PVOH fibers with robust mechanical properties.[32]

2.4.3.2 Application with Nanofillers

PVOH polymers have been utilized to produce functional fibers with various filler species embedded, including carbon nanotubes[66], soy protein [67], lignin[68], and silicon oxide[69]. It is found that a small amount of nanofillers could reinforce fibers for a better mechanical strength.[66,70] Most of these PVOH-filler fibers are produced via electro-spinning technique at laboratory scale, but

since dry-jet wet spinning is the selected method in this study, this section will mainly focus on the studies pursued with (dry-jet) wet spinning technique.

Carbon nanotubes (CNTs) are popular additives to PVOH fibers. A small amount of CNTs can improve PVOH fiber mechanical strength, as the uniform interface of nanotubes and PVOH benefits the pressure transfer inside the material. In one study, PVOH fibers were dry-jet wet spun with 0.3%wt single wall CNTs loading, and the final fibers exhibited a tenacity of 2.2 GPa compared to 1.7 GPa for corresponding pure PVOH fibers (Figure 2.28). [66] This tenacity value of PVOH-CNTs fibers (2.2 GPa) is considered very high compared to commercial grade PVOH fibers. In another study, Mercader successfully wet spun PVOH fibers with a high CNTs loading of 13 %wt, which was achieved by the introduction of nonionic surfactant into the spinning dope, $C_{18}H_{37}(OCH_2CH_2)_{20}OH$) (Brij® 78). This surfactant had a structure of hydrophobic-head and hydrophilic-tail, which greatly reduced the nanoparticle agglomeration and kept the solution homogeneous.[70]

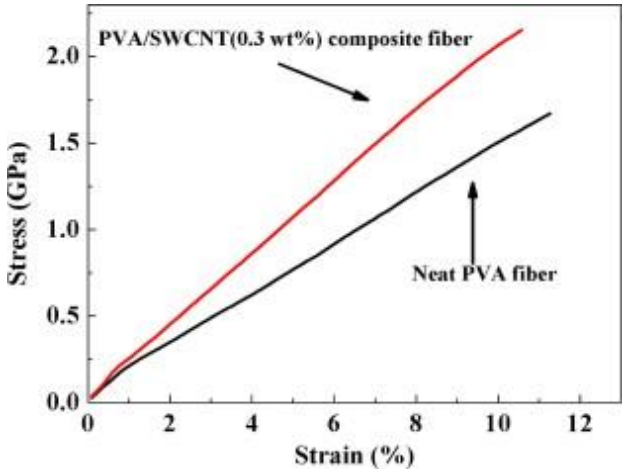

Figure 2.28 Tensile curves of pure PVOH fiber and PVOH/SWCNT fiber with SWCNT loading of 0.3%wt [66].

PVOH fibers have also been spun with SiO_2 nanoparticles embedded, forming a material that is biodegradable in body fluid for medical application. In one research, PVOH fibers were produced with 3%wt SiO_2 nanoparticle (particle diameter of 60-100 nm), and the fiber characterization presented a negative effect of particles on fiber strength and crystallinity. [69] The reason was not well explained in the study, and it could be due to agglomeration of the nanoparticles.

Another filler group for PVOH fibers are soy protein particles. In one study exploring the impact of soy protein particles ratio on fiber mechanical performance, the highest mechanical strength and thermal stability was achieved at 70%wt PVOH and 30%wt soy protein (Figure 2.29). Results of this study indicated that the crosslinking and hydrogen bonding between soy protein particles and PVOH polymer hydroxyl groups reached the maximum value at this ratio. When the soy protein particle loading grew even higher (e.g. > 30%wt), fibers exhibited porous structure and ended up with descending tensile strength and poor thermal stability. [67]

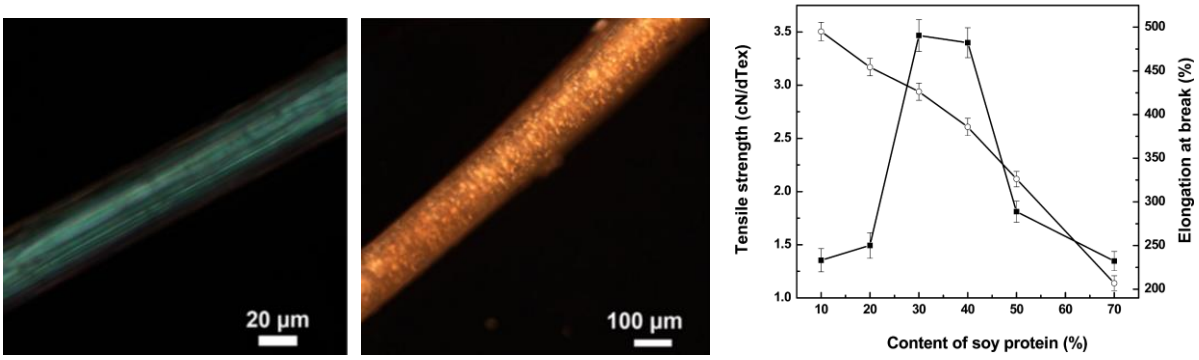

Figure 2.29 Polarized optical microscope images of pure PVOH fiber (left), PVOH fiber with 80%wt soy protein embedded (middle); Tensile strength (●) and elongation at break (○) of PVOH/soy protein blend fibers against soy protein concentration (right) [67].

2.4.3.3 Application with MNPs

Some researchers have examined electro-spinning processes utilizing PVOH with Fe_3O_4 nanoparticles to generate superparamagnetic nanofibers.[55]

In one study[71], poly(ethylene oxide) (PEO) was used as polymer shell for Fe_3O_4 nanoparticles in the PVOH spinning solution, in which PEO helped to maintain a uniform polymer-MNPs suspension. The TEM image of the final magnetic nanofiber is shown in Figure 2.30, in which MNPs lined up along fiber axis, possibly due to the magnetic coupling effect between MNPs. The saturated magnetization of this magnetic fiber was 7 emu/g, which was much lower than 45-55 emu/g for its corresponding bare Fe_3O_4 MNPs.

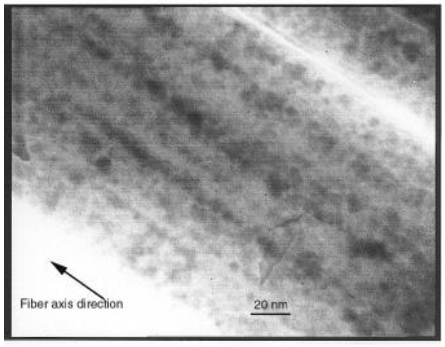

Figure 2.30 TEM of PVOH fibers with 8 %wt superparamagnetic Fe_3O_4 MNPs [55].

In another study, magnetic PVOH-Fe_3O_4 fibers were produced via wet spinning with a high MNPs loading of 23%wt. The saturation magnetization value of the final magnetic fiber product reached 13.38 emu/g. This study utilized a novel production method, wherein MNPs were synthesized directly in situ within PVOH spinning dope (Figure 2.31). The structure of final magnetic fiber was very porous (Figure 2.31) with breaking strength of 14- 48 MPa, while the breaking strength of pure PVOH fibers prepared in the same process was 48 MPa.[33] The tensile strength of pure PVOH fibers produced via wet spinning process can exhibit 1-1.6 GPa.[30]

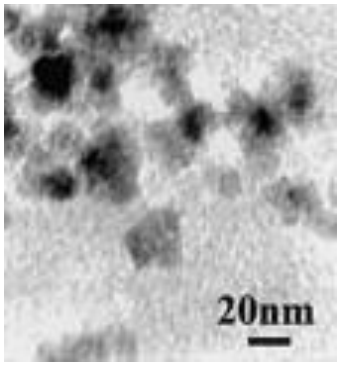

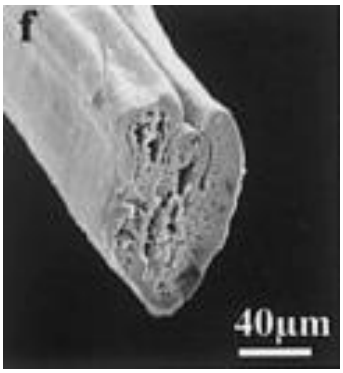

Figure 2.31 TEM of Fe_3O_4 magnetic particles synthesized in situ within PVOH solution at pH 12.01 (left); SEM of PVOH fibers containing 17.63%wt Fe ion nanoparticles synthesized through in situ method [33] (equals to 23%wt Fe_3O_4 loading) (right).

2.4.3.4 Dry-jet Wet Spinning PVOH Fibers

In this study, dry-jet wet spinning is selected as the PVOH magnetic fiber formation method, mainly because it could generate single fibers with good mechanical performance. The process of dry-jet wet spinning PVOH fibers and its effects on fiber structure are illustrated in detail below, which includes polymer raw materials, solvent system, dissolving condition, spinning process, coagulation bath, and post-treatments.

Raw Material

PVOH polymers, the raw materials used in fiber spinning, are usually synthesized via poly(vinyl acetate) hydrolysis (Equation 2-12).[72] PVOH polymers with high polymerization degree and high hydrolysis degree are preferred in fiber fabrication, as they can provide good mechanical properties for fibers.

$$[CH_2CH(OAc)]_n + C_2H_5OH \rightarrow [CH_2CH(OH)]_n + C_2H_5OAc \qquad 2\text{-}12$$

The hydrolysis degree of PVOH polymers, which is the percentage of acetate sites converted into hydroxyl groups, has a large impact on final fiber properties. A high degree of

hydrolysis frees a lot of hydroxyl sites, which could form hydrogen bonds between polymer chains, allowing fibers to achieve high crystallinity, strong tensile strength, and good solvent resistance. Industrialized PVOH fibers are typically made at two hydrolysis level: partially hydrolyzed (87-89%) and fully hydrolyzed (98%-99%). The tensile strength of PVOH fibers made in the partially hydrolyed level range from is 24-79 MPa, while PVOH fibers made in the fully hydrolyzed level range from 67-110 MPa.

The molecular weight of raw PVOH polymers also plays an important role in final fiber product performance. A higher polymerization degree provides extensive opportunities for polymer cross-chain entanglements, and thus results in outstanding crystallinity and tensile properties upon drawing. The molecular weight of PVOH polymer (M_w) used in industry ranges between 26,300 Da and 30,000 Da.

Spinning Dope

Dissolving is the first step in fiber dry-jet wet spinning process. PVOH polymers exhibit good solvent resistance because of strong intra- and intermolecular hydrogen bonding. Thus, PVOH is only dissolvable in highly polar solvents, such as water, dimethyl sulfoxide (DMSO), acetamide, and glycol. Typically, in industry, PVOH is dissolved in water with a polymer concentration of 10-20 %wt in spinning dope. At laboratory scale, other solvent systems are also used such as DMSO and DMSO-Water.[72] The highest tensile strength of PVOH fibers found in literature was 2.8 GPa with a Young's Modulus of 64 GPa, which fiber was fabricated via dry-jet spinning from the solvent system of DMSO/water (80%vol : 20%vol).[73]

The dissolving condition of PVOH polymers is determined by the hydrolysis degree and polymerization degree of polymer raw material. PVOH polymers with low hydrolysis of 70-80% can be dissolved in water at 10-40°C, while fully hydrolyzed PVOH polymer of 98-99% can only

be dissolved in water above 80°C. As seen in Figure 2.32, the larger the polymer molecular weight, the higher the dissolving temperature required. To prevent agglomeration, good agitation is necessary through the whole dissolving process.[74]

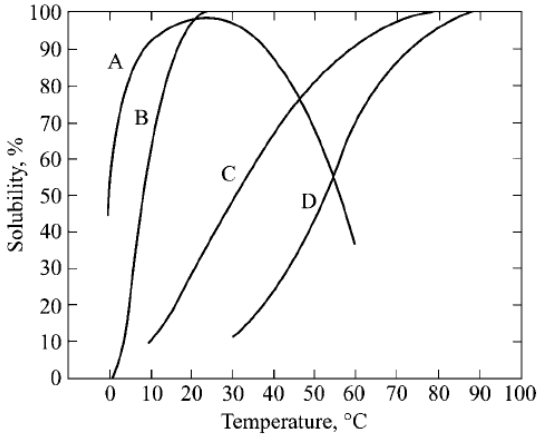

Figure 2.32 Water solubility of PVOH polymers: A, 78-81% hydrolyzed, degree of polymerization (DP)= 2000-2100; B, 87-89% hydrolyzed, DP= 500-600; C, 98-99% hydrolyzed, DP= 500-600; D, 98-99% hydrolyzed, DP= 1700-1800.

Another critical factor in the spinning solution is the polymer concentration. Fibers could possibly be formed via extrusion when the number of polymer entanglement is sufficient in solution. As shown in Figure 2.33, polymer chains start to interact with each other once the concentration reaches the polymer critical entanglement concentration (c^*). The value of c^* can be calculated according to the configuration of the polymer coil (radius of gyration, R_g). Once solution concentration exceeds c^*, Rg decreases as the polymer concentration increases until the concentration reaches the concentration above which Rg is constant and independent from polymer concentrations. The entanglement of polymers in spinning solution can be characterized as the viscosity of the solution (Figure 2.34). The higher the polymer concentration is, the greater the viscosity is, and the more polymer entanglements there are among polymer chains.[72]

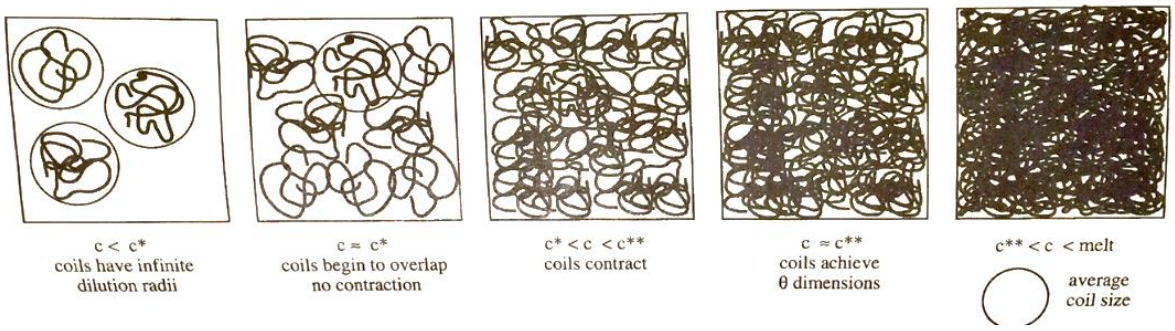

Figure 2.33 Interaction of polymer coils as polymer concentration increases from dilute solution (left) to melt (right) [58].

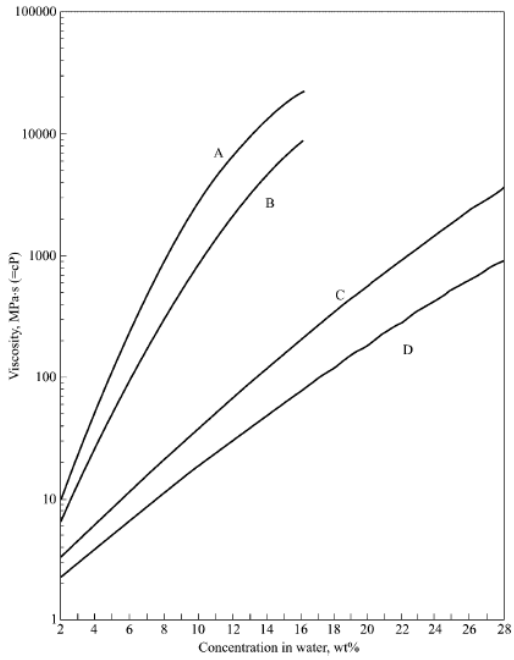

Figure 2.34 Solution viscosity against polymer concentration for 87-89% hydrolyzed PVOH polymer in water system at 20°C, the degree of polymerization for each curve is: A, 2200; B, 1500; C, 550; D, 220 [72].

The optimal polymer concentration for fiber spinning is achieved when the final fiber products exhibit the desired mechanical performance. A high concentration provides uniform and dense fiber microstructure, while low concentration allows fibers to be drawn to a higher crystallinity. As illustrated in Figure 2.35, the highest tensile strength and Young's modulus of

PVOH fibers is achieved at concentration of 6%wt in the solvent system of DMSO/Water (80%vol : 20%vol)[73], at which fibers displayed an optimum combination of uniform fiber structure and high draw-ability.

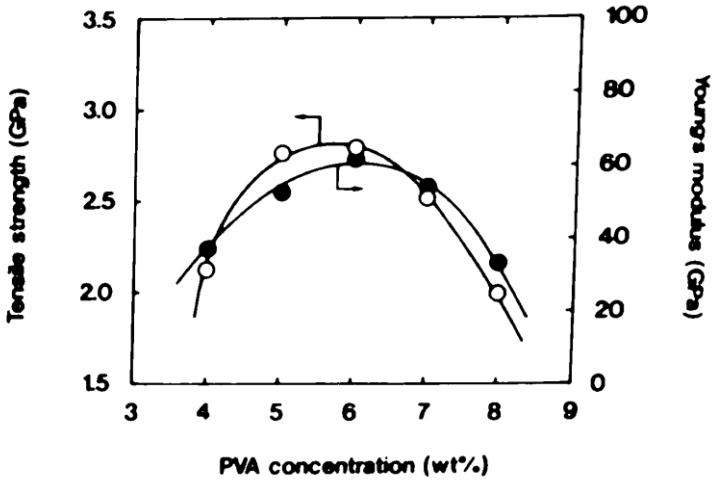

Figure 2.35 Tensile strength and Young's modulus of PVOH fibers produced from solvent system of DMSO/H_2O=80/20 vol% [73].

Extrusion

In industry, the production rate of PVOH fibers can vary from a hundred meters to thousand meters per minute, and a typical spinneret head has 10000-80000 holes with diameter of 50-150 μm. The diameter of spinneret hole affects the structure of final fibers. Specifically, fibers generated from large spinneret holes has large diameters, and it is more difficult for solvent in fiber core-section to diffuse out during the coagulation step, which could lead to phase separation problem between fiber skin and core and high porosity. Fibers spun from spinneret heads with small holes usually has a more solid and void-less structure with better mechanical performance. However, small spinneret holes require high extrusion pressure from the equipment, which may increase the overall cost of the fiber production.

Coagulation

Coagulation is one of the essential steps in fiber formation, as it has the highest impact on final fiber structure including fiber shape, porosity, crystallinity, thermal properties, and mechanical strength. Methanol has been found to be a good coagulant for PVOH in dry-jet wet spinning to achieve high fiber performance.

One of the key factors in this step is the coagulation bath temperature, which directly affects the solvent diffusion rate and fiber crystallization. The SEM images of PAN fibers from different coagulation temperature (5°C and 60°C) is illustrated here as an example (Figure 2.36).[75] When the bath temperature is too high, coagulating occurs so violently that the fiber skin forms much faster than the core section, which leads to an undesirable fiber with a kidney-shaped cross section that has poor mechanical strength. When the coagulation temperature is too low, fibers cannot be fully solidified through the coagulation bath, which results in a fragile porous structure. The optimal coagulation temperature is achieved when the fiber skin and core solidify at a similar speed, and the final fiber cross-section is a void-free circular shape.

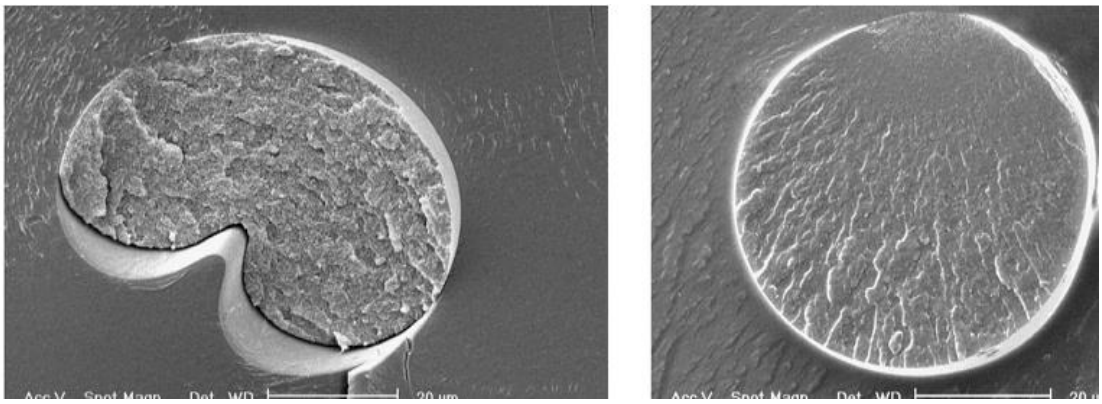

Figure 2.36 Cross-section SEM images of wet spun PAN fiber at different coagulation bath temperature: (Left) at 5°C, (Right) at 60°C [75].

Another important parameter in coagulation process is the residence time of fibers, which refers to the time fiber is held in the coagulation bath before wind-up. The residence time is determined by extrusion speed and coagulation bath length, which has a great influence on nascent

fiber structure. With a fixed coagulation bath length, if the extrusion speed is too fast, there may not be sufficient time for fibers to solidify completely during coagulation. Conversely, if the extrusion speed is too low, the production rate may be reduced unnecessarily. Therefore, a proper extrusion speed must be determined for the optimal fiber structure with the currently available coagulation setup.

Post-treatments

After coagulation, as-spun PVOH fibers still lack adequate fiber properties because most polymer regions are still in amorphous state. Post-drawing is an effective way to increase fiber crystallinity, and thus improve fiber mechanical strength, chemical resistance, and thermal stability.

One-stage or multi-stage drawing is applied at a high temperature slightly below the fiber melting point. The thermal energy provided by high temperature allows polymer chains to reorganize into a more crystalized structure with drawing force. During drawing, amorphous polymer regions are converted into extended chain crystal (ECC) regions, and/or small pieces of crystal regions are combined into larger crystallization zones. For example, the tenacity of pure PVOH was improved from 11 cN/tex for as-spun fibers (Figure 2.37) to 41 cN/tex with a multi-stage drawings (total draw ratio: 7.6).[69] In this study, multi-stage drawing is employed to pursue good fiber mechanical performance.

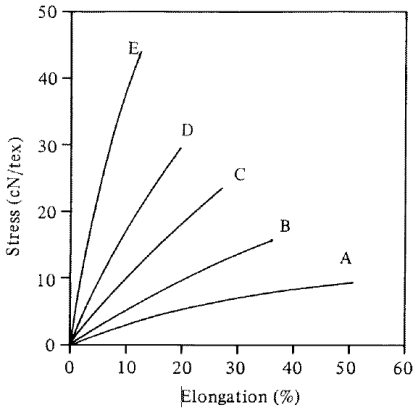

Figure 2.37 Stress-strain curves of wet spinning/multistep drawing of PVOH fibers with draw ratios of as-spun (A), 2.3 (B), 3.4 (C), 5.1 (D), 7.6 (E) [69].

2.4.3.5 Characterization

Morphology

The cross-section morphology of PVOH fibers can be observed via optical microscope, confocal microscope, and Scanning Electron Microscope (SEM). A circular cross-section shape indicates a uniform skin-core formation in coagulation process, while kidney and other shapes may tell different stories about the fiber spinning process.

The MNPs distribution in PVOH fibers can be observed with microscopy as well as with Transmission Electron Microscope (TEM). For TEM analysis, fiber samples need to be cut very thin so that electron beam can pass through.

Crystal Structure

Crystal structure is one of the basic and essential properties of PVOH fibers, as it provides structural information that helps to understand fiber performance related to mechanical strength, thermal stability, and solvent resistance.

WAXD is usually utilized to study fiber crystal structure, including crystallinity, crystal size, and polymer orientation factor. One example of PVOH fiber crystal pattern is shown in Figure

2.38, in which two wide peaks represent amorphous regions (*A)* and narrow peaks refer to crystallized regions. The strongest diffraction pattern peak of PVOH fibers is located at *2θ* angle of 18.0 -21.0°, which corresponds to PVOH 101 crystal phase.[32] It was also found that the index of polymer orientation along the fiber axis can be increased slightly by drawing (Figure 2.38). In one study [69], the index of polymer orientation increased from 0.46 to 0.55 with a draw ratio of 2, and interestingly, the alignment improvement was more apparent when nanoparticles are embedded.

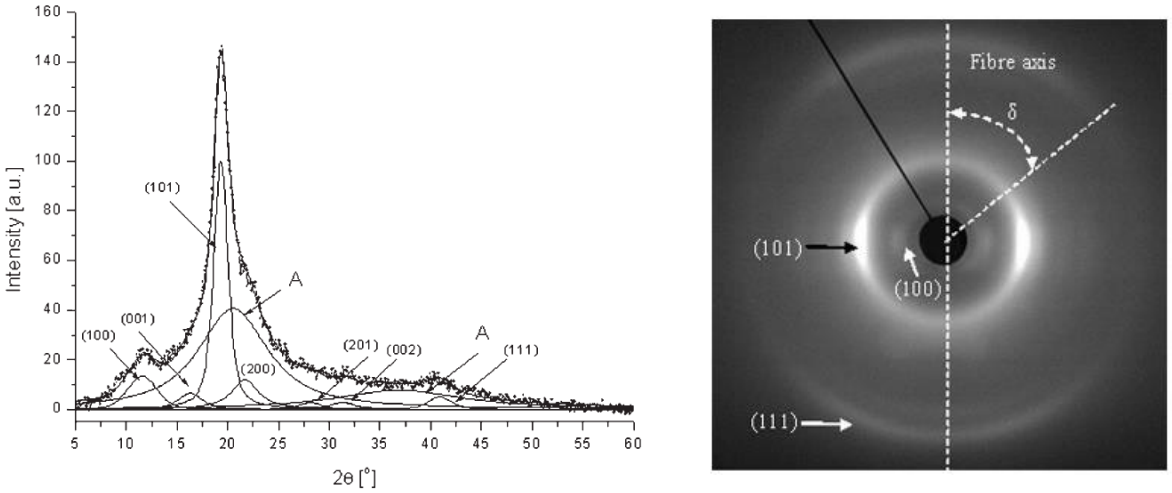

Figure 2.38 XRD pattern of PVOH fiber: 1D Diffraction pattern (left) and 2D diffraction pattern (right) [69].

Generally, fiber structures consist of many semi-crystalline regions, which are known as folded-chain crystal (FCC) sections. In some fibers, there are extended chain crystalline (ECC) regions in the structure which offers higher mechanical strength. PVOH crystal structure has been simulated with two different models: the Bunn and Peiser Model, and the Sakurada Model. In the Bunn Model (Figure 2.39), the lattice parameters of monoclinic PVOH units are a= 7.79 Å, b=5.49 Å, c=2.54 Å, and β=91.7 °, in which *b* refers to the direction along fiber axis.[76]

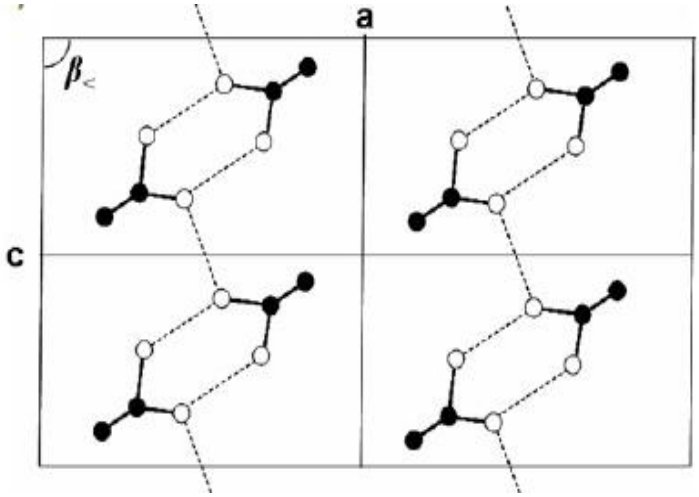

Figure 2.39 Crystal cell model of PVOH polymer with Bunn Model [76].

Thermal Performance

TGA is employed to study the thermostability of PVOH fibers by recording the weight loss in a controlled heating/cooling process. A sample TGA curve of PVOH fibers in nitrogen environment is displayed in Figure 2.40,[77] in which the *x* axis represented the temperature increase, and the *y* axis referred to remaining weight percentage. The thermal decomposition of PVOH occurred generally in three stages[67, 77]: 1st stage at 25- 200°C when the sample weight loss was mainly due to moisture evaporation and solvent volatilization; 2nd stage at 200-300°C when the inter-molecular bonding breaks down, and long polymer chains degrade into shorter ones; 3rd stage at 300-538°C when the PVOH polymer chains further break down and dehydrated into volatile products. The most common decomposition residue of PVOH after TGA process are vinyl alcohol and vinyl acetate copolymers.

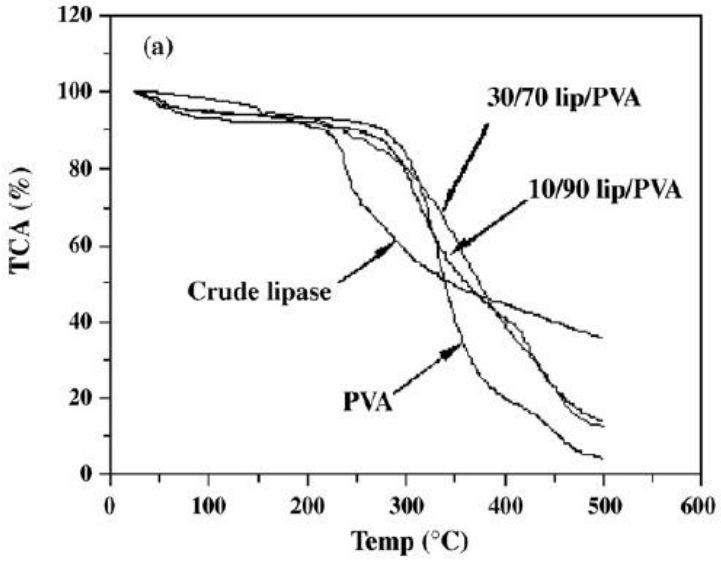

Figure 2.40 TGA graph of PVOH fibers with different ratios of crude lipase [77].

Mechanical Properties

The mechanical properties of fibers are determined by many factors, including the polymer raw materials, spinning system, coagulation condition, and post-treatments. Mechanical properties can be analyzed with a single fiber stress-strain test, and a sample tensile curve is shown in Figure 2.37. Generally, fibers with high crystallinity and few defects exhibit good mechanical performance. Industrial PVOH fibers produced via wet spinning process have been shown to have tensile strengths between 1-1.6 GPa and a tensile module of 10 GPa. PVOH fibers that are produced via dry-jet wet spinning can reach an even higher tensile strength of 3-6 GPa with tensile modulus of 50- 600 GPa.[30]

Magnetic Performance

Pure PVOH fibers fall into the category of diamagnetic materials, which are usually considered as “non-magnetic” material. The diamagnetic effect of PVOH fibers is unobservable

in the external magnetic field, and this magnetic response is much smaller than a paramagnetic or ferromagnetic response.

2.5 This Study

The goal of this research is to produce single magnetic fibers with high MNPs loadings via an industrialized fiber production method. Electro-spinning is the most popular method to fabricate magnetic fibers at laboratory scale, but it is difficult to produce continuous single fibers via this process. Likewise, the MNPs loadings in electro-spun magnetic fibers are usually low, in order to avoid MNPs accumulation on spinneret tip caused by electro-field in fiber spinning step. Furthermore, electro-spinning process faces further challenges including low production rate and higher cost as compared to other fiber production methods at industrial scale.

Therefore, dry-jet wet spinning is explored as the spinning method in this study to achieve the research goal. Dry-jet wet spinning can produce fibers with outstanding mechanical performance. Likewise, it is also possible to achieve higher MNPs loadings with dry-jet wet spinning process, as there is no electro-field involved in the process and the issue of MNPs accumulation from electro-field at high MNPs loading is negated. Dry-jet wet spinning has also been well-developed at industrial scale with a relatively low production cost, which makes it more feasible produce at scale. The research is divided into three sections.

2.5.1 Optimum Spinning Dope for Dry-jet Wet Spinning Magnetic PVOH Fibers

In section 4.1, in order to obtain optimum spinning dope for PVOH-Fe_3O_4 magnetic fibers, multiple spinning solution systems were prepared with polymers of different molecular weights and various solvents. PVOH fibers with 0%wt and 10%wt superparamagnetic Fe_3O_4 MNPs were fabricated and evaluated for fiber performance, including fiber morphology, crystal structure,

thermal properties, mechanical performance, and magnetic performance. The optimum system was selected and utilized in the following sections.

2.5.2 Effects of MNPs Concentration on Magnetic Fiber Performance

In section 4.2, PVOH fibers were produced with the optimum condition determined from section 4.1, with a wide range of superparamagnetic Fe_3O_4 MNPs loading ratios (MNPs 0, 10, 20, 40, and 60%wt, against PVOH polymer weight). The highest MNPs loading achieved for successful fiber production was 60%wt. The effects of MNPs loadings on fiber properties were analyzed for fiber morphology, crystal structure, thermal properties, mechanical performance, and magnetic performance.

2.5.3 Effects of MNPs Species on Fiber Performance at High MNPs Loadings

In section 4.3, magnetic fibers were fabricated with two species of MNPs at 60%wt high loading ratio: superparamagnetic Fe_3O_4 MNPs with diameter of 20nm, and ferrimagnetic Fe_3O_4 MNPs with diameter of 80nm. The magnetic fiber products were compared to understand the effects of MNPs size and magnetism performance on fiber properties, including fiber morphology, crystal structure, thermal properties, mechanical performance, and magnetic performance.

CHAPTER 3 EXPERIMENTS

3.1 Materials

Poly(vinyl alcohol) polymers (PVOH) with two degrees of polymerization were used in this study: 1) high molecular weight PVOH (HM), Mw= 146 000-186 000, Xn= 3 320-4 230, 99+% hydrolyzed, crystal form, purchased from Sigma-Aldrich; 2) low molecular weight PVOH (LM), Mw= 89 000-98 000, Xn= 2000-2200, 99+% hydrolyzed, fine powder form, purchased from Sigma Aldrich.

Two types of magnetic nanoparticles were utilized: 1) superparamagnetic Fe_3O_4 iron oxide black spherical nanopowder with diameter of 20-30 nm (>98%), purchased from SkySpring Nanomaterials Inc; 2) ferromagnetic Fe_3O_4 iron oxide black spherical nanopowder with diameter of 80nm (>99.5%), purchased from Nanoshel Company.

The organic solvent dimethyl sulfoxide (DMSO) was purchased from Sigma-Aldrich, with purity of >99.5%, while methanol was purchased from BDH Chemicals.

All materials were used as received without further treatments.

3.2 Procedure

3.2.1 Preparation of Spinning Dope

The spinning dopes of pure PVOH fibers are listed in Table 3.1. The spinning dope of low molecular weight PVOH polymers with water solvent (LM-H_2O) was prepared in three steps: 1) make 5 g/dl polymer solution by dissolving PVOH powders in DI water while stirring at 85- 90°C for 0.5h; 2) increase PVOH concentration to 20 g/dl by gradually adding PVOH powder into the solution in step 1 while stirring at 85-90°C; and 3) mix the solution well by stirring for another 2 hours. The spinning dope of LM-DMSO with DMSO solvent was prepared with the same

procedure as the LM-H_2O solution, except the solvent system was changed from water to DMSO. The last spinning dope of HM-DMSO was prepared following the same steps as described above, but with DMSO solvent and a final PVOH concentration of 10 g/dl. Good agitation was maintained throughout the entire process to prevent clumping.

Table 3.1 Spinning dopes of pure polymer fibers.

Spinning dope	Polymer	Solvent	Concentration (g/dl)
LM-H_2O	LM PVOH	DI water	20
LM-DMSO	LM PVOH	DMSO	20
HM-DMSO	HM PVOH	DMSO	10

For magnetic fibers, PVOH spinning dopes were prepared with LM/ HM PVOH polymers in water or DMSO solvent at various loadings of 20nm superparamagnetic Fe_3O_4 MNPs. Another species of MNPs, 80nm ferromagnetic Fe_3O_4 MNPs, was also integrated in magnetic fibers at the MNPs concentration of 60%wt. The spinning dopes of magnetic fibers were summarized in Table 3.2.

The preparation of magnetic fiber spinning dopes with DMSO solvent is listed as below. First, multiple samples of 200mg MNPs were dispersed in 300ml DMSO, and the samples were placed in a sonication bath overnight to obtain a homogenous phase. Separately, PVOH solution in DMSO was prepared at the concentration of 0.33-1.8 g/dl based on the needs of MNPs loading ratio in final fiber system. Then, two solutions, MNP-DMSO solution and PVOH-DMSO solution, were mixed together based on desired MNPs ratio and sonicated at 80°C for 4 hours. Finally, this blended solution was concentrated with rotatory evaporator to extract excessive DMSO solvent until the solution reached spinnable viscosity range. The solution viscosity of final spinning dopes was controlled between 5000 and 6000 cP at temperature of 60°C, which viscosity range was

verified in experiment trials with the capability to produce magnetic fibers with adequate mechanical strength via current dry-jet wet spinning setup. The viscosity was measured with Brookfield Ametek Lvdve115 viscometer equipped with spindle S63 at 50 rpm, and the readings were taken at 15s after the test started.

For magnetic fiber spinning dopes with DI water (LM-H_2O-10%MNPs), the preparation procedure was the same as that with DMSO solvent, except that the PVOH polymers and MNPs were dispersed in DI water.

Table 3.2 Spinning dopes of magnetic fibers.

Spinning dope	Polymer	Solvent	Fe_3O_4 MNPs size (nm)	MNPs loading * (%wt)
LM-H_2O-10%MNPs	Low HM	Water	20-30	10
LM-10%MNPs	Low HM	DMSO	20-30	10
HM-10%MNPs	High HM	DMSO	20-30	10
HM-20%MNPs	High HM	DMSO	20-30	20
HM-40%MNPs	High HM	DMSO	20-30	40
HM-60%MNPs	High HM	DMSO	20-30	60
HM-60%MNPs-80nm	High HM	DMSO	80	60

*Fe_3O_4 MNPs loading ratio by weight in fiber (%wt) = $\frac{MNPs\ Weight}{MNPs\ Weight + Polymer\ Weight} \times 100\%$

3.2.2 Fiber Spinning Process

In fiber spinning process, the prepared spinning dope from Section 3.2.1 was poured into a stainless-steel spinneret syringe, which was wrapped with a heating jacket to maintain the solution temperature at ~60°C. A sketch of the fiber spinning and solidification process was shown in Figure 3.1. As the spinning pump started, the solution was forced through a mass filter (200μm in pore size) at a constant rate, and then extruded through an #18-gauge syringe needle with round

cross-section (1mm inner diameter). This nascent fiber travelled through an air gap of 3-5 mm, and then immersed into the liquid coagulation bath of pure methanol at -30 ~ -25°C. The coagulation bath temperature was maintained with dry ice. The as-spun fiber travelled through the entire coagulation bath (1.5m in length) at the speed of 8 m/min, and finally wound onto a collector with draw ratio of one. The residence time of nascent fibers in the coagulation bath was ~11s, which was adequate to form desired fiber shape with current setup. The wound-up fibers were kept on the collectors, which were immersed in methanol bath at -20°C for 24 h until fiber fully solidified.

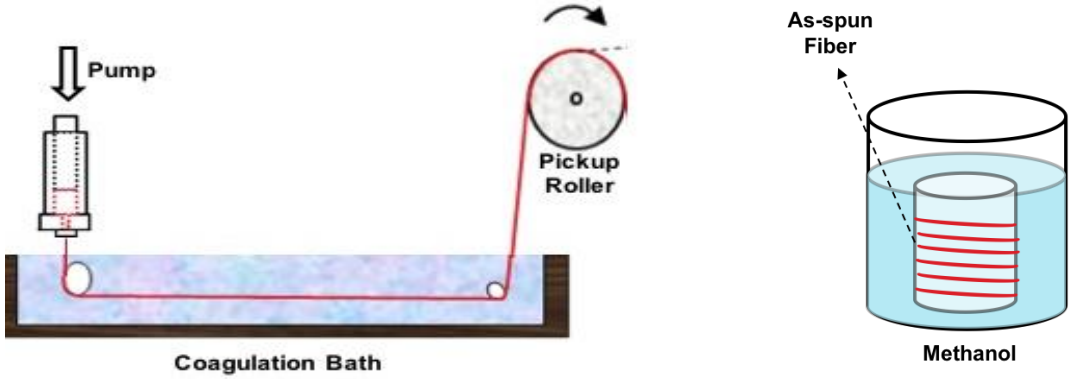

Figure 3.1 Schematic graphs of fiber dry-jet wet spinning (left) and solidification process (right) in experiments.

3.2.3 Fiber Post Treatment

After fully coagulated in methanol, as-spun fibers were post-processed with multi-stage drawing. Each stage of drawing was completed on a three-roller setup as shown in Figure 3.2. In each drawing, fibers were pulled from the feed-roller to a heat-roller at the same speed, then heated upon the contact with the heat-roller, and finally being collected on the pickup-roller which rotated at a higher speed upon pre-set draw ratio. The heat temperature and draw ratio of each drawing stage were summarized in Table 3.3. The drawing force was always applied along fiber axis, and

the contact time of fibers with the heated roller was no more than 0.5s to avoid over-heating. Total nominal DR was the product of the three stage DRs.

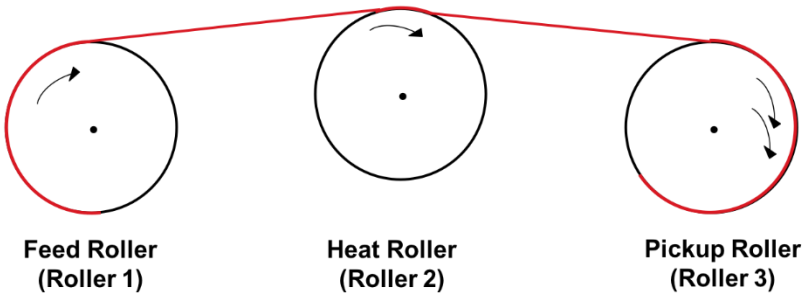

Figure 3.2 Schematic demonstration of drawing setup for each drawing stage.

Table 3.3 Parameters for fiber post-drawing process.

	Temperature of heat roller (°C)	Draw ratio
1st drawing stage	80	1.5
2nd drawing stage	90	2
3rd drawing stage	100	1.5

3.3 Characterization

3.3.1 Fiber Morphology

The morphology of fiber surface and cross-sections was characterized with Nikon H550S Optical Microscope and LEXT OLS4000 3D Laser Confocal Measuring Microscope.

For cross-section images, PVOH fibers were wrapped in the filling fiber of trilobal nylon, and the bundle of mixed fibers were immobilized in erasers and cut into flat and thin slices for observation. Fiber diameters were calculated as the equivalent cylindrical diameter of at least 15 specimens from the cross-section optical images with ImageJ Graphic Software. The distribution of MNPs clusters was observed with confocal microscope.

3.3.2 Crystal Structure

Wide-angle X-ray scattering (WAXD) was utilized to study the crystal structure of fibers. Two types of WAXD characterization were conducted, one-dimensional scanning and azimuthal scanning. Fiber samples were prepared by aligning a bundle of 15 parallel fibers on the sample holder as shown in Figure 3.3.

Figure 3.3 WAXD samples of pure polymer fibers (left) and PVOH-10%MNPs magnetic fibers (right).

In one-dimensional scanning, fiber samples were placed along the direction of beam source to detector on the instrument of PANalytical Empyrean Diffractometer which was equipped with PIXcel^{1D} detector and PIXCEL Monochromator filter. The radiation source was Cu-Kα with a wavelength (λ) of 1.54184 Å and beam power of 30 kV at 30 mA. The goniometer radius was 240 mm. Scanning was performed from 5° to 65° for 2θ angle with the increment of 0.026 °/s, and one data point was recorded per second.

The azimuthal scanning WAXD was performed on Bruker AXS General Area Detector Diffraction System (GADDS) equipped with HI-STAR two-dimensional area detector. The radiation source was Cu-Kα with wavelength of 1.54184 Å at the beam power of 45 kV and 40 mA. The collimator diameter of the beam spot on the sample was 800μm. The incident ω angle

was 5°, and the scans were recorded until 40°. The distance between sample holder and the detector was 6 cm.

To analyze one-dimensional WAXD patterns, MDI Jade 5.0 Software was applied to identify peaks and to provide more information. The baseline was subtracted with default MDI Jade software before the peak identification step. Detailed calculation of crystallinity and crystal structure was included in result sections. The reference pattern used for pure PVOH polymer crystal was PDF # 00-064-1489 from ICDD PDF database.

3.3.3 Thermal Performance

The thermostability of PVOH fibers were studied via thermal gravimetric analysis (TGA) with Perkin Elmer Pyris Model-1 instrument. Fiber samples of 0.2- 0.6g were heated in a platinum pan from 25°C to 950°C in nitrogen environment with the heating rate of 10°C/min. Sample weight loss was recorded as temperature increased during the degradation process. After TGA process, air was purged in to burn up the residues at 950°C.

3.3.4 Mechanical Properties

Single fiber tensile strength measurements were conducted with Q-test machine from Elite Controller- MTS according to ASTM D3379 Standard with the load cell of 5 lbs. The linear density of each fiber was determined by weighing 300cm length of fiber. Fiber specimens for tensile test were prepared at the length of 2.54 cm, and they were preconditioned at the standard environment of 25°C and relative humidity of 65% overnight before testing. The tensile strength and break elongation were calculated as the result of at least 5 specimens in each fiber system. Secant modulus at both 2% and 5% elongation were calculated, and the results were found with the same values for the same fiber sample, therefore the author assumed the secant modulus was the same

as Young's modulus and would be used throughout the remainder of this dissertation unless otherwise stated.

3.3.5 Magnetic Performance

The magnetic performance of fibers and pure magnetic nanoparticles (MNPs) were obtained with MPMS® SQUID (superconducting quantum interference devices) VSM DC Magnetometer, Quantum Design Company. A 6mm long bundle of each fiber sample was aligned and immobilized on a quartz holder. The tests were conducted in the magnetic field of -3T~ +3T in high vacuum environment at room temperature. The magnetic hysteresis loops of magnetism intensity versus external magnetic field were recorded for magnetic performance analysis.

CHAPTER 4 RESULTS AND DISCUSSION

4.1 Optimum System for Dry-jet Wet Spinning Magnetic PVOH Fibers

The goal of this section is to determine the optimum PVOH polymer system for spinning magnetic fibers to achieve good fiber properties. The tested spinning systems (Table 4.1) included two molecular weight PVOH polymers and two solvent systems (DMSO and water). Since the presence of MNPs would affect fiber properties, fibers were spun at both 0%wt and 10%wt superparamagnetic Fe_3O_4 MNPs loadings. Details about fiber spinning were presented in Section 3.2.2. Various fiber properties were tested to evaluate fiber performance, including fiber morphology (Section 4.1.1), crystal structure (Section 4.1.2), thermal properties (Section 4.1.3), mechanical performance (Section 4.1.4), and magnetic behavior (Section 4.1.5).

Table 4.1 Fiber systems for the study of optimal spinning system.

Fiber system	Polymer molecular weight	Solvent	Polymer concentration (g/dl)	Initial MNPs loading (%wt)
LM-H_2O	89 000-98 000	DI water	20	0
LM-H_2O-10%MNPs	89 000-98 000	DI water	20	10
LM-DMSO	89 000-98 000	DMSO	20	0
LM-DMSO-10%MNPs	89 000-98 000	DMSO	20	10
HM- DMSO	146 000-186 000	DMSO	10	0
HM-DMSO-10%MNPs	146 000-186 000	DMSO	10	10

4.1.1 Fiber Morphology

The solvent systems of water and DMSO were utilized to prepare spinning dopes, with the former being a strong polar solvent and the latter as a strong non-polar solvent. With water solvent, pure PVOH fibers were successfully produced via the dry-jet wet spinning process (Figure 4.1a).

However, magnetic fibers were not produced from the magnetic spinning dope with water system, instead, magnetic beads were formed (Figure 4.1b). The formation of beads was believed to be due to the Rayleigh-Tayler instability of the polymer solution at the spinning tip, when polymer jet tended to minimize the surface tension by reformation into spherical droplets.[78]

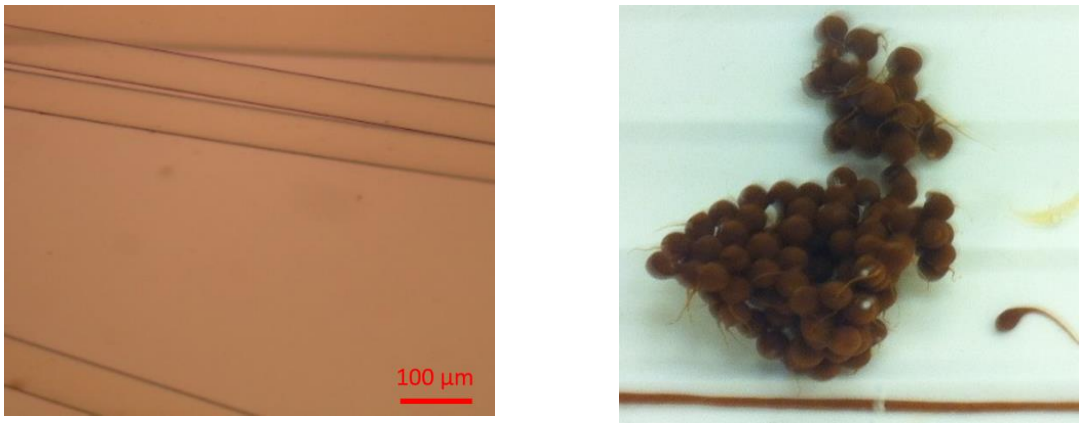

Figure 4.1 Products from LM-H_2O spinning dope as fibers(left), products from LM-H_2O-10%MNPs spinning dope as beads (right).

On the other hand, DMSO solvent was able to successfully produce continuous fiber products with and without MNPs, as well as with both molecular weight PVOH polymers (LM-DMSO, HM-DMSO, LM-DMSO-10%MNPs, HM-DMSO-10%MNPs). As seen in Figure 4.2, all fibers produced with DMSO solvent were uniform, smooth, and bead-free, regardless of polymer molecular weight and MNPs loadings. The cross-sections of fibers spun from DMSO solvent were circular to oval shapes (Figure 4.3), which suggested the coagulation process was efficient as the solidification of fiber skin and core occurred at the same time scale. Therefore, DMSO was selected as the solvent system for magnetic fiber research for continuous studies.

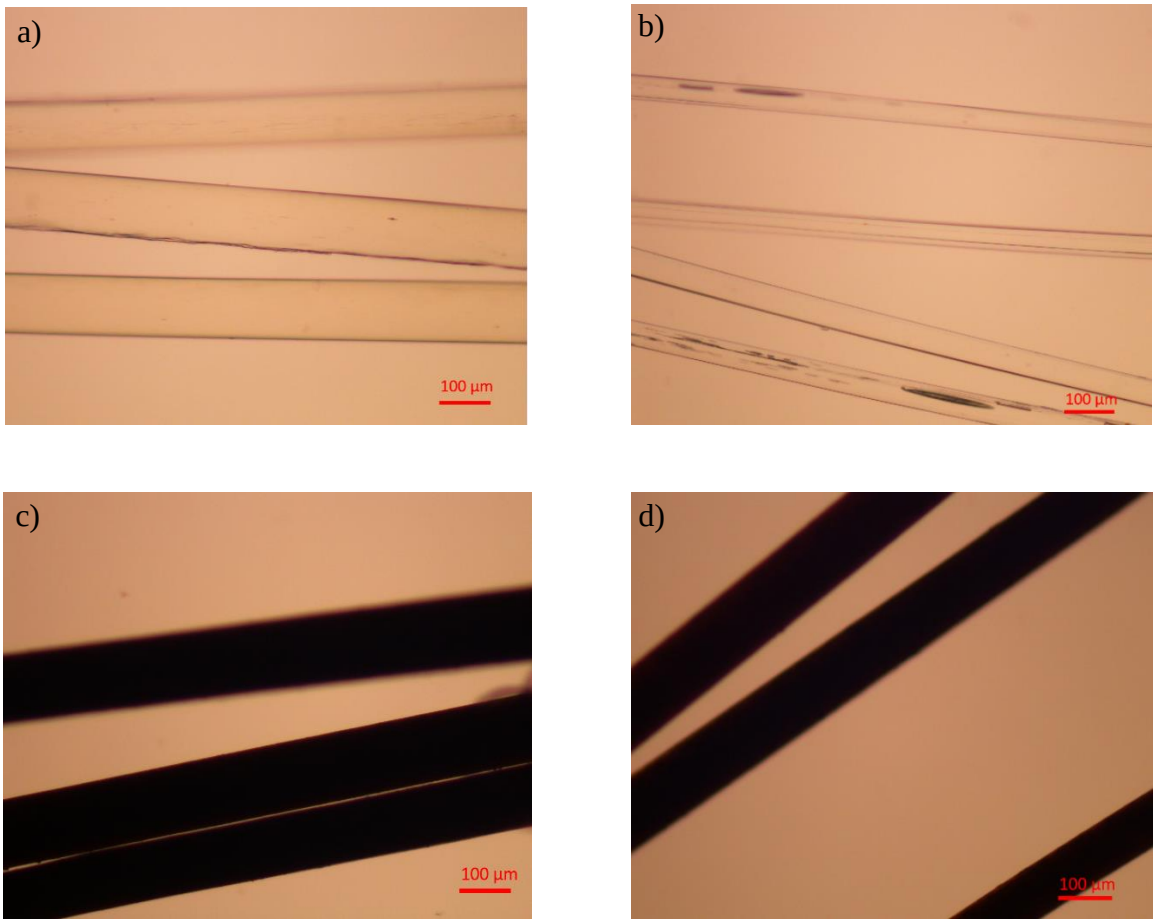

Figure 4.2 Optical images of pure and magnetic PVOH fibers (10%wt MNPs loading) produced with DMSO solvent: a) LM-DMSO, b) HM-DMSO, c) LM-DMSO-10%MNPs, d) HM-DMSO-10%MNPs.

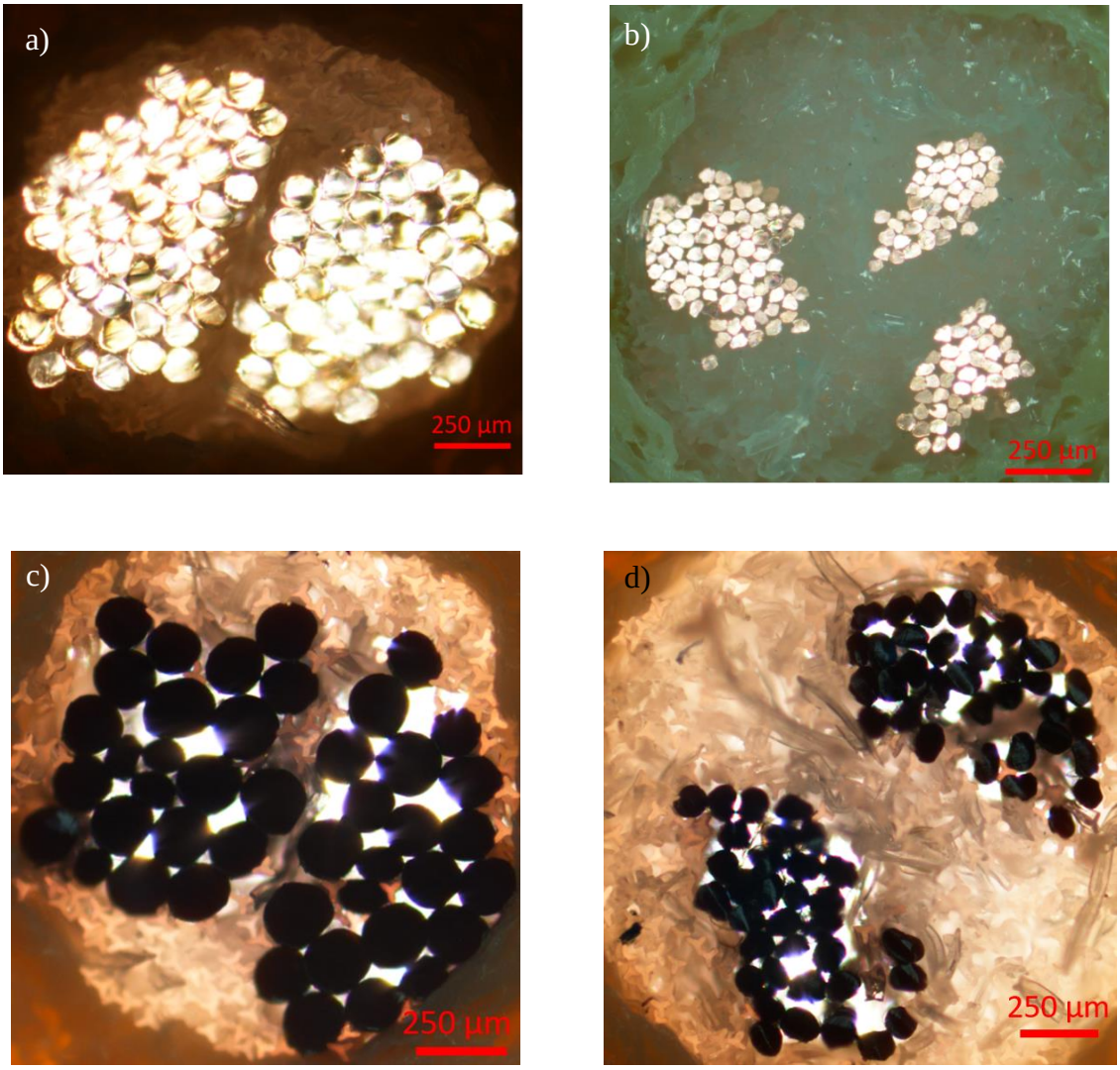

Figure 4.3 Cross-section optical images of pure and magnetic PVOH fibers (10%wt MNPs loading) produced with DMSO solvent: a) LM-DMSO, b) HM-DMSO, c) LM-DMSO-10%MNPs, d) HM-DMSO-10%MNPs.

Fiber diameters were calculated from the cross-section images in the range of 54- 163 µm (Table 4.2). It was noticed that fibers produced from HM PVOH polymers had slightly smaller diameters compared to the ones from LM PVOH polymers, which was valid for both pure and magnetic fibers. Since all fibers were extruded at the same volume rate from the same spinneret

head, this indicated more swelling effect exhibited for HM polymers spinning dope with larger nascent fiber diameters.[58]

Table 4.2 Diameters of pure polymer fibers and magnetic fibers with 10%wt MNPs.

Fiber system	Post-drawn fiber diameter (μm) *
LM-DMSO	124
HM-DMSO	54
LM-DMSO-10%MNPs	163
HM-DMSO-10%MNPs	105

*The draw ratio for all fibers was 4.5.

The MNPs distribution in fibers was observed via confocal microscopy (Figure 4.4). The bright dots in the cross-section were Fe_3O_4 MNPs clusters, which were commonly seen in magnetic fibers. This MNPs agglomeration was the result of MNPs dipole-dipole attraction as well as MNPs repelling effect from polymers.[26] Since the bright dots were spread-out on the cross-section, MNPs clusters was distributed all over the fiber structure. It was also seen that the cross-section of fibers was quite dense without many voids, which offered the possibility for good fiber mechanical properties.

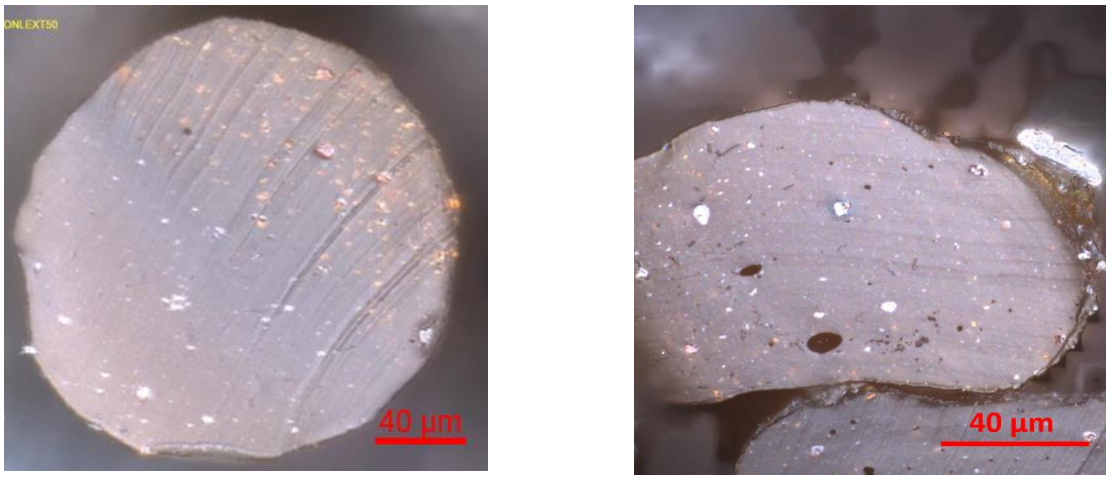

Figure 4.4 Cross-section confocal images of magnetic PVOH fibers (10%wt MNPs loading) with different polymer raw materials: (left) LM-DMSO-10%MNPs fibers, (right) HM-DMSO-10%MNPs fibers.

In summary, the water solvent system was eliminated from this study as it was not able to produce magnetic fibers, and DMSO was chosen as the solvent system for subsequent magnetic fiber studies. With DMSO solvent, PVOH polymers of both molecular weights were able to produce pure and magnetic fibers with a robust fiber structure and uniform MNPs distribution.

4.1.2 Crystal Structure

Crystal structure provides insights about fiber on micro-level, and it can help to understand fiber behaviors such as mechanical properties and thermal performance. Both 1D WAXD scanning and Azimuthal WAXD scanning were conducted on pure and magnetic PVOH fibers.

The crystal patterns of pure PVOH fibers (LM-DMSO, HM-DMSO, reference PVOH fibers) are presented in Figure 4.5, in which *x* axis represented 2θ angle and *y* axis was the relative intensity of the scattering. The diffraction peaks for PVOH crystal planar 101 and 200 were shown on both LM and HM fiber patterns, but HM-DMSO fibers had more distinguished and sharp crystal

peaks than LM-DMSO fibers. It was also found that the HM-DMSO fibers pattern aligned with the reference PVOH pattern (PDF #00-064-1489) much better, with more crystal peaks identified and matched (Table 4.3).

The WAXD patterns of magnetic fibers were shown in Figure 4.6, in which HM-DMSO-10%MNPs had more distinguished polymer crystal peaks than LM-DMSO-10%MNPs fibers, indicating a higher crystallinity.

Table 4.3 WAXD peaks position (2θ) of pure PVOH fibers.

Crystal phase	LM-DMSO (°)	HM-DMSO (°)	Reference Pure PVOH PDF #00-064-1489 (°)
100	11.72	11.37	11.38
001	-	15.96	16.11
-101	-	19.37	19.42
101	19.83	19.99	20.11
200	22.83	22.87	22.88
201	27.58	28.34	28.60
002	30.11	32.42	32.54

Crystallinity of fibers was estimated with Hermans-Weidinger method as shown Equation 4-1. The crystal peaks utilized in calculation were between 2θ angle of 15°- 25°, which included the crystal phases of 001, -101, 101, 200, and amorphous peaks as marked in Figure 4.5. Upon the crystallinity estimation, fibers produced with HM polymer achieved higher crystallinity than the ones spun from LM polymers, which was true for both pure and magnetic fiber products (Table 4.4).

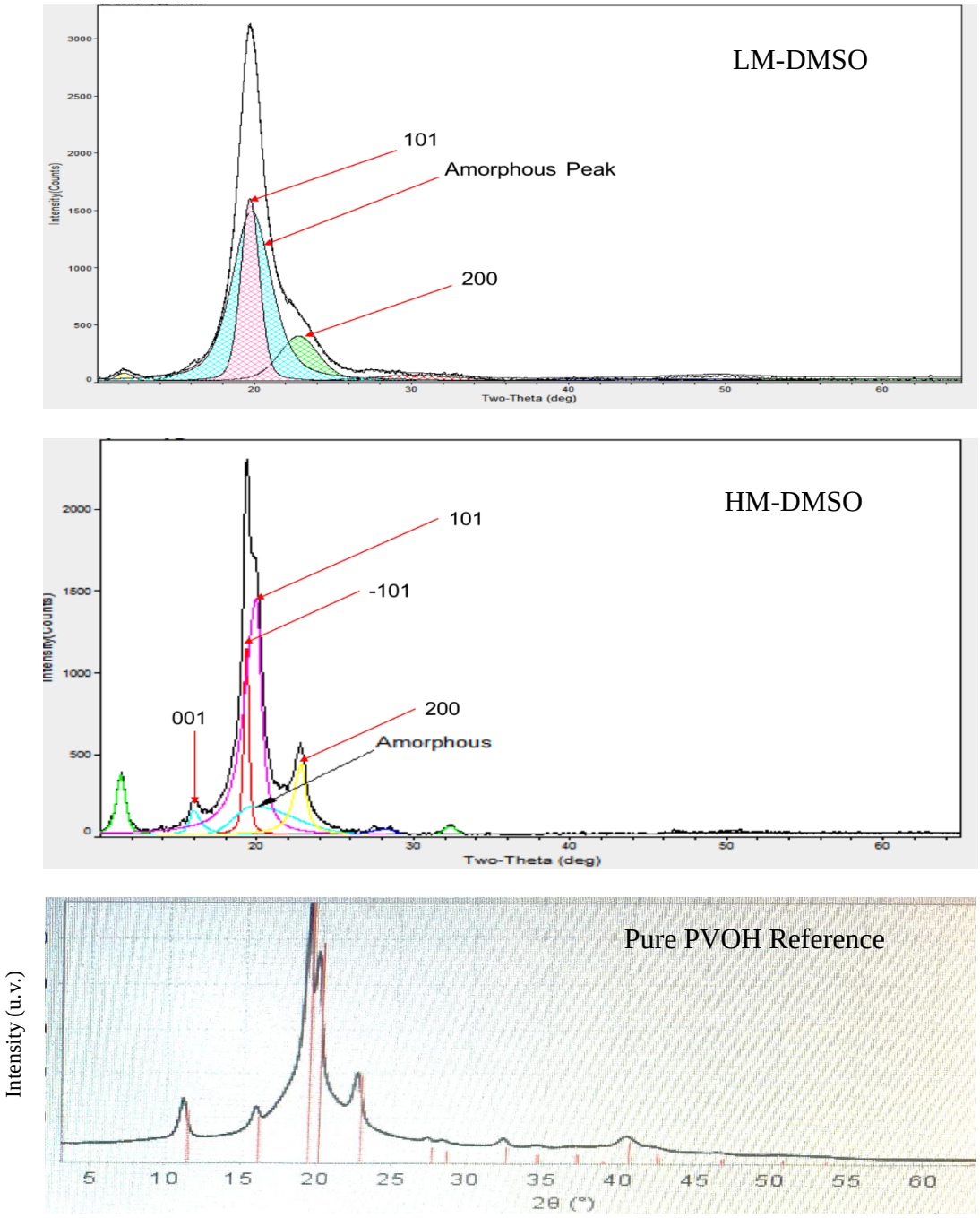

Figure 4.5 WAXD graphs of pure PVOH fibers made from low molecular weight polymer (top) and high molecular weight polymer (middle); reference PVOH pattern PDF #00-064-1489 (bottom).

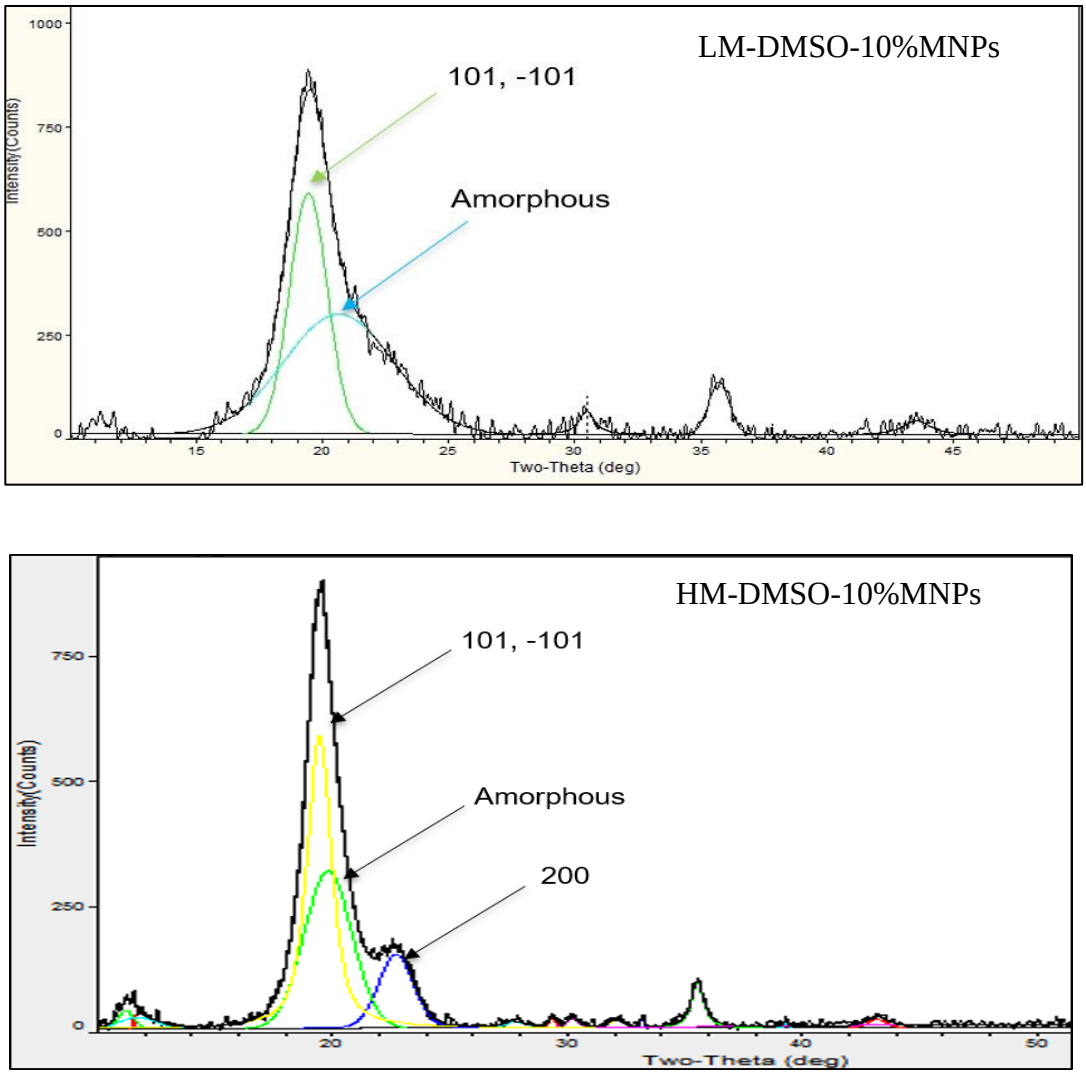

Figure 4.6 WAXD graphs of magnetic PVOH fibers made from low molecular weight polymers LM-DMSO-10%MNPs (top) and high molecular weight polymer HM-DMSO-10%MNPs (bottom).

$$\text{Est. Crystallinity } \% = 1 - \frac{\text{Area of amorphous peaks}}{\text{Area of amorphous peaks} + \text{Area of crystal peaks}} \qquad 4\text{-}1$$

Where the peaks were in the 2θ angle range of 15°- 25°.

Table 4.4 Crystallinity of pure polymer fibers and magnetic fibers with 10%wt MNPs.

Fiber System	Estimated crystallinity
LM-DMSO	42%
HM-DMSO	83%
LM-DMSO-10%MNPs	41%
HM-DMSO-10%MNPs	66%

In Azimuthal WAXD scanning patterns (Figure 4.7), rings implied the existence of crystal structure, and bright dots represented preferred polymer orientation. For pure PVOH fibers, HM-DMSO fibers had a narrower ring than LM-DMSO fibers indicating higher crystallinity. The preferred polymer orientation could not be compared visually from the images. For magnetic fibers, it was hard to identify the difference between HM-DMSO-10%MNPs and LM-DMSO-10%MNPs fibers patterns.

As a brief summary, pure polymer fibers and magnetic fibers made from HM PVOH exhibited higher crystallinity than the ones made from LM PVOH polymers, and the 1D WAXD crystal pattern of fibers made from HM polymer showed more polymer crystal peaks than the ones made from LM polymers.

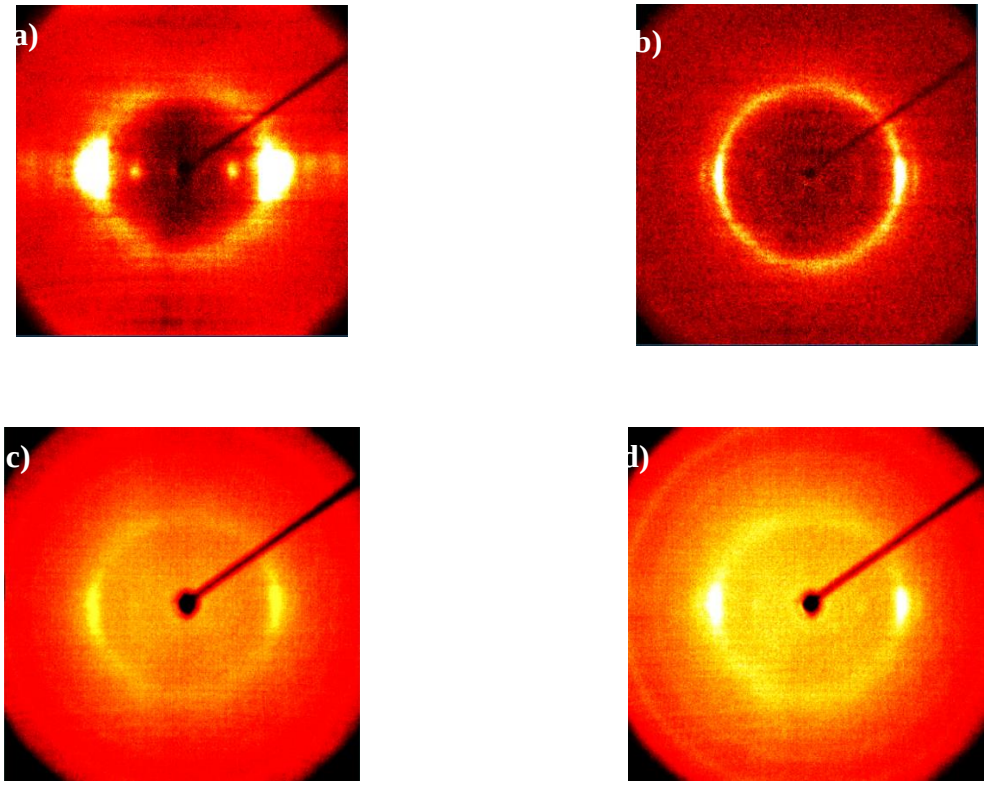

Figure 4.7 Azimuthal WAXD scanning graphs of pure polymer fibers and magnetic fibers with 10%wt MNPs: a) LM-DMSO fibers, b) HM-DMSO fibers, c) LM-DMSO-10%MNPs, d) HM-DMSO-10%MNPs.

4.1.3 Thermal Performance

The thermal properties were studied via TGA analysis for fibers produced with both molecular weight polymers, as well as fibers with and without MNPs.

For pure PVOH fibers, the degradation curves (Figure 4.8) were alike despite of polymer weights, except that LM PVOH fibers entered the main weight loss stage slightly earlier. Both pure PVOH fibers ended up with a final weight of zero at the end of the decomposition process.

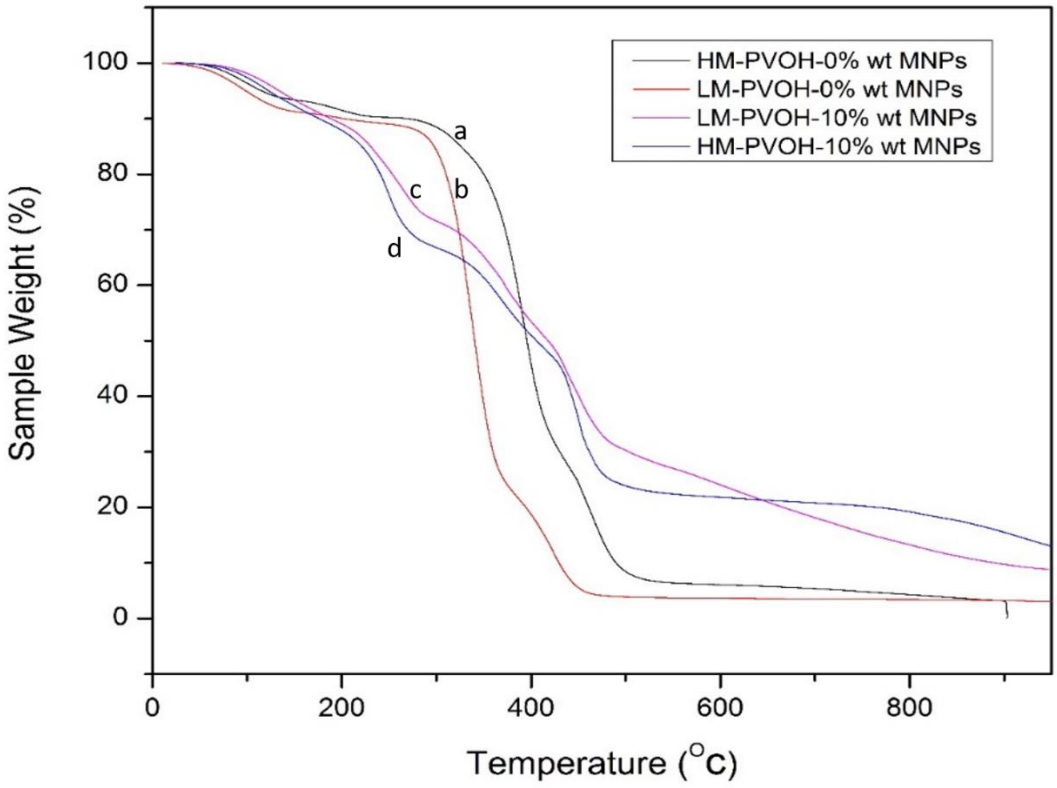

Figure 4.8 TGA graphs of pure PVOH fibers and magnetic PVOH fibers with 10%wt MNPs made from low and high molecular weight polymers: a) HM-0%MNPs, b) LM-0%MNPs, c) LM-10%MNPs, d) HM-10%MNPs.

For magnetic fibers, TGA decomposition curves were similar regardless of raw polymer weight. Since there was no residue for PVOH polymer after decomposition, all residues were considered coming from MNPs. Under the assumption that all Fe_3O_4 was turned into Fe_3C by the end of TGA process, actual MNPs loadings in each fiber system could be estimated upon TGA residue weight with Equation 4-2, and it was found HM-10%MNPs fiber had a higher MNPs loading of 17.7%wt than LM-10%MNPs ones of 11.5%wt (Table 4.5).

$$\text{MNPs \%wt in Fiber} = m_{TGA\ residue} \times \frac{M_{Fe3O4}}{M_{Fe3C}} \times 100\% \qquad 4\text{-}2$$

$m_{TGA\ residue}$: residue weight of magnetic fibers after TGA decomposition

M_{Fe3O4} : molecular weight of Fe_3O_4, 231.533

M_{Fe3C}: molecular weight of Fe_3C, 179.5457

Table 4.5 TGA results and MNPs ratio estimation of magnetic fibers with 10%wt MNPs.

Fiber system	Remaining weight after TGA (%wt)	Calculated MNPs loading (%wt)
LM-DMSO	0.0	--
HM-DMSO	0.0	--
LM-DMSO-10%MNPs	8.9	11.5
HM-DMSO-10%MNPs	13.7	17.7

The decomposition curves of pure PVOH fibers were very different from their corresponding magnetic fibers as seen in Figure 4.8. For HM polymer, pure PVOH fibers and HM-DMSO-10%MNPs magnetic fiber (Figure 4.8a and d) had a similar weight loss up to 200°C, which was attributed mostly to moisture and solvent volatilization.[67] In the temperature range of 200°C - 300°C, magnetic fiber experienced additional 19% weight loss compared to pure PVOH fibers, which was contributed by MNPs decomposition as well as extra polymer degradation. In other words, the involvement of MNPs had caused more polymer phase to degrade at a lower temperature. Since the crystallinity of PVOH was lower for magnetic fibers than pure polymer fibers, there were more amorphous regions in magnetic fiber which had lower degradation temperature, and thus aligned with the extra degradation observed here. Between 300°C and 538°C, PVOH polymers in both pure and magnetic fibers experienced major weight loss from hydrocarbon polymer chains breakdown, and the polymer weight was mostly gone.[77] Magnetic fibers also had iron oxide decomposition in this temperature range. Above 538°C, the small

amount of remaining PVOH polymers slowly decomposed until completely gone, and Fe_3O_4 was completely carbonized to Fe_3C composite.[32]

In summary, pure PVOH fibers with high and low molecular weights presented similar decomposition curves with final residue weights of zero, and the TGA curves of magnetic fibers were alike for two polymer weight systems. It appeared the high molecular weight PVOH polymer was able to embed more MNPs in the fiber system, and the incorporation of MNPs in fibers led to more weight loss in low temperature range compared to pure polymer fibers.

4.1.4 Mechanical Properties

Mechanical performance is one of the most important properties for fiber products, as it directly determines fiber application. Tensile tests were conducted on fibers after drawing, and tensile properties are were summarized in Table 4.6, including breaking strength, elongation length at break, and Young's modulus.

The tensile strength is reported in the range of 1-1.6 GPa for commercialized pure PVOH fibers, and the tensile strength of laboratory produced PVOH fibers can vary from 10 MPa up to 6 GPa.[56] Magnetic fibers fabricated in this section exhibited tensile strength of 91 MPa and 114 MPa after they were drawn. As shown in Table 4.6, the magnetic fibers produced from HW polymers (HM-10%MNPs) illustrated higher tensile strength and lower elongation at break, compared to those produced from LM-10%MNPs system. This could the outcome of higher crystallinity for HM-DMSO-10%MNPs fibers, and another possibility was that HM magnetic fibers was less susceptible to defects because of the more entanglements per polymer in the system.

Young's modulus was calculated as listed in Table **4.6**. HM-DMSO-10%MNPs fibers exhibited much higher Young's modulus (39.4 MPa) than LM-DMSO-10%MNPs fibers (24.0 MPa). This was likely because of higher crystallinity in the HM-10%MNPs fibers.[79]

Table 4.6 Tensile results of magnetic fibers with 10%wt MNPs.

Fiber system	Tensile strength (MPa)	Elongation at break (%)	Young's modulus (MPa)
LM-DMSO-10%MNPs	91.0 ± 9.2	73.9 ± 33.6	24.0 ± 2.9
HM-DMSO-10%MNPs	113.9 ± 18.0	20.3 ± 3.7	39.4 ± 3.7

As a summary, compared to magnetic fibers made from LM polymers, magnetic PVOH fibers produced with HM polymers showed better mechanical performance.

4.1.5 Magnetic Performance

To explore the effects of polymer molecular weight on fiber magnetic performance, SQUID magnetometer was utilized for fibers with both molecular weights and with/without MNPs. The magnetic hysteresis loops were recorded as shown in Figure 4.9.

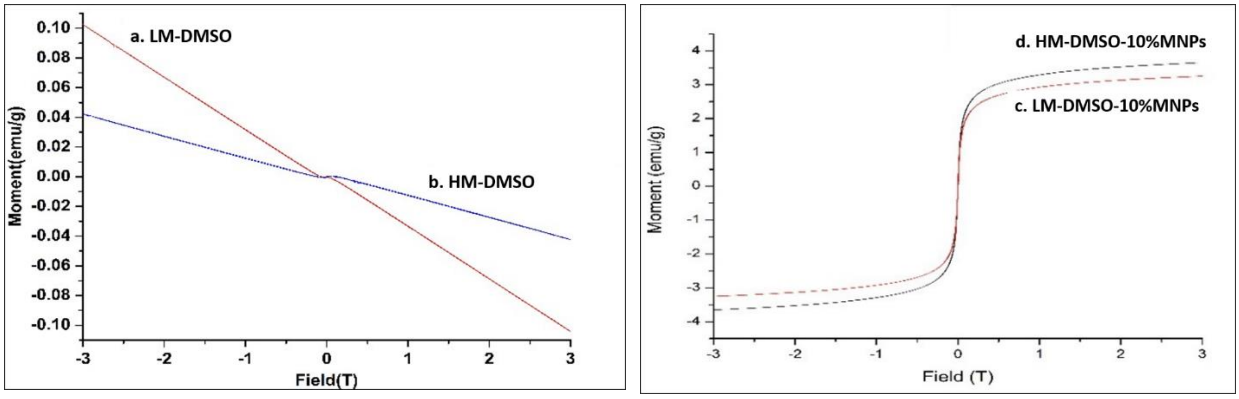

Figure 4.9 SQUID graphs of pure PVOH fibers and magnetic PVOH fibers with 10%wt MNPs made from low and high molecular weight polymers: a) pure LM-DMSO fibers, b) pure HM-DMSO fibers, c) LW-DMSO-10%MNPs fibers, and d) HW-DMSO-10%MNPs fibers.

Pure PVOH fibers showed typical paramagnetic magnetic behaviors in external magnetic field as expected (Figure 4.9a). Magnetic fibers with 10%wt MNPs displayed typical hysteresis loops of superparamagnetic material, which was consistent with the 20nm Fe_3O_4 MNPs embedded. The saturation magnetization value (*Ms)* was similar for both magnetic fibers around 3.5 emu/g, while that of bare Fe_3O_4 MNPs was 47.9 emu/g. With the assumption that superparamagnetic response of magnetic fiber was proportional to MNPs loadings, the MNPs in both magnetic fiber systems were estimated around 7.5%wt, which were smaller than the values calculated from TGA results. The value difference between two calculation methods could be due to the random distribution of defects in fibers, and since both tests only took a small amount of sample, errors might happen depending on which part of the fiber was sampled.

Table 4.7 Magnetism results of magnetic fibers with 10%wt MNPs.

Sample	Saturated Value, M_S, (emu/g)	MNPs loading estimated from SQUID (%wt)	MNPs loading estimated from TGA (%wt)
LM-DMSO-10%MNPs	3.5	7.3	11.5
HM-DMSO-10%MNPs	3.6	7.5	17.7
Fe_3O_4 MNPs	47.9	--	--

In summary, magnetic fibers exhibited the same superparamagnetic behavior as the MNPs embedded regardless of polymer molecular weights. The MNPs loadings calculated from magnetic performance were comparable for both magnetic fibers, and both were smaller than the estimation from TGA results. The estimated MNPs loading from SQUID and TGA results were both within reasonable range compared to the MNPs concentration added to the initial spinning dope.

4.1.6 Summary

In section 4.1, water solvent system was discovered to be not capable of generating magnetic fibers with current dry-jet wet spinning setup and was eliminated. The solvent system of DMSO was found with the capability to produce both pure PVOH fibers and magnetic fibers at 10%wt MNPs successfully. All fibers made from DMSO systems appeared with smooth surface and consistent diameters without spindle-shape unevenness. All DMSO-solvent based fibers were able to be drawn through multiple stages for better mechanical performance. The distribution of MNPs clusters in DMSO-based magnetic fibers was quite uniform in fiber structure. With all these results, DMSO solvent was chosen for magnetic fiber research for further magnetic fiber studies.

With DMSO solvent system, fibers were made with both high molecular weight (HM) and low molecular weight (LM) PVOH polymers at 0% and 10%wt MNPs loadings. Pure HM and LM PVOH fibers showed similar thermal decomposition curves, and so did HM and LM magnetic fibers. Both magnetic fibers demonstrated similar MNPs loadings and comparable magnetism behaviors despite of polymer weights. However, pure HM PVOH fibers were able to achieve higher crystallinity and more clearly identified sharp crystal peaks; and magnetic PVOH fibers made from HM polymers also demonstrated higher crystallinity, better tensile strength, as well as larger Young's modulus. Therefore, HM polymers were preferred as the raw material for magnetic fiber production in this study.

Overall, high molecular weight PVOH polymer with DMSO solvent was selected as the spinning system and were utilized in the rest of the study.

4.2 Effects of MNPs Concentration on Magnetic Fiber Performance

With the selected spinning system of DMSO solvent and PVOH polymer of Mw= 146,000-186,000. In this section, PVOH fibers were spun and post-drawn with Fe_3O_4 MNPs loadings of 0%wt, 10%wt, 20%wt, 40%wt, 60%wt. The effects of MNPs loadings on fiber structure and performance were studied with various characterizations, including fiber microstructure (Section 4.2.1), crystal structure (Section 4.2.2), thermal performance (Section 4.2.3), mechanical properties (Section 4.2.4), and magnetic performance (Section 4.2.5). The impact of drawing on magnetic fiber performance was also briefly studied with 10%wt and 20%wt MNPs fibers.

4.2.1 Fiber Microstructure

The microstructure of PVOH fibers was observed with optical microscope and confocal microscope for fiber cross-section, fiber diameter, fiber surface, and MNPs distribution.

As shown in Figure 4.2, pure polymer fiber and all magnetic fibers displayed a bead-free structure with consistent diameter, which indicated the spinning dope was homogeneous and the extrusion process was effective. The fiber surface was relatively smooth for fibers with MNPs loading up to 40%, while the surface was a little rougher for PVOH-60%MNPs fibers, which may be the results of high MNPs concentration. With a closer look at the fiber surface of PVOH-10%MNPs and PVOH-60%MNPs under Confocal microscope (Figure 4.11), neither samples displayed extensive MNPs clusters accumulation on the surface, which implied the MNPs phase did not separate from polymer phase during fiber formation, even at MNPs loadings as high as 60%wt.

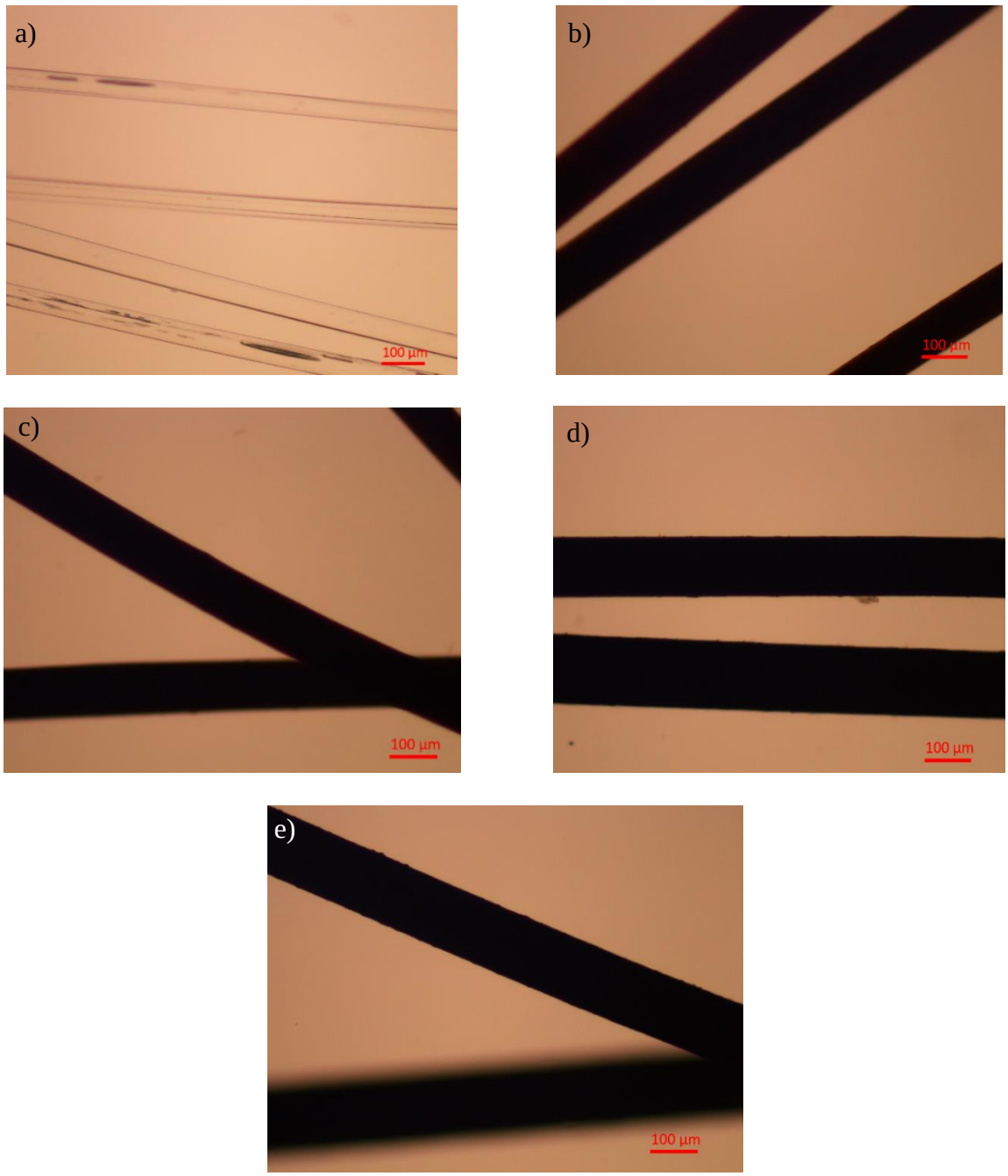

Figure 4.10 Optical images of PVOH fibers with different MNPs loadings from 0%wt to 60%wt: a) PVOH-0%MNPs, b) PVOH-10%MNPs, c) PVOH-20%MNPs, d) PVOH-40%MNPs, e) PVOH-60%MNPs.

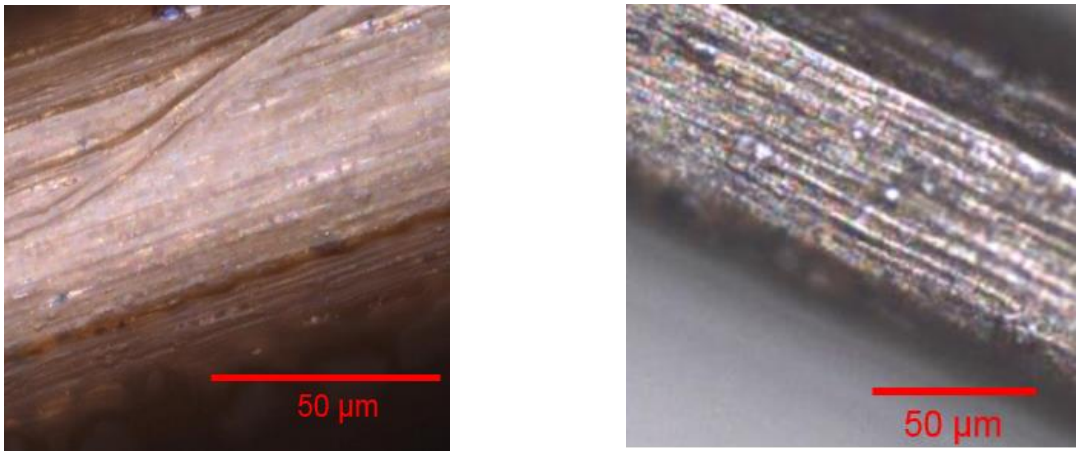

Figure 4.11 Confocal images of PVOH magnetic fibers surface: (left) PVOH-10%MNPs fiber, and (right) PVOH-60%MNPs fiber.

The cross-section of magnetic PVOH fibers was observed with optical microscope (Figure 4.12) and confocal microscope (Figure 4.4). The cross-section of all magnetic fibers showed oval-like shape without obvious shape changes among different MNPs loadings. The diameters of magnetic fibers (Table **4.8**) were in the same range. The slightly increase trend of diameter value along with MNPs loading could be due to a gentler drawing applied in the process, in order to avoid fiber breaking that were with high MNPS loadings and thus more defects. It could also be possible that the swelling effect at spinneret tip was higher for fibers with higher MNPs loadings, and swelling effect was considered as the results from yield behavior, high hysteresis, and increased nonlinear behavior caused by MNPs.[80]

The MNPs clusters distribution was seen with confocal microscope on fiber of PVOH-10%MNPs and PVOH-60%MNPs (Figure 4.4). The bright dots, Fe_3O_4 MNPs clusters, distributed all over the cross-section area, and more clusters were found in 60%wt MNPs fibers than 10%wt MNPs fibers as expected. It was pleasant to see PVOH-60%MNPs fibers had no major voids on

cross-section, which implied the spinning solution was homogeneous at such high MNPs concentration and the coagulation process was sufficient.

Table 4.8 Fiber systems for the study of MNPs loading effects.

Fiber system*	Initial MNPs loading (%wt)	Post-drawn fiber diameter (μm)
PVOH-0%MNPs	0	54
PVOH-10%MNPs	10	105
PVOH-20%MNPs	20	109
PVOH-40%MNPs	40	130
PVOH-60%MNPs	60	138

* The spinning dopes consisted of PVOH polymer (Mw= 146,000-186,000) at ~10 g/dl in pure DMSO solvent. The MNPs were 20nm superparamagnetic Fe_3O_4 nanoparticles.

In summary, the morphology analysis of PVOH fibers with different MNPs loading presented a successful production of magnetic fibers with MNPs loading up to 60%wt. Despite of MNPs concentration, all fibers represented an oval-like cross-section shape with very few voids. Magnetic fibers maintained consistent diameters without spindle shape, and fiber diameters were in the same range. Fe_3O_4 MNPs clusters were observed with uniform distribution all over the fiber structure, and no obvious accumulation of MNPs clusters was observed even at high MNPs loading of 60%wt.

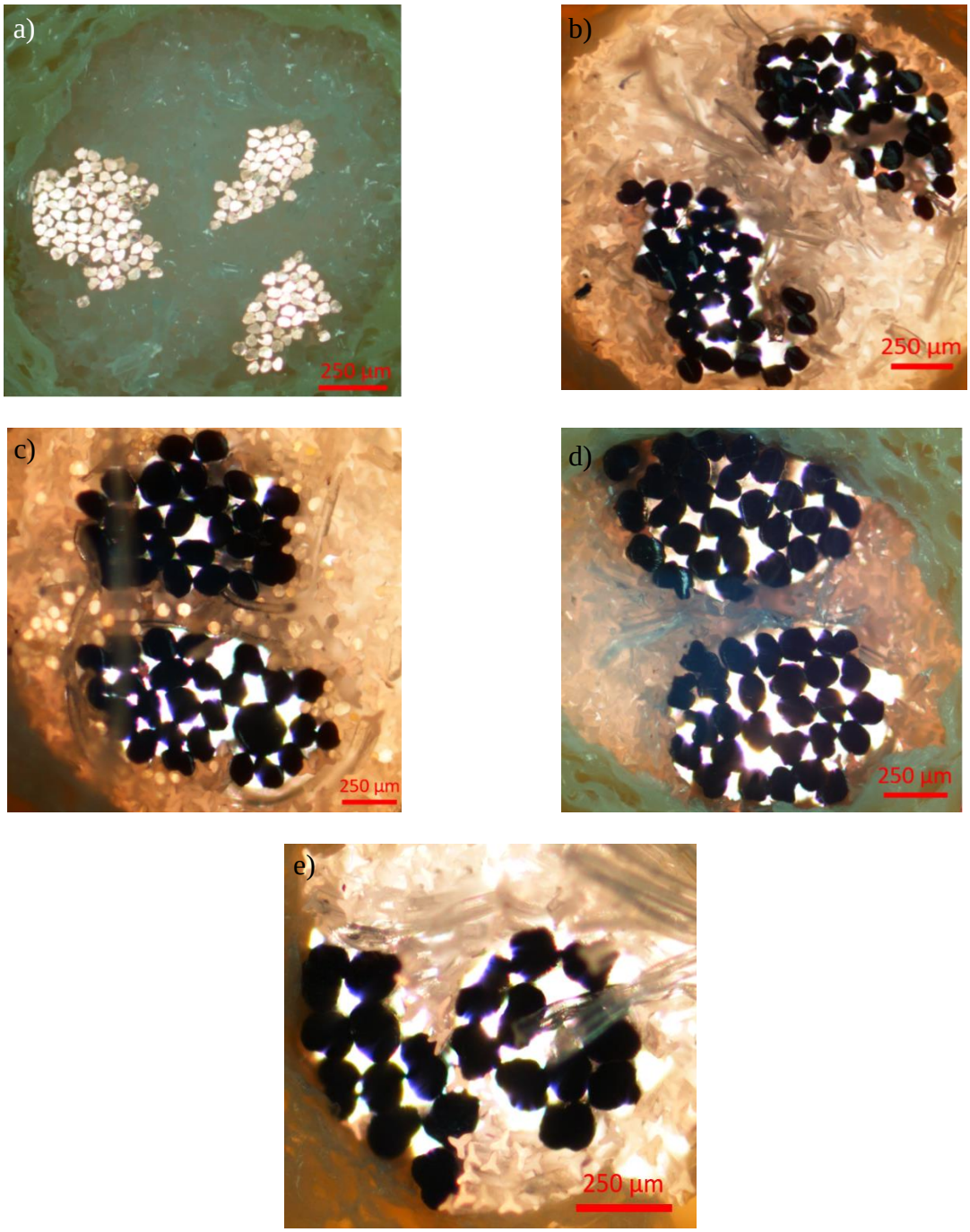

Figure 4.12 Cross-section optical images of PVOH fibers with different MNPs loading from 0%wt to 60%wt: a) PVOH-0%MNPs, b) PVOH-10%MNPs, c) PVOH-20%MNPs, d) PVOH-40%MNPs, e) PVOH-60%MNPs.

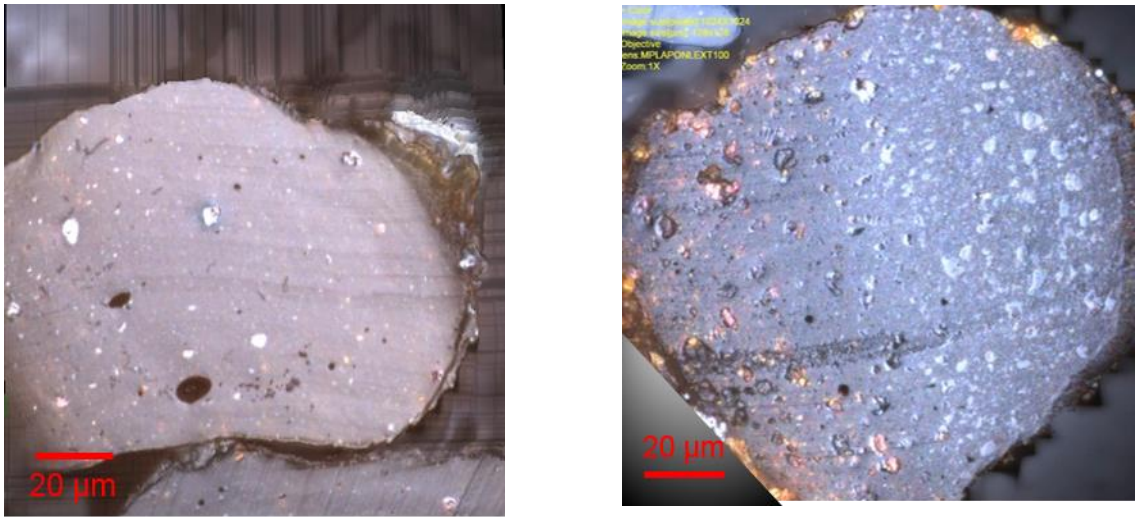

Figure 4.13 Confocal images of PVOH magnetic fiber cross-sections: a) PVOH-10%MNPs fiber; b) PVOH-60%MNPs fiber.

4.2.2 Crystal Structure

The crystal structure of PVOH fibers with various Fe_3O_4 MNPs loading ratio (0- 60%) was studied with one-dimensional WAXD scanning and azimuthal WAXD scanning. The one-dimensional WAXD provided information about fiber crystal structure such as crystal size (L), d-spacing, and crystallinity; and azimuthal WAXD scanning was able to provide information about polymer orientation preference in fibers.

The crystal patterns from WAXD 1D scanning were included in Figure 4.14, in which x-axis represented 2θ angle and y-axis as relative intensity of scattering. The strongest scattering peaks for PVOH polymer were $2\theta = 20.0°$ for crystal plane 101, and this crystal peak was chosen to represent polymer crystal structure. It was seen that the peak position of PVOH 101 crystal phase remained in the range of 19.4- 20.0 regardless of MNPs concentration, but it diminished from a high and sharp peak to a short and wide slope with the increase of MNPs concentration. This peak broadening effect indicated the increase of amorphous region in polymer matrix as

MNPs loading increased, while the reduction of peak height was the combination results from less polymer content as well as reduced crystallinity in the product for fibers of higher MNPs concentration.

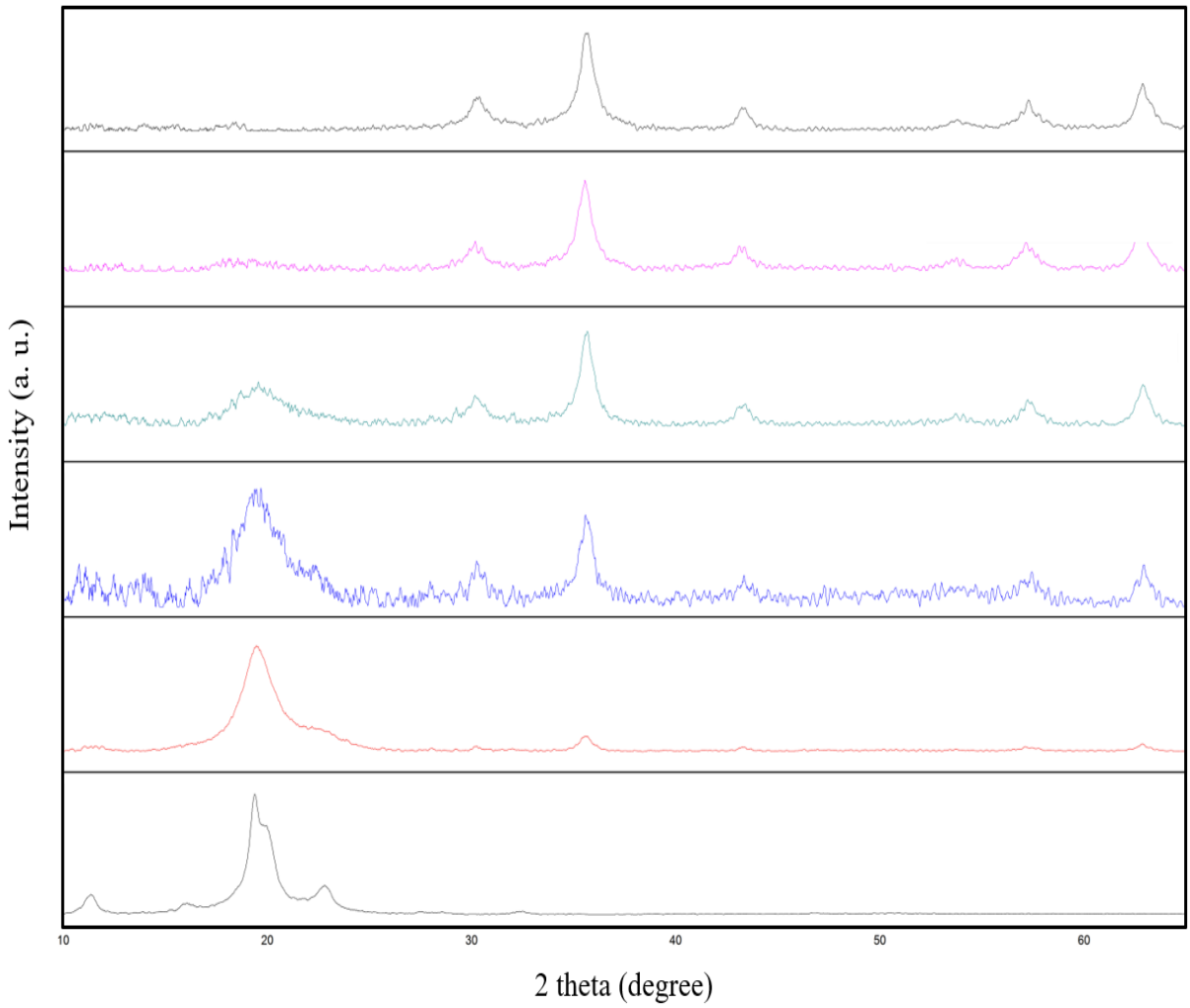

Figure 4.14 One-dimensional WAXD graphs of PVOH fibers with different 20nm Fe_3O_4 MNPs loadings (from bottom to top) of 0%wt, 10%wt, 20%wt, 40%wt, 60%wt, bare 20nm Fe_3O_4.

Table 4.9 Crystal structure of PVOH polymers in fibers with 0%wt- 60%wt MNPs.

Fiber system	PVOH-0%MNPs	PVOH-10%MNPs	PVOH-20%MNPs	PVOH-40%MNPs
Estimated polymer crystallinity	83%	66%	48%	--
2θ (°) *	20.0	19.5	19.4	19.5
d-spacing (Å) *	4.44	4.56	4.57	4.57
Crystal size (nm) *	6.7	6.1	4.4	3.4
Polymer orientation factor (*f*)	0.87	0.46	0.23	--

* 2θ, d-spacing, and crystal size were based on PVOH 101 crystal phase.

The polymer crystallinity was estimated with the area ratio of amorphous and crystal regions in the *2θ* range of 15- 25° as introduced in Section 4.1.2. From the calculation, the crystallinity of polymers (Table 4.9) decreased with the increase of MNPs concentration until crystal peaks cannot be distinguished from amorphous ones at MNPs loading of 40%wt.

The distance between crystal planes (*d*-spacing) of polymers was calculated with Bragg's law (Equation 4-3) on PVOH 101 crystal phase. The *d*-spacing results (Table 4.9) presented a consistent value of 4.44- 4.57 Å for PVOH polymers in every fiber system, indicating the packing density of polymer crystals stayed constant despite of MNPs loadings. This finding agreed with previous work, for example, An-ting Chien reported PAN magnetic fibers of 10%wt Fe_3O_4 MNPs exhibited the *d*-spacing value of 0.523nm, which was very close to the value of 0.524nm as for pure PAN fibers.[32]

$$d = \frac{n \times \lambda}{2 \sin \theta} \qquad 4\text{-}3$$

Where d is the spacing between crystallite layers at crystal phase defined by 2θ degree, n is chosen as 1, λ is 1.54184 Å as the wavelength of Cu-K_α radiation of the instrument.

The crystal size (L) of PVOH polymers were calculated with Debye-Scherrer model (Equation 4-4), and the results showed PVOH crystal size decreased tremendously from 6.7 nm for pure PVOH fibers to 3.4 nm for PVOH-40%MNPs ones. This reduction trend was likely due to the interruption of polymer crystal growth by MNPs, which effect became stronger as the MNPs loading increased.

$$L = \frac{K \times \lambda}{\beta(2\theta) \times \cos\theta} \qquad 4\text{-}4$$

Where L is the crystal size, K is a constant taken as 0.9 assuming crystallites are all spherical, λ is 1.54184 Å as the wavelength of Cu-K_α radiation of the instrument, θ is Bragg's angle, $\beta(2\theta)$ refers to the full width at half maximum (FWHM).

Azimuthal WAXD scanning was able to provide information about effect of Fe_3O_4 MNPs loadings on polymer orientation in the fiber. As seen in Figure 4.15, the crystal ring of PVOH polymer became wider and less focused as MNPs loading increased, and eventually the ring disappeared when MNPs concentration reached 40%wt. The bright dots in the rings represented preferred polymer orientation direction, which was along fiber axis at ϕ~90°.

The preferred polymer orientation factor (f) was calculated with Herman's equation (Equation 4-5 and 4-6) along fiber axis direction. [81, 82] The results (**Table** 4.9) showed a decrease trend on preferred polymer orientation factor from 0.87 for pure polymer fibers to 0.23 for magnetic fibers with 40%wt MNPs loading, implying polymers were less aligned with the addition of MNPs. This negative effect of MNPs on polymer orientation has been reported in the literature before, for instance, An-ting Chien stated a reduction of polymer orientation in magnetic PAN fibers with 10%wt MNPs loading compared to its pure polymer fibers.[32]

$$cos^2\phi = \frac{\int_0^{\pi/2} I(\phi) cos^2\phi \sin\phi d\phi}{\int_0^{\pi/2} I(\phi) \sin\phi d\phi} \quad 4\text{-}5$$

Where ϕ is the azimuthal angle as shown in Figure 4.15, and $I(\phi)$ is the scattered intensity at angle ϕ.

$$f = \frac{1}{2}(3cos^2\phi - 1) \quad 4\text{-}6$$

Where *f* is the Herman's orientation factor. When *f* = 1, all polymers align along reference direction; when *f = 0*, all polymers are randomly oriented without preference along reference direction; and when *f*=-0.5, all polymers align perpendicular to reference direction.

For Fe_3O_4 MNPs, the peak of 2θ =35.5° as Fe_3O_4 MNPs phase 311 was chosen as the identical peak. This intensity pattern (Figure 4.14) grew from flat to a tall and sharp peak as MNPs concentration increased as expected. Despite of MNPs loading ratios, the 2θ angle of phase 311 remained in the range of 35.6- 35.9°, and the *d*-spacing value was stable, which implied the crystal cell structure of Fe_3O_4 MNPs stayed consistent despite of loading concentrations. The size of MNPs crystals decreased from 12.1 nm for PVOH-10%MNPs fibers to 9.8 nm for PVOH-60%MNPs fibers. It was interesting to notice the pattern of PVOH-60%MNPs fibers were very similar to that of pure Fe_3O_4 MNPs.

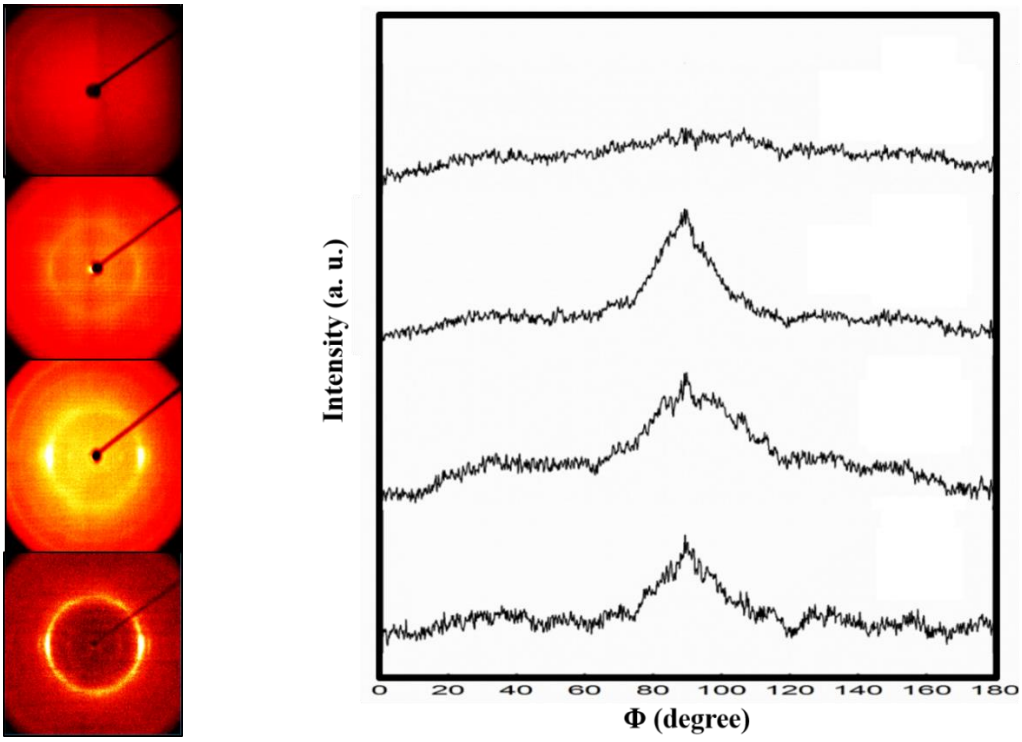

Figure 4.15 Azimuthal WAXD graphs (left) and their scattering intensity graphs (right) of PVOH fiber with MNPs loading (from bottom to top) at 0%wt, 10%wt, 20%wt, 40%wt.

Table 4.10 Crystal structure of Fe_3O_4 MNPs in fibers with 0%wt- 60%wt MNPs.

Fiber system	PVOH-0%MNPs	PVOH-10%MNPs	PVOH-20%MNPs	PVOH-40%MNPs	PVOH-60%MNPs	Bare 20nm Fe_3O_4 MNPs
2θ (°) *	--	35.9	35.7	35.6	35.6	35.6
d-spacing (Å) *	--	2.52	2.52	2.52	2.52	2.52
Crystal size (nm) *	--	12.1	11.6	11.5	10.9	9.8

* 2θ, d-spacing, and crystal size were based on Fe_3O_4 311 crystal phase.

The effects of drawing on fiber crystal structure has barely been studied on magnetic fibers before, especially when MNPs loadings exceeded a high concentration of 10%wt. In this section,

the author briefly studied the effect of drawing on the crystal structure of magnetic fibers PVOH-10%MNPs and PVOH-20MNPs fibers.

For magnetic fiber system of 10%wt MNPs loading ratio, the polymer crystallinity increased along drawing, as the relative height of polymer crystal peaks over MNPs crystal peak (Figure 4.17 right) grew higher with draw ratio. The preferred polymer orientation also developed to a higher value under drawing for 10%wt magnetic fibers, which was displayed as the more focused crystal rings and higher peak value in Azimuthal patterns (Figure 4.17). However, for PVOH-20%MNPs magnetic fibers, neither the crystal ring or scattering peak density had improved obviously with the increase of draw ratio (Figure 4.18).

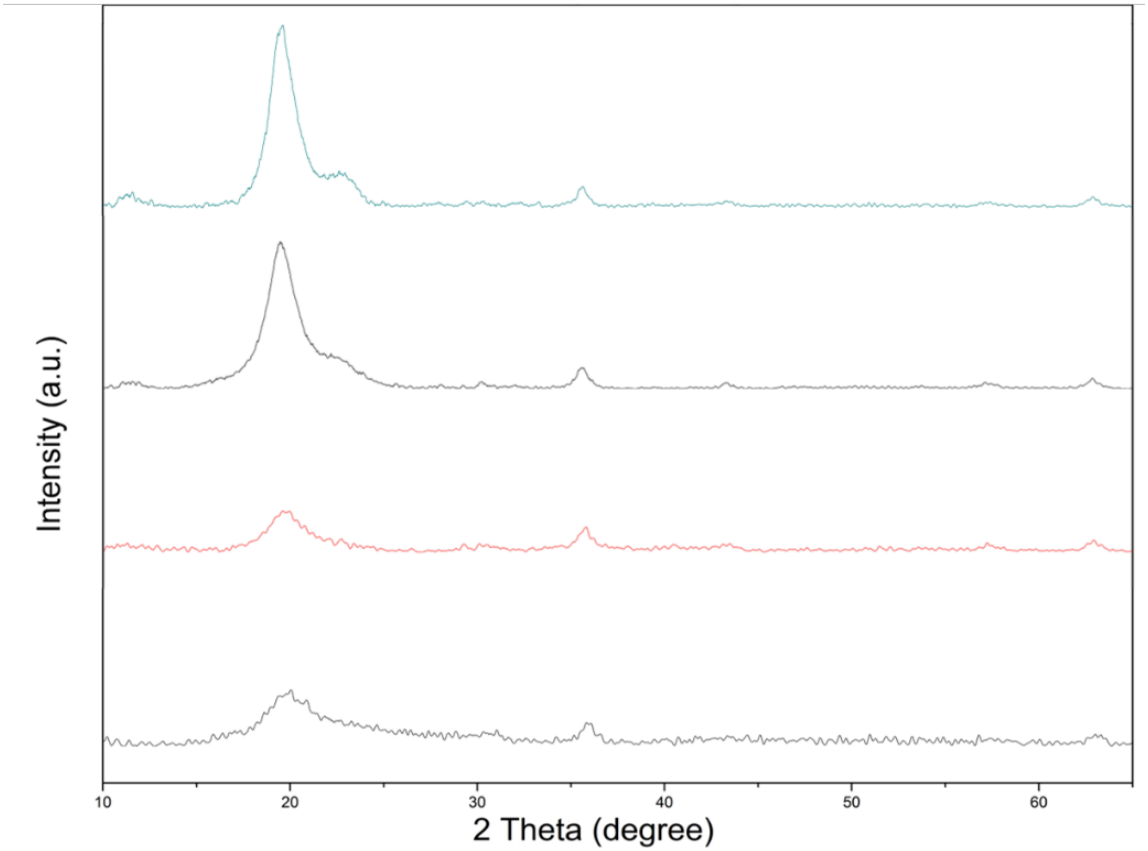

Figure 4.16 1D WAXD graphs of PVOH-10%MNPs fibers against draw ratio, from bottom to top, nominal DR=1.0, 1.5, 3.0, 4.5.

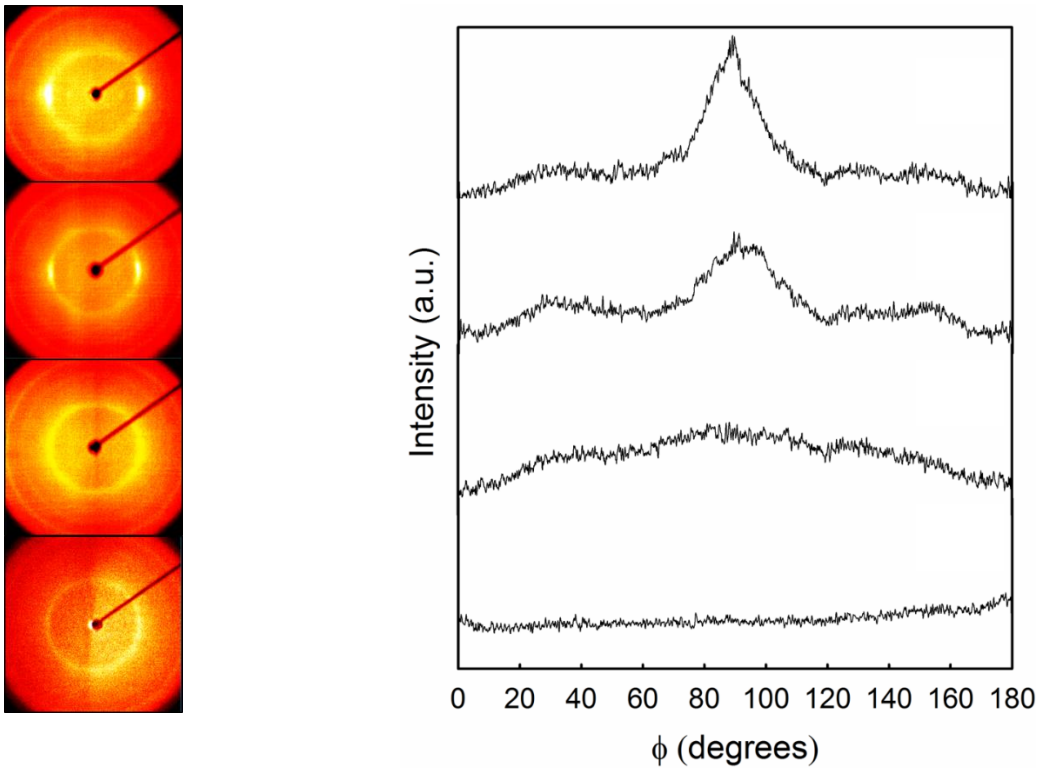

Figure 4.17 Azimuthal WAXD graphs (left) and 1D WAXD graphs (right) of PVOH-10%MNPs fibers against draw ratio, from bottom to top, nominal DR=1.0, 1.5, 3.0, 4.5.

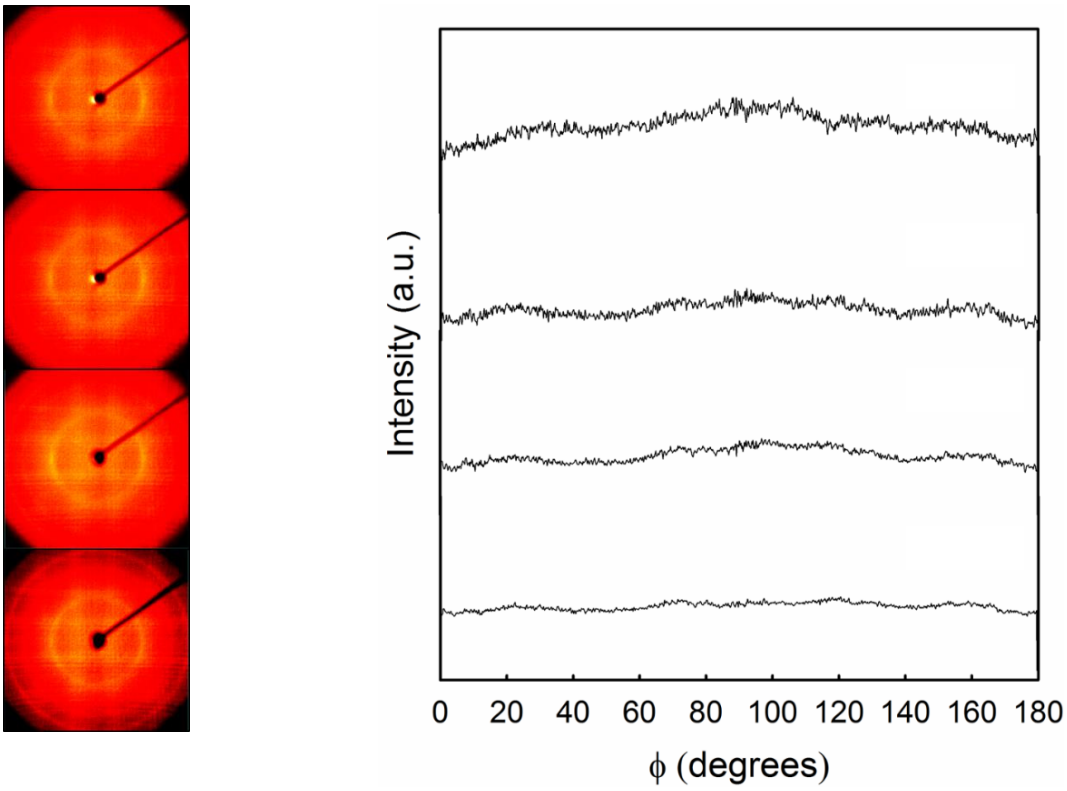

Figure 4.18 Azimuthal XRD graphs and their scattering density graphs of PVOH-20%MNPs fibers against draw ratio, from bottom to top, nominal DR=1.0, 1.5, 3.0, 4.5.

In summary, the presence of Fe_3O_4 MNPs had little influence on packing density of polymer crystal structure but led to smaller polymer crystals in size. The polymer crystallinity and preferred polymer orientation was weakened as the increase of Fe_3O_4 MNPs loading. These were the results of the interruption of polymer crystal development by the MNPs. Drawing was found effective to improve polymer crystallinity and polymer orientation at MNPs loading of 10%wt, but it was less effective at higher MNPs loadings. For Fe_3O_4 MNPs, the crystal packing density remained consistent no matter in the format of bare particles or embedded in magnetic fibers, while the crystal size of Fe_3O_4 MNPs was larger for MNPs embedded in polymer matrix.

4.2.3 Thermal Performance

Thermal performance is an important factor that determines fiber application range. Some previous research has revealed an enhancement on fiber thermostability when MNPs concentration was very low in the system. However, fiber thermostability will be sacrificed as the MNPs loading continues to grow, since the development of polymer crystals will be hindered by too many MNPs. There have been few studies about the effect of MNPs on magnetic fiber thermal properties beyond the loading ratio of 10%. In this section, magnetic fiber thermostability was explored with magnetic fibers with MNPs loading of 0%-60%wt.

The TGA result curves were displayed in Figure 4.19, with weight loss analysis in Figure 4.21. The estimated MNPs loading for each magnetic fiber system was calculated upon TGA residue weight with the equations described in Section 4.1.3, and the results were summarized in Figure 4.20.

Upon the comparison among TGA curves (Figure 4.19), the overall weight loss of fibers after the decomposition decreased as the MNPs loading increased. Since PVOH polymers completely disappeared after TGA process while the Fe_3O_4 MNPs had residues, the higher MNPs loading there was in the fiber, the higher residue weight the sample would remain.[32] Previous study conducted by Zhu J reported the reduction of weight loss for magnetic PAN fibers with the increased concentration of Fe@FeO MNPs.[35]

Under the assumption that Fe_3O_4 MNPs were completely converted into Fe_3C compound after the decomposition process, the MNPs loadings in each fiber system could be estimated from the remaining weights as described in Section 4.1.3. From the calculation (Figure 4.20), it was found that most magnetic fibers (PVOH-10%MNPs, PVOH-20%MNPs, PVOH-40%MNPs) contained higher MNPs loading than that initially added into the spinning dopes. The highest

MNPs loading achieved in this study was 56.6%wt for PVOH-60%MNPs fibers, equivalent to 23.8%vol, which was a very high loading for inorganic nanoparticle in polymer system.

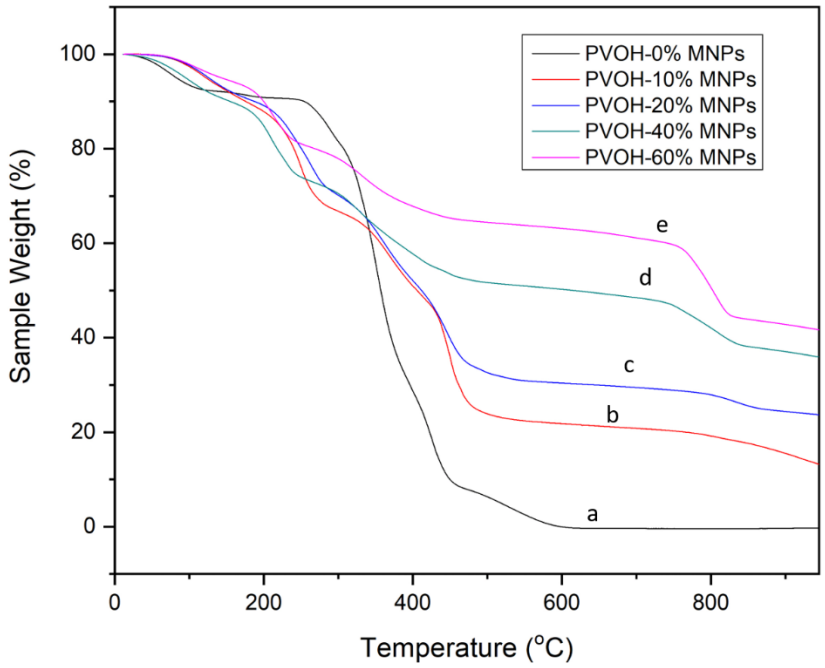

Figure 4.19 TGA graphs of PVOH fibers with different MNPs loadings, from bottom to top, a) 0%wt, b) 10%wt, c) 20%wt, d) 40%wt, e) 60%wt.

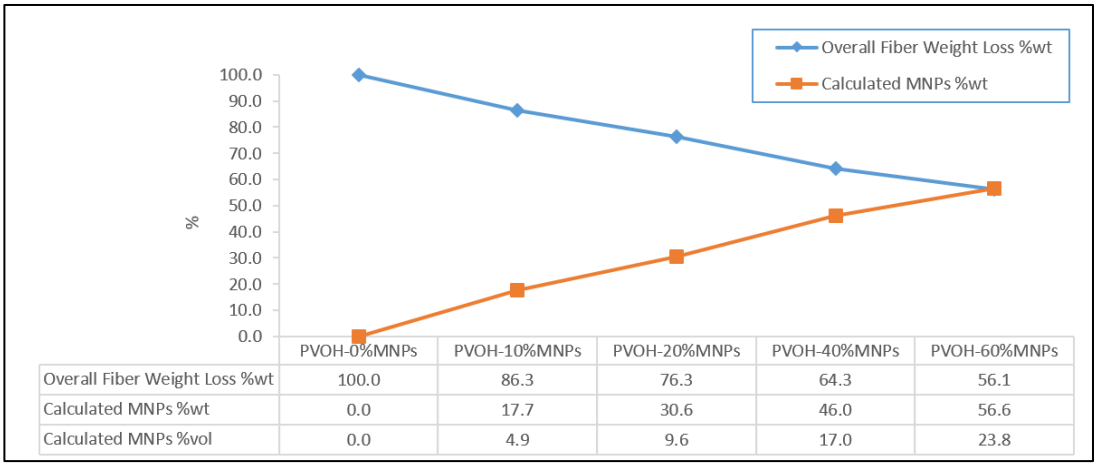

	PVOH-0%MNPs	PVOH-10%MNPs	PVOH-20%MNPs	PVOH-40%MNPs	PVOH-60%MNPs
Overall Fiber Weight Loss %wt	100.0	86.3	76.3	64.3	56.1
Calculated MNPs %wt	0.0	17.7	30.6	46.0	56.6
Calculated MNPs %vol	0.0	4.9	9.6	17.0	23.8

Figure 4.20 TGA results and estimated MNPs loadings accordingly of PVOH fibers with different initial MNPs loadings of 0%wt, 10%wt, 20%wt, 40%wt, 60%wt.

A detailed investigation of weight loss at different temperature stage was conducted to understand the impact of MNPs on fiber decomposition process (Figure 4.21).

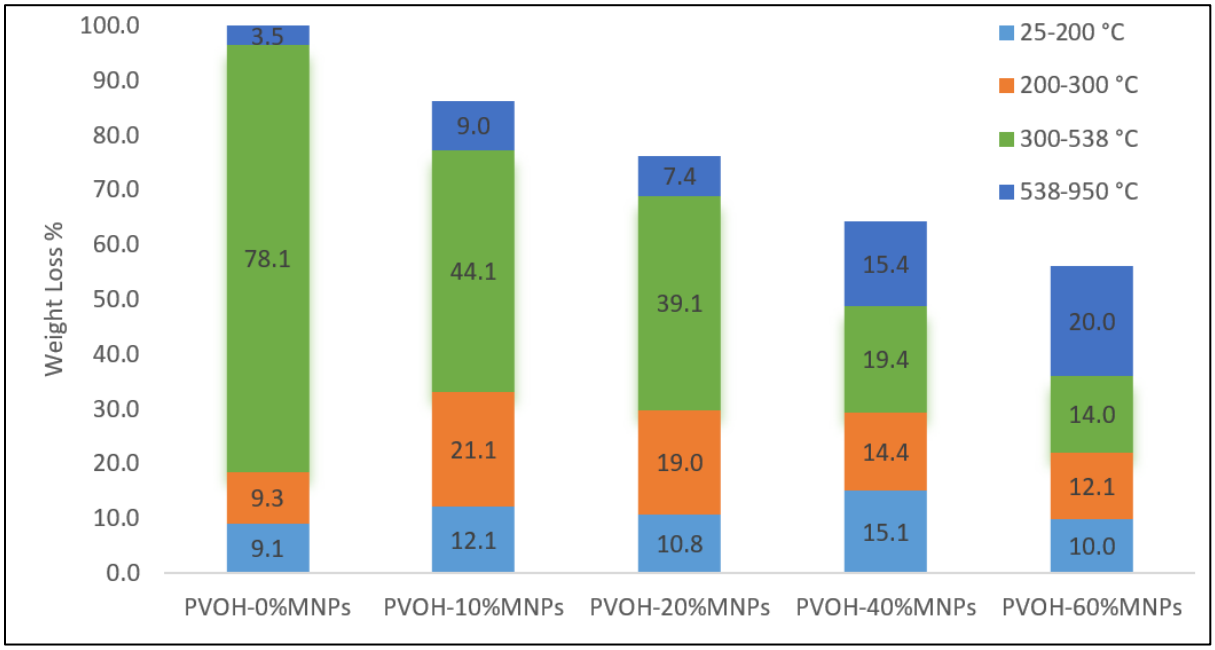

Figure 4.21 Weight loss analysis in TGA decomposition for PVOH fibers with different MNPs loading from 0% to 60%, the temperature range are divided (from bottom to top) as 25-200°C, 200-300°C, 300-538°C, 538-950°C.

From the analysis, the weight loss of fibers below 200°C was in the range of 9%-15%wt across the fiber systems, which was mainly due to moisture evaporation and solvent volatilization without major polymer decomposition.[67]

In the temperature range of 200°C to 300°C, pure PVOH fibers had a weight loss of 9%, while all magnetic fibers experienced a higher weight loss, such as 21%wt for PVOH-10%MNPs fibers, 19%wt for PVOH-20%MNPs fibers. This increased weight loss was due to the reduction of the crystallinity of polymers in magnetic fibers, since amorphous regions had lower degradation temperature than crystal regions.

The major weight loss of fibers occurred in the temperature range of 300- 538°C, in which PVOH polymers dehydrated into volatile products along with polymer chains breaking down, as well as continued decomposition of Fe_3O_4 MNPs.[77] It was found that pure PVOH fibers experienced 78% weight loss in this range, while magnetic PVOH fibers experienced much lower weight loss (e.g. 44% weight loss for PVOH-10%MNPs, 14% weight loss for PVOH-60%MNPs). This trend was mainly the result of less polymer quantity content in the fiber system as MNPs concentration increased, but also because lower crystallinity had shifted some polymer decomposition to lower temperature range.

Above 538°C, pure PVOH fibers experienced 4% weight loss, while fibers with MNPs had much higher weight loss, which was due to Fe_3O_4 MNPs continuous carbonization into Fe_3C. The weight loss in this temperature range increased as the MNPs loading grew, as the weight loss of pure PVOH fibers was 4%wt, and that of PVOH-60%MNPS was 20%wt, except that PVOH-20%MNPs system did not show an increase on value compared to PVOH-10%MNPs.

The optical image after TGA process was shown in Figure 4.22, which was from PVOH-20%MNPs magnetic fibers. It appeared the fiber sample had retained its fiber shape with a hollow core structure after degradation. The red color is likely from Fe_2O_3, which composite was formed as air purged into the chamber after the decomposition process.

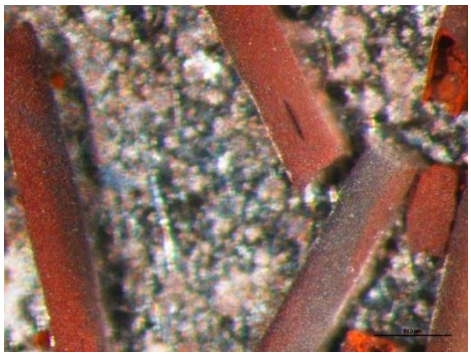

Figure 4.22 Optical image of PVOH-20%MNPs fibers after TGA process and air purging.

In summary, the overall weight loss of fibers decreased as MNPs loading increased for magnetic fibers. Fibers with higher MNPs concentration degraded faster in this process due to lower crystallinity of polymers caused by the incorporation of MNPs. Magnetic fibers presented fiber shape with hollow core after decomposition process. The actual MNPs loadings in magnetic fiber systems were estimated based on TGA residue weight.

4.2.4 Mechanical Properties

Mechanical performance is one of the essential properties for fibers, as it directly determines the application range of final products. In the literature, most of the mechanical performance studies were conducted on magnetic fibers with MNPs loadings less than 10%wt, and there were few studies done on fibers with high MNPs concentrations. In this section, the author studied the mechanical properties of magnetic fibers in a wide range of 0%- 60%wt MNPs loadings with single fiber tensile strength test.

As shown in Table 4.11, fiber tensile strength was measured between 18 MPa and 117 MPa for all fibers. Compared to the tensile strength of pure PVOH fibers reported (10 MPa- 6GPa) in the literature, the values of these magnetic fibers were on the lower side due to incorporation of MNPs. The relatively high values of elongation ratio at breaking indicated the fibers were not fully drawn, which was mainly limited by the current drawing setup. This could possibly be improved with a milder drawing condition such as a heating bath in the future. Current tensile results presented no correlation between tensile strength and MNPs loadings.

Young's modulus was calculated and plotted for each fiber system against draw ratio in Figure 4.24. For each fiber system, Young's modulus increased as the draw ratio became higher. For instance, PVOH fiber improved from 18 MPa to 47 MPa through drawings, while PVOH-60%MNPs fibers increased from 2 MPa to 9 MPa along the drawing process. These results implied

that drawing could improve fiber strength for magnetic fibers, but the improvement was less effective as MNPs loadings increased.

Table 4.11 Tensile results of fibers with 0%wt- 60%wt MNPs.

Fiber system	Tensile strength (MPa)	Elongation at break (%)
PVOH-0%MNPs	52.8 ± 8.5	6.6 ± 0.9
PVOH-10%MNPs	113.8 ± 18.0	20.3 ± 3.7
PVOH-20%MNPs	44.3 ± 8.0	55.3 ± 12.1
PVOH-40%MNPs	79.4 ± 4.0	117.4 ± 32.6
PVOH-60%MNPs	18.5 ± 2.1	93.4 ± 14.1

Between fiber systems at the same draw ratio, Young's modulus decreased as the MNPs loadings increased, which was true at all draw ratios. This trend agreed with the previous studies, for example, Lin reported a reduction of 50% on fiber initial modulus for PVOH fibers with 18%wt magnetic iron embedded.[33] This negative impact of MNPs loading on fiber mechanical performance at high loading was mainly due to the reduced polymer crystallinity and less polymer content in the product.

Young's modulus was also plotted per polymer weight in each fiber system, with the polymer ratio estimated from TGA results. As shown in Figure 4.23, pure PVOH fiber exhibited the highest Young's modulus per polymer weight, and the modulus value decreased as the MNPs loading increased.

In summary, Young's modulus of magnetic fibers decreased with the increase of MNPs loadings, as the combination result from lower polymer crystallinity (Section 4.2.2) and less polymer content in fibers. Specifically, MNPs had negative effect on polymer mechanical strength, as the Young's modulus per polymer weight decreased with the increase of MNPs loading.

Drawing was found capable of improving fiber mechanical performance, but it was less effective when MNPs loading became higher.

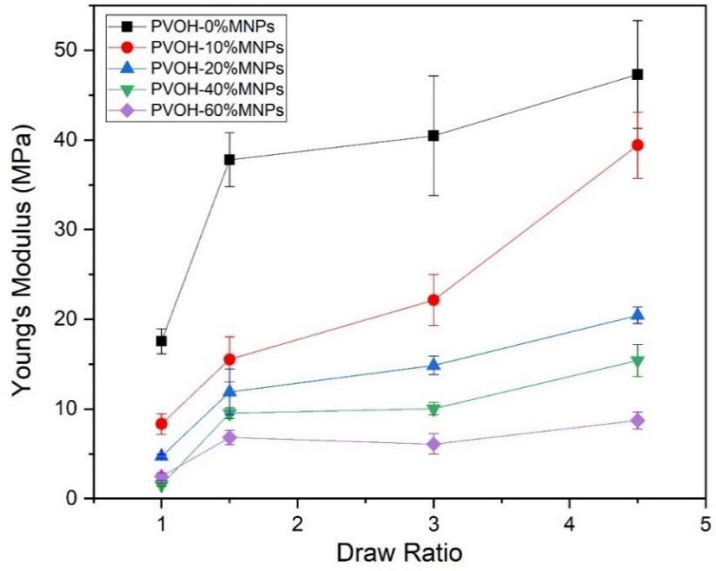

Figure 4.23 Young's modulus (MPa) against draw ratio for PVOH fibers with MNPs loadings from 0%wt to 60%wt.

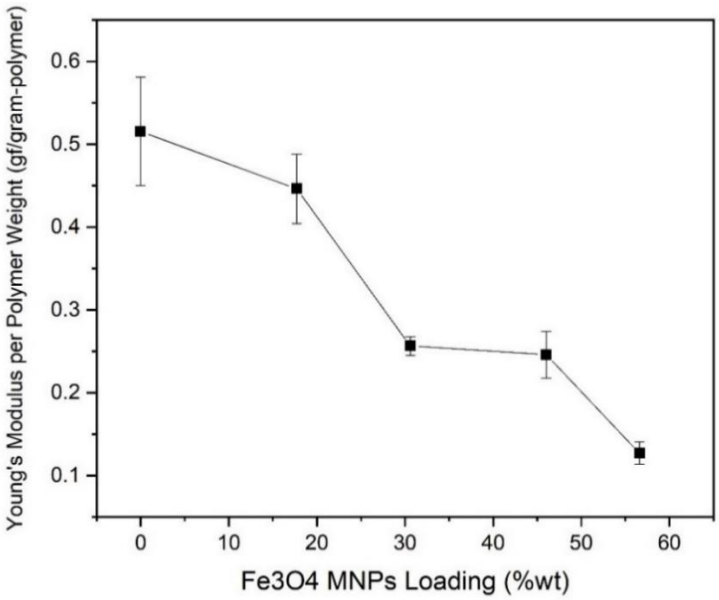

Figure 4.24 Young's modulus (gf/polymer denier) for post-drawn PVOH fibers with different MNPs loadings from 0%wt to 60%.

4.2.5 Magnetic Performance

It is essential to study the magnetic performance of magnetic fibers to determine the application range as magnetic materials. The magnetization value of magnetic fibers (emu/gram-fiber) was plotted against external magnetic field (T) as shown in Figure 4.25, with major characteristics summarized in Table 4.12, including saturation value (M_S), remnant value (M_R), and estimated MNPs loadings.

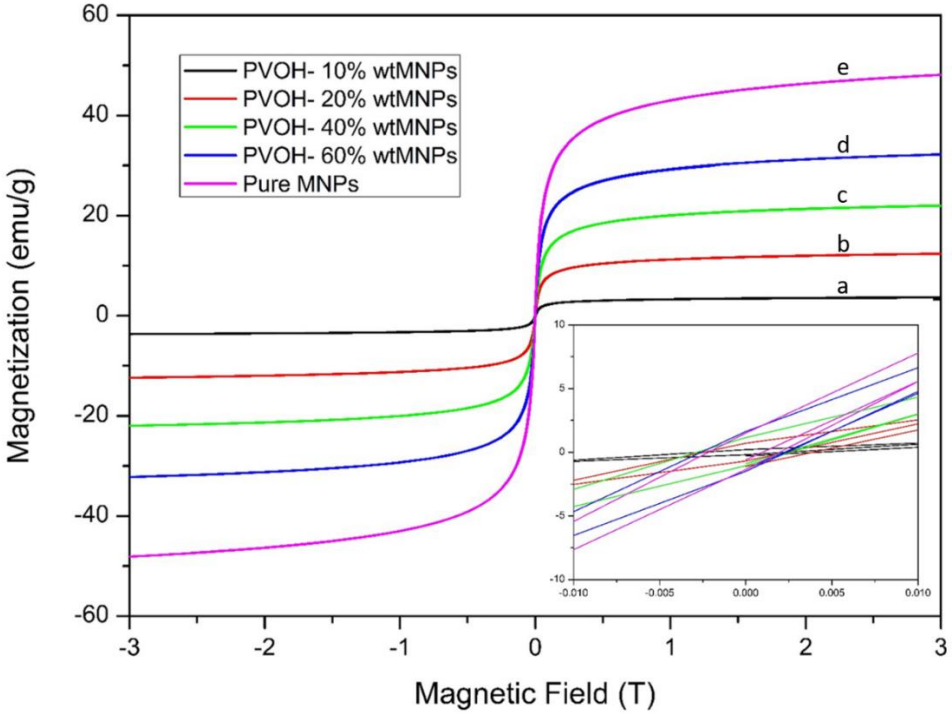

Figure 4.25 Magnetic hysteresis loops of PVOH magnetic fibers and pure Fe_3O_4 MNPs in external magnetic field of -3T ~3T: a) PVOH-10%MNPs fibers, b) PVOH-20%MNPs fibers, c) PVOH-40%MNPs fibers, d) PVOH-60%MNPs fibers, and e) bare 20nm Fe_3O_4 MNPs.

All hysteresis loops of magnetic fibers followed the trend of superparamagnetic 20nm Fe_3O_4 MNPs that were embedded. The saturation magnetism value (M_S) increased as the MNPs loading increased. Since M_S were considered solely determined by MNPs weight ratios, the actual MNPs loading was estimated with M_S values via Equation 4-7. The calculated MNPs loadings

(Table 4.12) confirmed the MNPs loadings added initially in the spinning dope, and most fiber systems (PVOH-20%MNPs, PVOH-40%MNPs, PVOH-60%MNPs) demonstrated higher MNPs loadings in fiber than the values in the initial solution. This estimated MNPs loadings were comparable to the ones calculated from TGA characterization for most magnetic fiber systems, except for PVOH-10%MNPs system which has been discussed in Section 4.1.5.

Table 4.12 Magnetism results and MNPs ratio estimation of fibers.

Fiber system	Saturated value, M_S, (emu/g)	Coercivity per fiber weight, $H_{C\text{-}fiber}$, (Oe/g)	Coercivity per MNPs weight, $H_{C\text{-}MNPs}$, (Oe/gram-MNPs)	Remnant value, M_R, (emu/g)	MNPs loading estimated from SQUID (%wt)	MNPs loading estimated from TGA (%wt)
PVOH-10%MNPs	3.6	24	240	0.1	7.5%	17.7%
PVOH-20%MNPs	12.3	25	125	0.7	25.7%	30.6%
PVOH-40%MNPs	22.0	25	63	1.1	45.9%	46.0%
PVOH-60%MNPs	32.1	26	43	1.6	67.0%	56.6%
Bare Fe_3O_4 MNPs	47.9	23	23	1.5	--	--

$$\textbf{MNPs \%wt in Fiber} = \frac{\boldsymbol{M_R(magnetic\ fiber)}}{\boldsymbol{M_R\ (Virgin\ MNPs)}} \times \mathbf{100}\% \qquad 4\text{-}7$$

The coercivity (H_C) represents the ability of magnetic fibers to withstand external magnetic field without becoming magnetized, which is the internal reverse driving field to demagnetize the external magnetic field. The higher H_C is, the higher resistance the material exhibits to withstand external magnetic field. As presented in Table 4.12, all magnetic fibers had similar $H_{C\text{-}fiber}$ values of 23-26 Oe/gram-fiber. However, once H_C was corrected to per MNPs weight ($H_{C\text{-}MNPs}$), PVOH-10%MNPs fibers displayed a significant high coercivity value at 240 Oe/gram-MNPs compared

to 23 Oe/gram-MNPs for pure MNPs, which was known as MNPs hardening effect. The finding agreed with earlier research work, for instance, Di Zhang[30] reported the MNPs hardening effect of $H_{C\text{-}MNPs}$ =20.1 Oe for pure MNPs to $H_{C\text{-}MNPs}$= 206 Oe once dispersed in polymer matrix. This hardening effect was because the dipole-dipole interaction among MNPs was reduced once embedded in polymer matrix, and therefore the magnetism of each MNPs was enhanced. This MNPs hardening effect was weakened as the MNPs concentration increased.

Another magnetism characteristic is remnant value (M_R), which represents the remaining magnetism in material (M_R, *emu/g*) once external magnetic field is removed (at $x=0$). A magnified plot of M_R for all magnetic fibers was seen in Figure 4.25 , with M_R values summarized in Table 4.12. It was observed that M_R values of all fibers and virgin MNPs were small but not zero, which was due to the magnetically soft nature of MNPs. The M_R value of magnetic fibers increased as the MNPs loadings grew, and PVOH-60%MNPs magnetic fibers reached a similar value to that of virgin MNPs.

In summary, the highest saturation magnetism value (*Ms*) was achieved with 60%wt MNPs magnetic fiber system at 32.1 emu/g, as of 67% compared to pure Fe_3O_4 MNPs value. To the author's best knowledge, this was the highest magnetic response and highest MNPs loading of magnetic fibers available in the literature so far, especially with full scope of fiber properties analysis. Along MNPs loading from 10%wt to 60%wt MNPs, all magnetic fibers presented superparamagnetic behaviors consistent with the 20nm Fe_3O_4 MNPs embedded. Magnetic hardening effect was observed on MNPs in fibers, which became stronger as MNPs concentration was smaller. The M_S of magnetic fibers increased as MNPs loading became higher, and MNPs loading estimation from SQUID results verified the MNPs concentration in each fiber system.

4.2.6 Summary

The major achievement in this section was the successful production of superparamagnetic fibers with the highest magnetism saturation value (*Ms*=32.1 emu/g) in the literature, which was 67% of bare Fe_3O_4 MNPs. This high *Ms* was achieved with a high MNPs loading around 60%wt (estimated 56.6%wt in TGA, estimated 67.0% in SQUID), which was also the highest MNPs loading for magnetic fibers available in the literature. This magnetic fiber system with high MNPs loading showed decent mechanical properties as fiber. Besides, the effect of MNPs concentration on magnetic fiber properties in a wide MNPs loading range of 10- 60%wt was studied for various fiber properties.

All magnetic fiber revealed a quite uniform shape without spindles, and the fiber structure was quite dense with MNPs distributed all over the area. The diameter of magnetic fibers maintained in the same range as pure PVOH fibers. The polymer crystallinity and crystal size decreased as the MNPs loading increased, which was mainly due to the interruption of polymer crystal development by MNPs. Correspondingly, the thermo-degradation for magnetic fibers became faster as MNPs loading grew, as a result of more polymer amorphous regions in the structure. The stiffness of fibers decreased with the increase of MNPs concentration, which was the combination outcome of lower polymer crystallinity and less polymer content in the product. The magnetism performance of fibers was consistent with the superparamagnetic Fe_3O_4 MNPs embedded, and the magnetic saturation value (*Ms*) increased for magnetic fibers with the increase of MNPs loading. MNPs hardening effect was observed in magnetic fibers, and the effect was stronger in low MNPs loading systems. The actual MNPs loadings in magnetic fibers were estimated from TGA residue weight as well as from magnetic saturation values, and the results verified the high MNPs concentrations added in the initial spinning solution.

Drawing was found as an effective method to increase magnetic fiber crystallinity as well as mechanical performance. The Young's modulus of magnetic fibers with high MNPs loading at 60%wt could still be enhanced via drawing, but the improvement was much smaller compared to the ones with lower MNPs ratios.

It is worthwhile to mention that polymer solution with 80%wt MNPs loading was attempted for spinning, but it failed to produce continuous fibers as product. It is still of interest to try higher MNPs loadings, which might be feasible with the presence of additives or upon surface modification of MNPs.

4.3 Effects of MNPs Species on Magnetic Fiber Performance

Magnetic fibers with 20nm superparamagnetic Fe_3O_4 MNPs was successfully spun and characterized at a high MNPs loading of 60%wt. It is considered more challenging to incorporate MNPs with large diameters into magnetic fibers, especially at high MNPs loadings, because large MNPs are more likely to agglomerate to form defects which compromises fiber properties.[30] In this section, PVOH-60%-MNPs-80nm fibers were produced and characterized, and the effects of MNPs species (superparamagnetic and ferromagnetic MNPs) on magnetic fiber were studied with fiber property including microstructure, crystal structure, thermal performance, mechanical properties, and magnetic performance.

4.3.1 Fiber Microstructure

The microstructure of magnetic fibers was studied with optical and confocal microscopes, including fiber diameter, fiber surface, cross-section, and MNPs distribution. Unless otherwise stated, all fiber samples in this section were the post-drawn fibers from each spinning system.

The fiber surface was captured with optical microscope (**Figure 4.26**), in which both magnetic fibers showed smooth skin and consistent diameters without spindle-shape. This suggested both spinning solutions were homogenous, and the fiber production process was effective. A closer look at the fiber surface by confocal microscope (**Figure 4.27**) displayed some MNPs clusters as bright dots, while the surfaces were still relatively smooth for both fibers.

The cross-section of PVOH-60%MNPs-20nm magnetic fibers (**Figure 4.28**b) displayed an oval-shape cross-section that was similar to pure PVOH fibers (**Figure 4.28**a); while PVOH-60%MNPs-80nm fiber (**Figure 4.28**c) had more irregular cross-section shape. Since the nascent fiber of PVOH-60%MNPs-80nm system were more in oval-like shape as displayed in **Figure 4.28**d, the irregular shape of post-drawn fibers was likely formed during drawing. The diameters

of both magnetic fibers were similar in value (Table 4.13), which was much higher than the diameter of pure PVOH fibers.

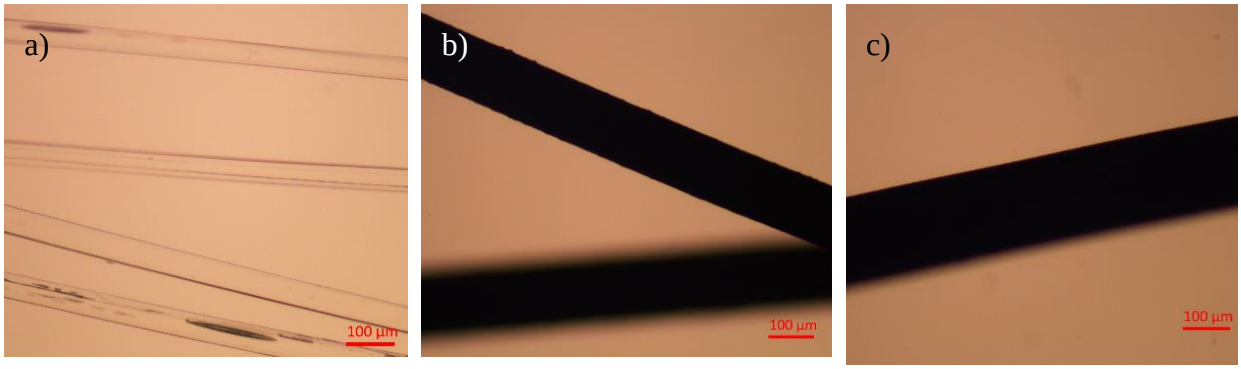

Figure 4.26 Optical images of pure PVOH fibers and magnetic PVOH fibers with different MNPs species at MNPs loading of 60%wt: a) PVOH-0%MNPs fibers, b) PVOH-60%MNPs-20nm fibers, c) PVOH-60%MNPs-80nm fibers.

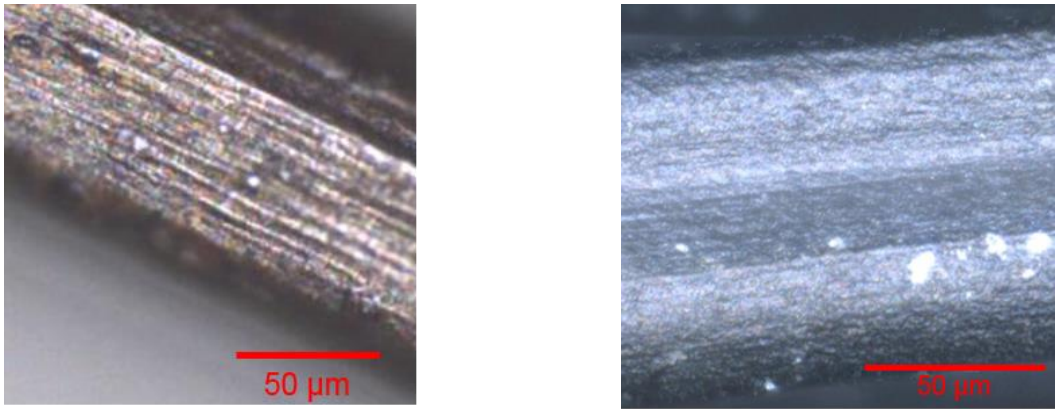

Figure 4.27 Confocal images of fiber surfaces for PVOH magnetic fibers with different MNPs species at MNPs loading of 60%wt: (left) PVOH-60%MNPs-20nm fibers, (right) PVOH-60%MNPs-80nm fibers.

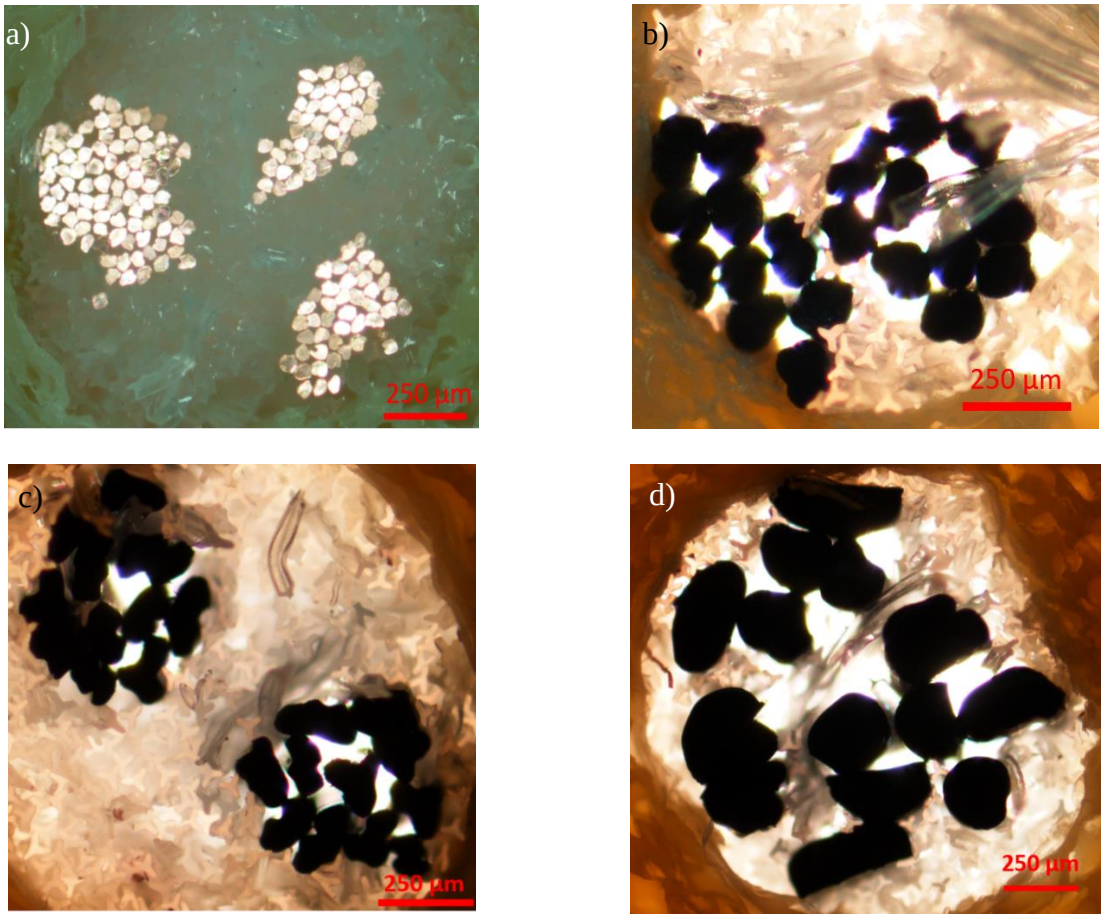

Figure 4.28 Cross-section optical images of pure PVOH fibers and magnetic PVOH fibers with different MNPs species at MNPs loading of 60%wt: a) PVOH-0%MNPs post-drawn fibers, b) PVOH-60%MNPs-20nm post-drawn fibers, c) PVOH-60%MNPs-80nm post-drawn fibers, d) PVOH-60%MNPs-80nm as-spun fibers.

Table 4.13 Fiber systems for the study of MNPs species effects.

Fiber system *	Initial MNPs loading (%wt)	Post-drawn fiber diameter (µm) **
PVOH-0%MNPs	0	54
PVOH-60%MNPs-20nm	60	138
PVOH-60%MNPs-80nm	60	117

*The spinning dopes consisted of PVOH polymer (Mw= 146,000-186,000) at ~10 g/dl in pure DMSO solvent.

**The draw ratio for all fibers was 4.5.

Both magnetic fibers showed dense structure without many voids in the cross-section (Figure 4.4), which was a good sign for mechanical strength. The MNPs agglomeration (bright dots in the images) distributed all over the cross-section area, while the clusters appeared much larger in size for the PVOH-60%MNPs-20nm fibers compared to PVOH-60%MNPs-80nm fibers, which could possibly lead to compromised mechanical performance for the former fiber system.

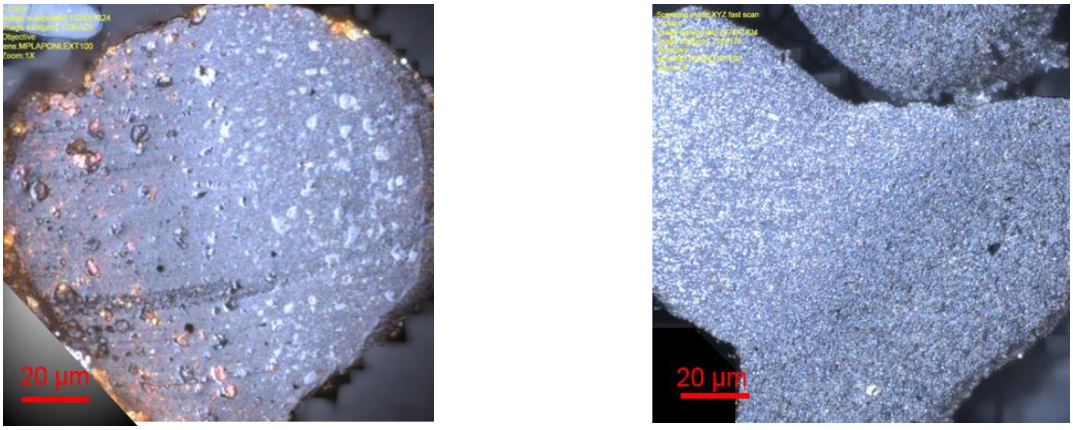

Figure 4.29 Confocal images of magnetic PVOH fibers with different MNPs species at 60%wt MNPs loading: (left) PVOH-60%MNPs-20nm fibers, (right) PVOH-60%MNPs-80nm fibers.

In summary, both magnetic fibers with 20nm and 80nm Fe_3O_4 MNPs at high loading of 60%wt presented a bead-free shape with relatively smooth surface. The diameters of these magnetic fibers were in the comparable range and were much higher than pure PVOH fibers. The shape of magnetic fibers cross-section with 20nm MNPs was oval-like, while magnetic fibers with 80nm MNPs was more irregular. Magnetic fiber with 80nm MNPs had finer MNPs clusters and was possible to exhibit better mechanical performance.

4.3.2 Crystal Structure

The crystal structure provides structure information about fibers at molecular level. In this section, WAXD analysis of both one-dimensional scanning and azimuthal scanning were employed for such purpose.

Upon the WAXD graphs (Figure 4.30), both magnetic fibers presented clear and sharp crystal peaks for MNPs but barely noticeable peaks for polymer phase. This indicated that MNPs maintained crystal phase and fiber polymers were mostly in amorphous state in these magnetic fibers The crystal peaks of MNPs for both magnetic fibers matched the pattern of their bare MNPs quite well, which agrees with previous work[9].

In Azimuthal WAXD scanning, neither of the magnetic fibers showed clear crystal rings (for crystal regions) nor bright dots (for preferred fiber orientation direction) like those in pure PVOH fibers (Figure 4.31). The bright blurs of magnetic fibers were mostly from the scattering effects of Fe_3O_4 MNPs.

In summary, PVOH polymers were mostly in amorphous phase in both magnetic fibers, and the MNPs were in crystal phase. The crystal peaks position of Fe_3O_4 MNPs remained consistent after MNPs embedded in polymer matrix for both magnetic fibers systems.

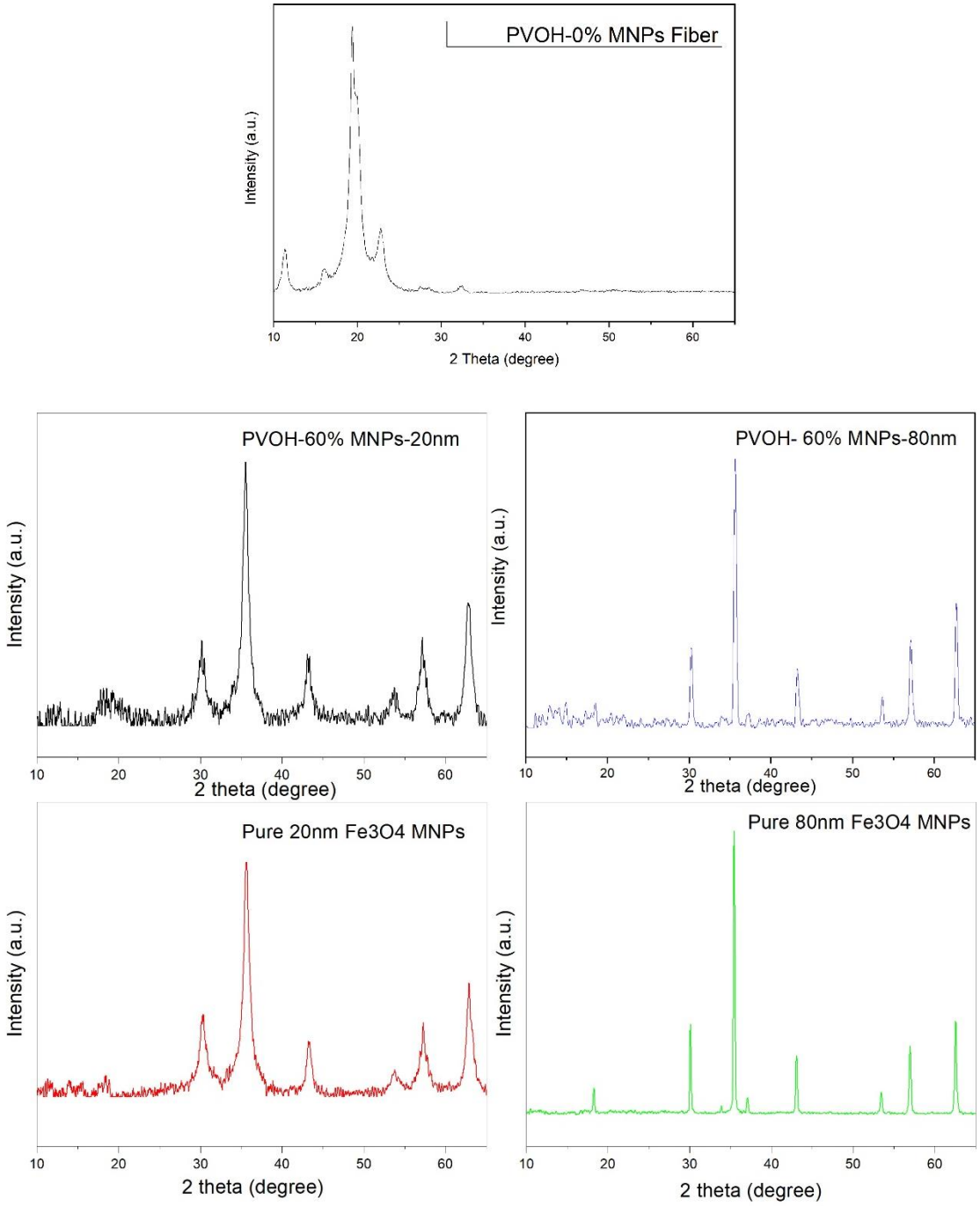

Figure 4.30 WAXD graphs of pure PVOH fiber, magnetic PVOH fibers with different MNPs species at MNPs loading of 60%wt, and corresponsive bare MNPs.

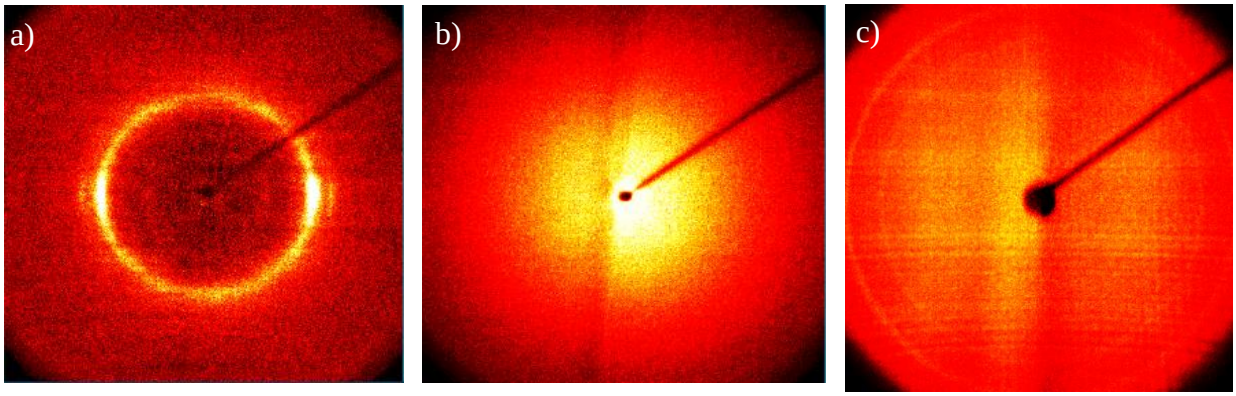

Figure 4.31 Azimuthal WAXD graphs of pure PVOH fibers and magnetic PVOH fibers with different MNPs species at MNPs loading of 60%wt: a) PVOH-0%MNPs fibers, b) PVOH-60%MNPs-20nm fibers, c) PVOH-60%MNPs-80nm fibers.

4.3.3 Thermal Performance

The effects of Fe_3O_4 MNPs species on fiber thermostability at high MNPs loading of 60%wt was investigated. The TGA curves were shown in Figure 4.32, with other results such as weight loss and estimated MNPs loading included in Table 4.14.

The overall decomposition curves of both magnetic fibers (Figure 4.32) were alike to each other. The final remaining weights were similar (44%wt and 47%wt), which were much higher than that of pure PVOH fibers. Assuming all Fe_3O_4 were converted into Fe_3C by the end of degradation, MNPs loadings in magnetic fibers were estimated. The PVOH-60%-20nm fibers exhibited MNPs loading of 61%wt, and the MNPs loading of PVOH-60%-80nm fibers was estimated at 57%wt. These calculated MNPs concentration were close to the original concentration in the initial spinning solution.

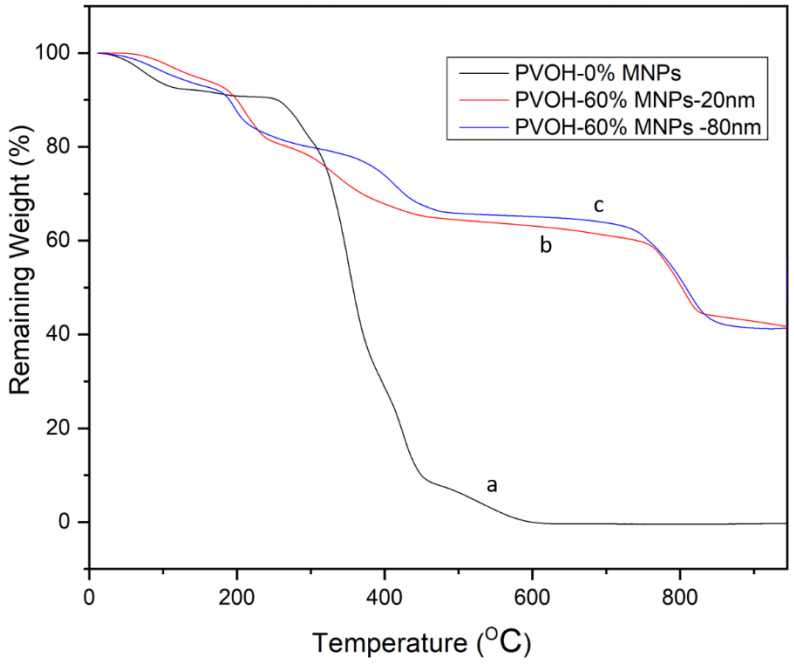

Figure 4.32 TGA graphs of pure PVOH fibers and magnetic PVOH fibers with different MNPs species at MNPs loading of 60%wt: a) PVOH-0%MNPs fibers, b) PVOH-60%MNPs-20nm fibers, c) PVOH-60%MNPs-80nm fibers.

Table 4.14 TGA results of fibers with 20nm and 80nm MNPs at 60%wt MNPs loading.

Fiber System	Remaining weight %wt	Calculated MNPs %wt
PVOH-0%MNPs	0.0	0.0
PVOH-60%MNPs-20nm	43.9	56.6
PVOH-60%MNPs-80nm	47.3	61.0

In summary, the decomposition process and overall weight loss of both magnetic fibers were similar despite the MNPs species. The actual MNPs loadings in fibers were verified upon TGA residue weight calculation.

4.3.4 Mechanical Properties

In this section, single fiber tensile strength was conducted on magnetic fibers at high MNPs loading 60%wt to study the mechanical performance. As shown in Table 4.15, Young's modulus

for both magnetic fibers were lower than that of pure PVOH fibers, indicating a negative effect of MNPs on fiber mechanical performance at such high loading. Young's modulus of 80nm MNPs fibers was higher than that of 20nm MNPs fibers, one reason for that could be the finer MNPs clusters in 80nm-MNPs fibers as displayed in the fiber cross-section images in Section 4.3.1.

Table 4.15 Tensile results of fiber with 20nm and 80nm MNPs at 60%wt MNPs loading.

Fiber system	Young's modulus (MPa)
PVOH-0%MNPs	47 ± 6
PVOH-60%MNPs-20nm	8.7 ± 0.9
PVOH-60%MNPs-80nm	21.9 ± 2.4

4.3.5 Magnetic Performance

The magnetic performance of both magnetic fibers with MNPs loading of 60%wt were shown in Figure 4.25, with major magnetism results summarized in **Table 4.16**, including saturation value (M_S), remnant value (M_R), and estimated MNPs loadings.

In the magnetism hysteresis loops (Figure 4.25), both magnetic fibers inherited the magnetism behaviors from the corresponding MNPs: PVOH-60%MNPs-20nm fibers presented superparamagnetic performance, while PVOH-60%MNPs-80nm fibers displayed ferromagnetism.

The magnetism saturation value (*Ms*) was 32.1 emu/g for PVOH-60%MNPs-20nm fibers and was 37.6 emu/g for PVOH-60%MNPs-80nm fibers, which values were among the highest magnetism response reported for magnetic fibers in the literature. The actual MNPs loadings was calculated as proportional to MNPs loading ratio. From the calculation, PVOH-60%MNPs-20nm fibers implied MNPs loading of 67.0%wt, and PVOH-60%MNPs-80nm fibers presented a lower MNPs loading ratio of 46.0%wt. The MNPs loadings estimated from TGA analysis and SQUID

were quite high for both systems, and the value difference between calculation method could be caused by the uneven MNPs distribution in fiber as well as by the small size of samples taken for each test.

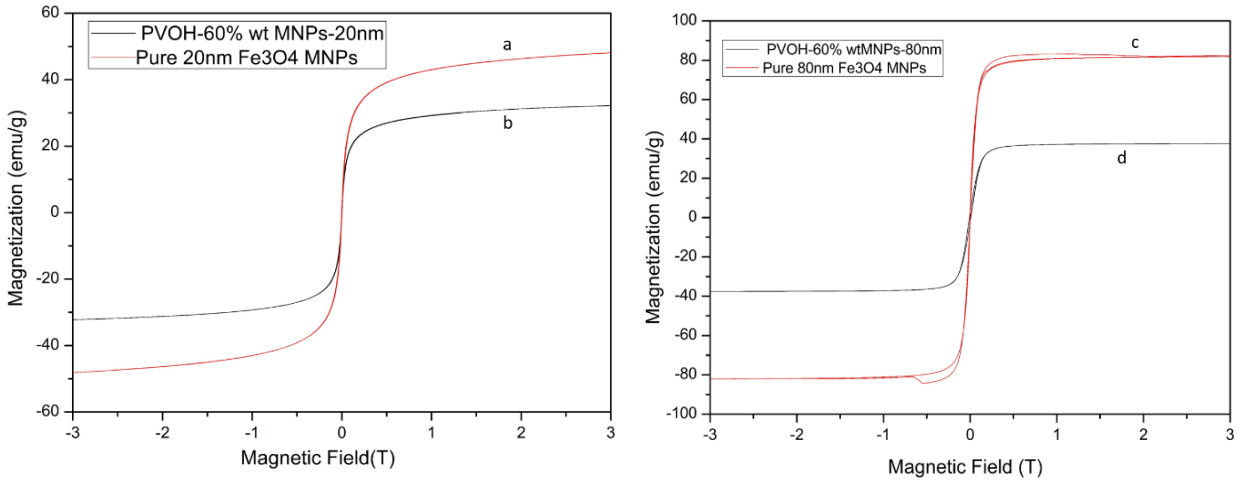

Figure 4.33 Magnetic hysteresis loops of PVOH magnetic fibers at 60% MNPs loading and their corresponsive bare Fe_3O_4 MNPs. Left: a) bare 20nm Fe_3O_4 MNPs, b) PVOH-60%MNPs-20nm fibers; Right: c) bare 80nm Fe_3O_4 MNPs, d) PVOH-60%MNPs-80nm fibers.

Both magnetic fibers exhibited a much higher coercivity value ($H_{C\text{-}MNPs}$) compared to bare MNPs, which was the result of MNPs hardening effect in polymer matrix. This hardening effect was more obvious for 80nm MNPs fibers than for 20nm MNPs. The remnant values (M_R) of both magnetic fibers and pure MNPs were close to zero as magnetically soft materials.

Overall, magnetic fibers inherited the magnetism behavior from the corresponsive Fe_3O_4 MNPs, and MNPs hardening effects were observed for both fiber systems. The estimated MNPs loadings verified high MNPs loadings in the system, and both systems presented very high magnetism saturation value.

Table 4.16 Magnetism results of magnetic fibers with 20nm and 80nm MNPs at 60%wt MNPs loading and bare Fe_3O_4 MNPs.

Fiber system	Saturated value, M_S, (emu/g)	Coercivity per fiber weight, $H_{C\text{-}fiber}$, (Oe/gram-fiber)	Coercivity per MNPs weight, $H_{C\text{-}MNPs}$, (Oe/gram-MNPs)	Remnant value, M_R, (emu/g)	MNPs ratio estimated from SQUID results (%wt)	MNPs ratio estimated from TGA results (%wt)
PVOH-60%MNPs-20nm	32.1	26	43	1.6	67.0	56.6
Bare 20nm MNPs	47.9	23	23	1.5	--	--
PVOH-60%MNPs-80nm	37.6	73	159	2.2	46.0	61.0
Bare 80nm MNPs	81.8	14	14	3.6	--	--

4.3.6 Summary

In section 4.3, PVOH magnetic fibers with 20nm superparamagnetic and 80nm ferromagnetic Fe_3O_4 MNPs at high MNPs loading of 60%wt were successfully produced via the dry-jet wet spinning process.

Both magnetic fibers demonstrated a bead-free structure with uniform fiber diameters and few-voids cross-section as MNPs dispersed all over the fiber structure. The crystal patterns of both magnetic fibers aligned with the patterns of their corresponsive MNPs very well, representing the consistent crystal structure of MNPs. The polymers in the magnetic fibers were mostly in amorphous structure without obvious crystal peaks, which led to lower Young's modulus for high-MNPs-loading magnetic fibers compared to the pure polymer fibers. The thermal decomposition process was similar for both magnetic fiber systems regardless of the MNPs species. The MNPs loadings estimated from TGA and SQUID results verified the high MNPs loadings in each fiber system. Both magnetic fibers followed the same magnetism hysteresis behaviors of their

corresponding MNPs, with MNPs hardening effect observed in both systems. The saturation magnetism values (*Ms)* of magnetic fibers were 46% and 67% as that of their corresponding MNPs, which were the highest magnetic response achieved on magnetic fibers in the literature to the author's best knowledge. This competitive high magnetic response provides such organic magnetic fibers the potential to be used in traditional inorganic magnetics application, while offering unique properties as fibers.

CHAPTER 5 CONCLUSION

The overall objective of this study was to fabricate highly magnetic responsive single fibers via the industrialized fiber production technique of dry-jet wet spinning, which has been fully achieved via three sections of research.

First, the optimum spinning dope was selected, which included high molecular weight PVOH polymer and DMSO solvent. This system was capable of producing uniform magnetic fibers with uniform structure and acceptable mechanical performance using a dry-jet wet spinning process (Section 4.1).

Second, with the spinning dope identified earlier, magnetic fibers were successfully fabricated with 20nm superparamagnetic Fe_3O_4 MNPs within MNPs loading range of 0% to 60% by weight. The highest magnetic saturation value (*Ms*) of the fibers exhibited 32 emu/g, as compared to the bare MNPs of 48 emu/g, a 67% ratio (Section 4.2). The effects of MNPs on magnetic fiber performance were also studied. It was found that with the addition of MNPs loaded into the fiber, the resulting magnetic fiber diameter grew, polymer crystallinity decreased, thermal degradation occurred faster, and mechanical performance decreased. Higher concentrations of MNPs in the system resulted in even greater increases in magnetic fiber diameter growth, decreases in polymer crystallinity, quicker thermal degradation, and lower mechanical performance. Higher concentrations of MNPs in the dope were also correlated with stronger *Ms*. Drawing was able to improve the mechanical properties of magnetic fibers at all MNPs loadings, but it became less effective at higher concentrations of MNPs in the fiber system.

Finally, to further understand the effect of MNPs species on magnetic fibers at high concentrations of MNPs in the system, ferromagnetic fibers with 80nm Fe_3O_4 MNPs were successfully spun with a MNPs loading of 60% by weight. These fibers exhibited a *Ms* value of

38 emu/g, or 47% as compared to corresponsive bare MNPs (Section 4.3). Comparing superparamagnetic and ferromagnetic fibers at high MNPs loadings, it was demonstrated that polymers in these fibers were mostly in an amorphous phase, but fibers still exhibited robust mechanical strength, which could be utilized in practical applications, such as for artificial muscles or as filters for metal ions.

Overall, this study demonstrated a unique dry-jet wet spinning process, which can be used as a powerful technique to produce magnetic fibers at a wide concentration of MNPs and open new possibilities for making magnetic fiber production a commercial reality.

CHAPTER 6 FUTURE WORK

Upon the successful fabrication of highly magnetic responsive fibers with magnetic nanoparticles and PVOH polymer, some limitations were realized in the current work, additionally, some interesting topics were discovered for future work.

One limitation in the study was the scale of the spinning dope due to current setup. Two factors contributed to the small number of fibers produced: first, the spinning dope in the study was small; second, solution was wasted during spinning and drawing to achieve a steady-state fiber. Due to the limited sample length of fibers produced, it was possible that this contributed to the wide variation of fiber specimen mechanical performance, as some specimens may not have reached steady-state during production. This limitation could be improved with a larger scale system that can produce more fiber quantity at the same steady state.

To continue pursuing magnetic fiber for even higher MNPs loading, spinning dope with 80%wt MNPs was tried in this study, but this failed to generate continuous fiber. Future studies could examine strategies to generate such a continuous fiber by adding surfactant or other additives to the spinning solution, or chemically modifying the MNPs surface with organic components, which could potentially offer better compatibility between the MNPs and polymers.

It would be also interesting to mix superparamagnetic MNPs and ferromagnetic MNPs in the same spinning dope at high loadings and various ratio, which could generate fiber with various magnetic performance. There are fiber properties that were not studied for the magnetic fibers in this, but are worthy to study based on the application, such as fiber solubility, biodegradation, and UV resistance.

This study did not have the opportunity to electro-spin the spinning solutions that were prepared for dry-jet wet spinning, which would be beneficial to compare these two magnetic fiber spinning processes together directly.

For future work, magnetic fibers in this study were not further processed into final products such as yarns or cloth, nor were they tested for application performance as magnetic-field induced switch or artificial muscles. These application-oriented characterizations are of interest and are necessary for magnetic fiber industrialization.

REFERENCES

(1) Yang, W.; Xie, R.; Pang, X.; Ju, X.; Chu, L. Preparation and characterization of dual stimuli-responsive microcapsules with a superparamagnetic porous membrane and thermo-responsive gates. *J. Membr. Sci.* 2008, *321*, 324-330.

(2) Ye, X.; Liu, Z.; Wang, Z.; Huang, X.; Xu, Z. Preparation and characterization of magnetic nanofibrous composite membranes with catalytic activity. *Mater Lett* 2009, *63*, 1810-1813.

(3) Wang, L., Yu, Y., Chen, P.C., Zhang, D.W., Chen, C.H Electrospinning synthesis of C/Fe3O4 composite nanofibers and their application for high performance lithium-ion batteries. *J. of Power Sources* 2008, *183 (2)*, 717-723.

(4) Turek, K.; Opila, J. Magnetic fibers. *J Magn Magn Mater* 1990, *83*, 279-280.

(5) Zhang, H.; Xia, J.; Pang, X.; Zhao, M.; Wang, B.; Yang, L.; Wan, H.; Wu, J.; Fu, S. Magnetic nanoparticle-loaded electrospun polymeric nanofibers for tissue engineering. *Materials Science and Engineering: C* 2017, *73*, 537-543.

(6) Nasouri, K.; Shoushtari, A. M. Fabrication of magnetite nanoparticles/polyvinylpyrrolidone composite nanofibers and their application as electromagnetic interference shielding material. *J. Thermoplast. Compos. Mater.* 2018, *31*, 431-446.

(7) Matos, R. J. R.; Chaparro, C. I. P.; Silva, J. C.; Valente, M. A.; Borges, J. P.; Soares, P. I. P. Electrospun composite cellulose acetate/iron oxide nanoparticles non-woven membranes for magnetic hyperthermia applications. *Carbohydrate Polymers* 2018, *198*, 9-16.

(8) Tan, S. T.; Wendorff, J. H.; Pietzonka, C.; Jia, Z. H.; Wang, G. Q. Biocompatible and Biodegradable Polymer Nanofibers Displaying Superparamagnetic Properties. *ChemPhysChem* 2005, *6*, 1461-1465.

(9) Minoru Miyauchi, Trevor J. Simmons, Jianjun Miao, Jennifer E. Gagner, Zachary H. Shriver, Udayanath Aich, Jonathan S. Dordick, and Robert J. Linhardt Electrospun Polyvinylpyrrolidone Fibers with High Concentrations of Ferromagnetic and Superparamagnetic Nanoparticles. - *ACS Appl. Mater. Interfaces* 2011, *3*, 1958-1964.

(10) Kamachi, M. Magnetic Polymers*. *Journal of Macromolecular Science: Polymer Reviews* 2002, *42*, 541.

(11) Nathan Tafla Rabinovitch US Patent US20140231035A1, 2013-02-15.

(12) Iii Vincenzo Casasanta, Aya Seike France Patent WO2014084853A1, 2012-11-30.

(13) Arup K. Sengupta, Ping Li, Brendan J. Murray, Stuart D. Harrison, Gregory M. Vero US Patent US7540965B2, 2003-04-04.

(14) Farshad, M.; Le Roux, M. Compression properties of magnetostrictive polymer composite gels. *Polym. Test.* 2005, *24*, 163-168.

(15) R Samatham and I-S Park and K J Kim and J-D Nam and N Whisman and,J.Adams Electrospun nanoscale polyacrylonitrile artificial muscle. *Smart Mater. Struct.* 2006, *15*, N152.

(16) Shiga, T.; Okada, A.; Kurauchi, T. Magnetroviscoelastic behavior of composite gels. *J Appl Polym Sci* 1995, *58*, 787-792.

(17) Javad Foroughi, Geoffrey M. Spinks, Gordon G. Wallace, Jiyoung Oh, Mikhail E. Kozlov, Shaoli Fang, Tissaphern Mirfakhrai, John D. W. Madden, Min Kyoon Shin, Seon Jeong Kim, Ray H. Baughman Torsional Carbon Nanotube Artificial Muscles. *Science* 2011, *Oct.*

(18) Bennett Fitch Applications and Benefits of Magnetic Filtration. *http://www.machinerylubrication.com/Read/794/magnetic-filtration* (accessed 9, 2005).

(19) Künkül, A.; Abbasov, T. Removal of corrosion products from viscous aqueous suspensions by magnetic filtration. *Powder Technol* 2004, *149*, 23-28.

(20) Li, L.; Wang, F.; Lv, Y.; Liu, J.; Zhang, D.; Shao, Z. Halloysite nanotubes and Fe3O4 nanoparticles enhanced adsorption removal of heavy metal using electrospun membranes. *Applied Clay Science* 2018, *161*, 225-234.

(21) Shan, D.; Shi, Y.; Duan, S.; Wei, Y.; Cai, Q.; Yang, X. Electrospun magnetic poly(l-lactide) (PLLA) nanofibers by incorporating PLLA-stabilized Fe3O4 nanoparticles. *Materials Science and Engineering: C* 2013, *33*, 3498-3505.

(22) Marcos R. Mauricioa, Heloise Ribeiro de Barrosa, Marcos Rogério Guilhermea, Eduardo Radovanovica, Adley F. Rubiraa, Gizilene M. de Carvalhob, Synthesis of highly hydrophilic magnetic nanoparticles of Fe3O4 for potential use in biologic systems. - *Colloids and Surfaces A: Physicochemical and Engineering Aspects* 2013, *417*, 224--229.

(23) Zhang, Q.; Luan, L.; Feng, S.; Yan, H.; Liu, K. Using a bifunctional polymer for the functionalization of Fe3O4 nanoparticles. *React Funct Polym* 2012, *72*, 198-205.

(24) Chen, C.; Jiang, X.; Kaneti, Y. V.; Yu, A. Design and construction of polymerized-glucose coated Fe3O4 magnetic nanoparticles for delivery of aspirin. *Powder Technol* 2013, *236*, 157-163.

(25) Koichiro Hayashi, Kenji Ono, Hiromi Suzuki, Makoto Sawada, Makoto Moriya, Wataru Sakamoto and Toshinobu Yogo One-Pot Biofunctionalization of Magnetic Nanoparticles via Thiol−Ene Click Reaction for Magnetic Hyperthermia and Magnetic Resonance Imaging. - *Chem. Mater.* 2010, *22 (12)*, 3768–3772.

(26) Mincheva, R.; Stoilova, O.; Penchev, H.; Ruskov, T.; Spirov, I.; Manolova, N.; Rashkov, I. Synthesis of polymer-stabilized magnetic nanoparticles and fabrication of nanocomposite fibers thereof using electrospinning. *European Polymer Journal* 2008, *44*, 615-627.

(27) Song, T.; Zhang, Y.; Zhou, T.; Lim, C. T.; Ramakrishna, S.; Liu, B. Encapsulation of self-assembled FePt magnetic nanoparticles in PCL nanofibers by coaxial electrospinning. *Chemical Physics Letters* 2005, *415*, 317-322.

(28) Roskov, K. E.; Atkinson, J. E.; Bronstein, L. M.; Spontak, R. J. Magnetic field-induced alignment of nanoparticles in electrospun microfibers. - *RSC Adv.* 2012, *2*, 4603-4607.

(29) Wang, H.; Tang, H.; He, J.; Wang, Q. Fabrication of aligned ferrite nanofibers by magnetic-field-assisted electrospinning coupled with oxygen plasma treatment. *Mater. Res. Bull.* 2009, *44*, 1676-1680.

(30) Zhang, D.; Karki, A. B.; Rutman, D.; Young, D. P.; Wang, A.; Cocke, D.; Ho, T. H.; Guo, Z. Electrospun polyacrylonitrile nanocomposite fibers reinforced with Fe3O4 nanoparticles: Fabrication and property analysis. *Polymer* 2009, *50*, 4189-4198.

(31) Nazari, A. Treatment of enzymatic wool with Fe3O4 nanoparticles and citric acid to enhance mechanical properties using RSM. *Journal of the Textile Institute* 2017, *108*, 1572-1583.

(32) Chien, A.; Newcomb, B. A.; Sabo, D.; Robbins, J.; Zhang, Z. J.; Kumar, S. High-strength superparamagnetic composite fibers. *Polymer* 2014, *55*, 4116-4124.

(33) Lin, H.; Watanabe, Y.; Kimura, M.; Hanabusa, K.; Shirai, H. Preparation of magnetic poly(vinyl alcohol) (PVA) materials by in situ synthesis of magnetite in a PVA matrix. *J Appl Polym Sci* 2003, *87*, 1239-1247.

(34) Liu, F.; Ni, Q.; Murakami, Y. Preparation of magnetic polyvinyl alcohol composite nanofibers with homogenously dispersed nanoparticles and high water resistance. *Textile Research Journal* Mar 2013, *Vol. 83, Iss. 5*, 510-518.

(35) Zhu, J.; Wei, S.; Rutman, D.; Haldolaarachchige, N.; Young, D. P.; Guo, Z. Magnetic polyacrylonitrile-Fe@FeO nanocomposite fibers - Electrospinning, stabilization and carbonization. *Polymer* 2011, *52*, 2947-2955.

(36) Sahoo B, Devi KS, Banerjee R, Maiti TK, Pramanik P, Dhara D. Thermal and pH Responsive Polymer-Tethered Multifunctional Magnetic Nanoparticles for Targeted Delivery of Anticancer Drug. - *ACS Appl. Mater. Interfaces* 2013 May, *5(9)*, 3884-93.

(37) Liao, M.; Chen, D. Preparation and characterization of a novel magnetic nano-adsorbent. *J. Mater. Chem.* 2002, *12*, 3654--3659.

(38) Stone, R.; Hipp, S.; Barden, J.; Brown, P. J.; Mefford, O. T. Highly scalable nanoparticle?polymer composite fiber via wet spinning. *J Appl Polym Sci* 2013, *130*, 1975-1980.

(39) Hyeon, T. Chemical synthesis of magnetic nanoparticles. *Chem. Commun.* 2003, *8*, 927.

(40) Lu, A.; Salabas, E. L.; Schüth, F. Magnetic Nanoparticles: Synthesis, Protection, Functionalization, and Application. *Angewandte Chemie International Edition* 2007, *46*, 1222-1244.

(41) Jongnam Park, Kwangjin An, Yosun Hwang, Je-Geun Park, Han-Jin Noh, Jae-Young Kim, Jae-Hoon Park, Nong-Moon Hwang and Taeghwan Hyeon Ultra-large-scale syntheses of monodisperse nanocrystals. *Nature Materials* 2004, *3*, 891-895.

(42) Hou, Y.; Xu, Z.; Sun, S. Controlled Synthesis and Chemical Conversions of FeO Nanoparticles. *Angewandte Chemie International Edition* 2007, *46*, 6329-6332.

(43) Nguyen Thai Ha, Nguyen Hoang Hai, Nguyen Hoang Luong, Nguyen Chau, Huynh Dang Chinh Effects of the conditions of the microemulsion preparation on the properties of Fe3O4 nanoparticles. *The Open Surface Science Journal* 2008, *24*, 9-15.

(44) Deng, H.; Li, X.; Peng, Q.; Wang, X.; Chen, J.; Li, Y. Monodisperse Magnetic Single-Crystal Ferrite Microspheres. *Angewandte Chemie International Edition* 2005, *44*, 2782-2785.

(45) Zheng-Ming Huang, Y. Z. Zhang, M. Kotaki, S. Ramakrishna A review on polymer nanofibers by electrospinning and their applications in nanocomposites. *Composites Science and Technology* 2003, *63*, 2223–2253.

(46) Wu, S.; Sun, A.; Zhai, F.; Wang, J.; Xu, W.; Zhang, Q.; Volinsky, A. A. Fe3O4 magnetic nanoparticles synthesis from tailings by ultrasonic chemical co-precipitation. *Mater Lett* 2011, *65*, 1882-1884.

(47) Xueai Li, Bin Zhang, Chunhua Ju, Xijiang Han, Yuchen Du, and Ping Xu Morphology-Controlled Synthesis and Electromagnetic Properties of Porous Fe3O4 Nanostructures from Iron Alkoxide Precursors. *J. Phys. Chem. C* 2011, *115 (25)*, 12350-12357.

(48) Liu, J.; Cheng, J.; Che, R.; Xu J.; Liu M.; Liu Z. Synthesis and Microwave Absorption Properties of Yolk–Shell Microspheres with Magnetic Iron Oxide Cores and Hierarchical Copper Silicate Shells. *ACS Appl. Mater. Interfaces* 2013, *5(7)*, 2503-9.

(49) Amarjargal, A.; Tijing, L. D.; Park, C.; Im, I.; Kim, C. S. Controlled assembly of superparamagnetic iron oxide nanoparticles on electrospun PU nanofibrous membrane: A novel heat-generating substrate for magnetic hyperthermia application. *European Polymer Journal* 2013, *49*, 3796-3805.

(50) Yang, X.; Zhang, X.; Ma, Y.; - Huang, Y.; Wang, Y.; Chen, Y. Superparamagnetic graphene oxide-Fe3O4nanoparticles hybrid for controlled targeted drug carriers. *J. Mater. Chem.* 2009, *19*, 2710-2714.

(51) Yavuz, C. T.; Mayo, J. T.; Yu, W. W.; Prakash, A.; Falkner, J. C.; Yean, S.; Cong, L.; Shipley, H. J.; Kan, A.; Tomson, M.; Natelson, D.; Colvin, V. L. Low-Field Magnetic Separation of Monodisperse Fe3O4 Nanocrystals. *Science* 2006, *314*, 964-967.

(52) Schmidt, A. M. Electromagnetic Activation of Shape Memory Polymer Networks Containing Magnetic Nanoparticles. *Macromolecular Rapid Communications* 2006, *27*, 1168-1172.

(53) Liu, F.; Cao, P. ; Zhang, H. ; Tian, J. ; Xiao, C. ; Shen, C. ; Li, J. ; Gao, H. Novel Nanopyramid Arrays of Magnetite. *Adv Mater* 2005, *17*, 1893-1897.

(54) Wang, S., Wang, C., Zhang, B., Sun, Z., Li, Z., Jiang, X., Bai, X. Preparation of Fe3O4/PVA nanofibers via combining in-situ composite with electrospinning. *Materials Letters* 2010, *64 (1)*, 9-11.

(55) Wang, M.; Singh, H.; Hatton, T. A.; Rutledge, G. C. Field-responsive superparamagnetic composite nanofibers by electrospinning. *Polymer* 2004, *45*, 5505-5514.

(56) Byung Wook Ahn, Tae Jin Kang Preparation and characterization of magnetic nanofibers with iron oxide nanoparticles and poly(ethylene terephthalate). *Journal of Applied Polymer Science* 2012, *125*, 1567-1575.

(57) Li, Y.; Zhu, H.; Gu, H.; Dai, H.; Fang, Z.; Weadock, N. J.; Guo, Z.; Hu, L. Strong transparent magnetic nanopaper prepared by immobilization of Fe3O4 nanoparticles in a nanofibrillated cellulose network. *J. Mater. Chem. A* 2013, *1*, 15278-15283.

(58) Arthur N. WIlkinson, Anthony J. Ryan In *Polymer Processing and Structure Development;* Kluwer Academic Publishers, Ed.; 1998; , pp 577.

(59) Strobl G. In *The Physics of Polymers;* Springer-Verlag, Ed.; 1996; , pp 445-173-176.

(60) Cakmak, M.; Teitge, A.; Zachmann, H. G.; White, J. L. On-line small-angle and wide-angle x-ray scattering studies on melt-spinning poly(vinylidene fluoride) tape using synchrotron radiation. *Journal of Polymer Science Part B: Polymer Physics* 1993, *31*, 371-381.

(61) P Bajaj, K. D. Some recent advances in the production of acrylic fibres for specific end uses. *Indian Journal of Fibre & Textile Research* 1991, *16*, 89-99.

(62) Leon Segal In *The rheology of wet-spun fiber extrusion;* 1970; , pp 190.

(63) Robert J. Lancashire Unit - Chemistry of Garments: Synthetic (man-made) Fibres. *http://wwwchem.uwimona.edu.jm/courses/CHEM2402/Textiles/Synthetic_Fibres.html* (accessed 08, 2011).

(64) Robert R Mather In *High Performance Fibres;* The Chemistry of Textile Fibres; Royal society of chemistry: 2011; Vol. Chapter 6, .

(65) Nataraj, S. K.; Yang, K. S.; Aminabhavi, T. M. Polyacrylonitrile-based nanofibers—A state-of-the-art review. *Progress in Polymer Science* 2012, *37*, 487-513.

(66) Xu, X.; Uddin, A. J.; Aoki, K.; Gotoh, Y.; Saito, T.; Yumura, M. Fabrication of high strength PVA/SWCNT composite fibers by gel spinning. *Carbon* 2010, *48*, 1977-1984.

(67) Liu, D.; Zhu, C.; Peng, K.; Guo, Y.; Chang, P. R.; Cao, X. Facile Preparation of Soy Protein/Poly(vinyl alcohol) Blend Fibers with High Mechanical Performance by Wet-Spinning. *Ind. Eng. Chem. Res.* 2013, *52(18)*, 6177-6181.

(68) Lu, C.; Blackwell, C.; Ren, Q.; Ford, E. Effect of the Coagulation Bath on the Structure and Mechanical Properties of Gel-Spun Lignin/Poly(vinyl alcohol) Fibers. *ACS Sustainable Chem. Eng.* 2017, *5*, 2949-2959.

(69) Mikołajczyk, T.; Rabiej, S.; Boguń, M.; Szparaga, G.; Draczyński, Z. Nanocomposite polyvinyl alcohol fibers for medical applications. *J Appl Polym Sci* 2011, *120*, 1234-1244.

(70) Mercader, C.; Denis-Lutard, V.; Jestin, S.; Maugey, M.; Derré, A.; Zakri, C.; Poulin, P. Scalable process for the spinning of PVA?carbon nanotube composite fibers. *J Appl Polym Sci* 2012, *125*, E191-E196.

(71) Wang, M.; Singh, H.; Hatton, T. A.; Rutledge, G. C. Field-responsive superparamagnetic composite nanofibers by electrospinning. *Polymer* 2004, *45*, 5505-5514.

(72) M. K. Lindemann In *Vinyl Alcohol Polymers;* Vinyl Alcohol Polymers; EPST: Air Products and Chemicals, Inc., Vol. 14, pp 149-207.

(73) Won-Ill Cha, Suong-Hyu Hyon, Yoshito Ikada Gel spinning of poly(vinyl alcohol) from dimethyl sulfoxide/water mixture. *J. of Polymer Science Part B: Polymer Physics* 1994, *32 (2)*, 297-304.

(74) Krzysztof Matyjaszewski In *Encyclopedia of polymer science and technology electronic resource];* John Wiley & Sons Inc: Hoboken, New Jersey, 2014; Vol. 8.

(75) Sobhanipour, P.; Cheraghi, R.; Volinsky, A. A. Thermoporometry study of coagulation bath temperature effect on polyacrylonitrile fibers morphology. *Thermochimica Acta* 2011, *518*, 101-106.

(76) Lewin, M. In *Handbook of Fiber Chemistry;* CRC Press: Boca Raton, 2007; Vol. 3rd ed.

(77) Wang, Y.; Hsieh, Y. -. Immobilization of lipase enzyme in polyvinyl alcohol (PVA) nanofibrous membranes. *J. Membr. Sci.* 2008, *309*, 73-81.

(78) R. T. Weitz, L. Harnau, S. Rauschenbach, M. Burghard, and K. Kern Polymer Nanofibers via Nozzle-Free Centrifugal Spinning *Nano Letters* 2008, *Vol. 8, No.4*, 1187-1191.

(79) Takasa, K.; Miyashita, N.; Takeda, K. Young modulus and degree of crystallization of highly-elongated polyoxymethylene. *J Appl Polym Sci* 2006, *101*, 1223-1227.

(80) Kejian Wang Description of Extrudate Swell for Polymer Nanocomposites. *Materials (Basel)* 2010, *3(1)*, 386-400.

(81) A. K. Haghi In *Research Progress in Nano and Intelligent Materials;* Apple Academic Press: 2011; , pp 111.

(82) Zhang, X.; Liu, T.; Sreekumar, T. V.; Kumar, S.; Hu, X.; Smith, K. Gel spinning of PVA/SWNT composite fiber. *Polymer* 2004, *45*, 8801-8807.